AN IMPROVED METHOD OF INVESTIGATION OF COMBUSTION PARAMETERS IN A NATURAL GAS FUELLED SI ENGINE WITH EGR AND H_2 AS ADDITIVES

by

WEI-CHIN CHANG

A thesis submitted to
The University of Birmingham
for the degree of

DOCTOR OF PHILOSOPHY

School of Manufacturing and Mechanical Engineering
The University of Birmingham
Birmingham B15 2TT
England
August 2002

ABSTRACT

An improved approach to the classical Rassweiler and Withrow's mass fraction burned model and an improved data acquisition/processing procedure are employed with the intention of increasing precision while retaining simplicity. A new method to predict the trends of MFB and emissions, based on the online analysis of cylinder pressure is introduced. A diagnostic method to study the heat release rate in a natural gas fuelled engine has been developed for future use.

Natural gas fuelled vehicles are environmentally friendly and it is possible to use a high compression ratio engine with all its associated benefits for efficiency. However, one of the problems associated with the use of natural gas is NO_x emission. EGR can be used to reduce NO_x, but it leads to unstable combustion. The stability problem can be resolved by the addition of hydrogen, which can be provided by fuel reforming. Based on the beneficial effects of exhaust gas fuel reforming, the effects of EGR, H_2 and H_2/CO as additives to natural gas are analysed and discussed in terms of combustion indicators derived by the new diagnostic method, in particular in terms of combustion duration (CA for 5/50/95% MFB), IMEP and cycle by cycle variation (COV of IMEP, COV of peak pressure).

ACKNOWLEDGMENTS

I would like to thank Dr. Miroslaw Wyszynski for his academic supervision and guidance throughout my study, and Dr. A. Megaritis for his encouragement and help.

I wish to thank my colleague, Mr. Steven Allenby (soon to be Ph.D), for his friendly support and help with the English language.

I also wish to thank Mr. Eric Chiang, the chairman of Chun-Hsin Electric and Machinery Mfg. Corp., Taiwan, for the financial support in the first year of this study.

Finally, I have to thank my long-suffering wife, Pin-Wei, for her unfailing support, and my son, Chun-Hsiang, and my daughter, Yu-Hua, for forgiving me for being unable to be a good farther during the last few years. Without their support and everlasting love, this work would not have been possible.

CONTENTS

NOMENCLATURE / SUBSCRIPT

Nomenclature:

9PWS	9 points weighted smoothing method
BDC, ABDC, BBDC	Bottom dead centre, After BDC, Before BDC
TDC, ATDC, BTDC	Top dead centre, After TDC, Before TDC
BMEP	Brake mean effective pressure (bar)
CA	Crank angle (degree)
CNG	Compressed natural gas
CO	Carbon monoxide
COV, COV_{IMEP}	Coefficient of variation, COV of IMEP
DAQ	Data acquisition
DC	Direct current
EGR	Exhaust gas recirculation
EOC	End of combustion
EVO	Exhaust valve open
HC	Hydrocarbon
Hz	Hertz (frequency unit)
IG	Ignition
IMEP	Indicated mean effect pressure (bar)
IVC	Inlet valve close
LPF	Low pass filter method
NG	Natural Gas
NO_x, NO	Oxide of nitrogen, Nitric oxide
MBT	Minimum advance for best torque (crank angle)
MFB	Mass fraction burned (-)
P	Cylinder pressure (bar)
PMEP	Pumping mean effective pressure (bar)
R&W	Rassweiler and Withrow model
SI	Spark ignition
SOC	Start of combustion
T	Temperature (K)
TDC	Top dead centre
UHC	Unburned hydrocarbon
V	Engine cylinder volume (m^3)

WOT	Wide open throttle
cps	Cycles per second
deg.	Degree
n	Polytropic index
n_c	Compression polytropic index
n_e	Expansion polytropic index
$\overline{p}$	Average value of relevant parameter *P*
P_{max}	Peak pressure (bar)
psi	pounds per square inch
r-R&W	Revised R&W model
r_c	Compression ratio
s	Standard deviation
x	MFB
θp_{max}	CA of peak pressure
θ_{xb5}	CA of 5% MFB
λ	air/fuel ratio
γ	Ratio of specific heats

Subscript:

c	Referring to clearance volume
n	Referring to net IMEP
g	Referring to gross IMEP
s	Referring to swept volume

LIST OF FIGURES

LIST OF TABLES

1. INTRODUCTION

Although the internal combustion engine has been developed for more than one century, combustion conditions inside the engine cylinder are still not precisely predictable yet, mainly because of the cycle-by-cycle variations from unexpected fuel-air mixture charge and the unknown heat transfer condition. Moreover, research has emphasized alternative fuels recently. The combustion behaviour might be very different from traditional fuels, i.e. petrol and diesel. An optical engine is capable of being used to explore the combustion process inside the cylinder by observing the flame behaviour with a high-speed camera [1] or in-cylinder flow in a motored engine with particle image velocimetry [2]. However, the costs of such an engine and instruments are prohibitively high for most engine research, and the destruction of engine is impracticable for a performance diagnosis on a mass produced engine. A good experimental rig that can accurately collect combustion information from a firing engine and also foretell the emissions trends will be a helpful diagnostic tool for alternative fuel (i.e. natural gas) engine development.

Amann [3] said that the cylinder pressure indicator is the most important diagnostic tool in engine investigation, he also presented several applications using pressure data as engine performance indicators. The extent of pressure data applications covers a very wide range, e.g. closed loop feedback control using pressure signals as a data source [4], heat release related

analysis [5-7], abnormal combustion detection [8, 9] and emission prediction [10], all have been well studied and proved accurate.

Obviously using pressure data alone will not yield too much meaningful information from the cylinder, it has to be associated with some other parameters collected simultaneously from the engine. The time resolved pressure data is known to be useful, from which much information can be extracted regarding combustion phenomena inside the engine cylinder, and none of the expensive instruments, installations and troublesome hardware modifications are necessary.

Combustion is the most important chemical behaviour inside an engine cylinder, a series of quick reactions are triggered by a spark plug in an SI engine. Engine combustion is complex and happens suddenly in a very short time, the behaviour of the flame strongly depends on the inlet charge mixtures. Understanding the combustion progress can help researchers to develop better knowledge for car engine design and improved emission results. By using an IBM compatible personal computer and modern data acquisition rig, real-time data acquisition and analysis become feasible. With some attention to signal collecting and processing, e.g. phasing of TDC, data smoothing, etc, the dependable data can be collected, therefore a simple and reliable analysis method is an essential process to not only present an engine combustion performance, but also to predict the emissions behaviour.

Apparently, many researchers have made efforts to simulate the combustion conditions for

engine research. Heywood [11, Ch. 14] classified these models into thermodynamic and fluid dynamic groups, Ramos [12, Ch. 4] defined thermodynamics and dimensional models for spark-ignition engine research work, Chow and Wyszynski [13] used the first and second thermodynamics law to distinguish their differences. There are so many different mathematic methods to model the engine combustion, but only a few can be applied to real time analysis because of calculation time or information availability problems. One of the real-time applicable models is by Rassweiler and Withrow [14]. They produced a widely used classic method to analyse burn rate and reveal combustion conditions inside engine. Regardless of heat transfer and crevice leakages but still maintaining accuracy, the pressure rise due to combustion is proportional to the mass of burned charge.

Since first discovered in the U.S.A. at Fredonia, New York, in 1821, natural gas has, in just half century after World War II, become a highly demanded energy source. Natural gas is currently the basis for 19% of the world's energy supply, and it has long been used as a stationary engine fuel. Because natural gas is a much cleaner fuel than gasoline/diesel, it could perhaps bridge a transition to a renewable-powered transportation system.

The application of natural gas as a vehicle fuel is not popular enough so far, there are a few automakers producing natural gas fuelled automobiles, however the fuel supply infrastructure is still not widespread for this kind of vehicle, nevertheless it is optimistic to investigate the

use of natural gas because of the abundant stock and low emission characteristics. Even for the newest fuel cell car development, producing hydrogen by catalytic steam reforming of natural gas is one of the potential possibilities [15, 16], besides the infrastructure system for fuel supply can still be used for future developments.

Hydrogen related car research, such as the pure hydrogen engine [17, 18] and fuel cell cars [19-21], has shown the potential for features of nearly free emissions. Before these technologies become more mature and the costs come down to an acceptable range, natural gas will be the best choice in terms of environmental concerns. With its high octane number rating, the compression ratio of natural gas fuelled engine can increase up to 15 without incurring knocking problems, which means better thermal efficiency can be achieved easily.

Several improved approaches to Rassweiler and Withrow's model were employed in this study to pursue more precise, but still simple, estimation of heat release rate; hence real time analysis can be performed. Some important engine combustion characteristics, e.g. indicated mean effective pressure, peak pressure, cycle to cycle variation, ignition delay and combustion duration were discussed as indicators of engine performance.

1.1. The Work Presented in this Thesis

A series of engine tests has been carried out on a spark ignition engine with natural gas fuel,

all pressure data were collected by an improved data acquisition rig to ensure the accuracy of analysis sources. By applying the improved methods to mass fraction burned calculation, some combustion indicators were used to decide the engine performance. Effects of exhaust gas recirculation (EGR) and hydrogen as additives on combustion were particularly implemented as a test on the beneficial effects of fuel reforming.

Emissions results were analysed in relation to the patterns deduced from the first and second derivative of pressure data. A new method for predicting the trends of emissions behaviour was introduced based on the analysis of pressure data online. In addition, the data acquisition itself can be more efficient by only selecting for analysis, and showing, the most relevant pressure data.

2. LITERATURE SURVEY

2.1. Acquisition of Volume and Pressure Data

For understanding the combustion inside an engine cylinder, many researchers work on either experimental tests or computer model simulations. Because of booming computing technology and growing hardware ability, mathematic simulations methods have become increasingly popular and economic. However, an experimental result is the fundamental validation measure for complex mathematic models, hence it is necessary and needs to be accurate and reliable, moreover, easy and efficient.

Chun and Heywood [6] said the principle diagnostic in analysing the combustion process of the internal combustion engine is the time-history of the cylinder pressure. As the working media of the reciprocating internal combustion engine, cylinder pressure transforms the chemical energy of the inlet mixture to mechanical work, hence it can be used to evaluate the distribution of cycle work, to estimate the net heat release rate during combustion and to diagnose abnormal combustion [3, 5]. To more practically use pressure data, the association with volume variables has proved very useful, and consequently an accurate crank angle indicator to display the volume data is required.

2.1.1. Engine Volume

2.1.1.1. Clearance Volume

It has been suggested that the clearance volume not to be derived from a manufacturer's compression ratio by calculation because the mean figure may not be accurate enough for experimental test. An alternative of using the acoustic device or liquid displacement to validate the value [3] is highly recommended.

2.1.1.2. Optical Crankshaft Encoder

Tracing the position of crank angle by using an optical crankshaft encoder is cost-efficient and convenient, as long as the signal is well calibrated. Nowadays, this type of shaft encoder usually generates at least two different signals: one is position identifying normally with a frequency of one pulse per revolution; the other one is the crank-angle marking signal, from 0.2 to 10 crank angles per pulse depends on the accuracy. The shaft encoder is normally coupled with engine crank shaft, hence it is convenient to track the engine speed. Taraza and co-workers [22] used shaft encoder signals and internal clock pulses from data acquisition card to verify the speed of a diesel engine, Chan [23] used shaft encoder together with pressure transducer to present the thermodynamic cycle and entropy change. Both indicate very useful applications to engine study of this versatile instrument.

TDC is the best point to correspond with the piston position, and it can be correlated with the TDC signal of the shaft encoder synchronously. To avoid the difficulty of finding the correct position of TDC from the high piston speed section of the stroke, the strategy is to take an offset to the slow-moving crank angle so the marking pulse can be correlated easily.

2.1.2. Piezoelectric transducer

In 1880 Pierre and Jacques Curie first discovered the piezoelectric effect, which did not attract too much attention until the 1940s. They found that under mechanical loading, some crystals can exhibit very tiny electrical charges, but this phenomenon was very hard to detect and no convenient instrument was available then. Until Kistler made the charger amplifier principle practicable in 1950, then researchers started using very high input impedance amplifiers to amplify their signals, and it became very popular in several applications within various disciplines. The detail of a quartz piezoelectric transducer can be found in Figure 2-1.

The electrical output can be produced only when the crystals experiences a change in load, therefore, a static measurement is impossible with this technology, a reference datum will always be needed. Besides, a dead weight method using hydraulic mechanism is necessary to calibrate the whole system (piezoelectric transducer and charger amplifier) before using it.

Although some researchers criticized that the use of piezoelectric transducer in pressure data

acquiring as a disturbance of engine combustion [24], this technology has been developed very well.

Brown [25] evaluated the pressure measurement system of piezoelectric transducer and checked a wild range of possible errors. He suggested that the errors for IMEP determination could be classified into four categories:

(1) phase shift: delay of circuits, passage effect and crankshaft

(2) calibration accuracy, sensitivity, stability and linearity

(3) read-out system

(4) hysteresis, thermal strains, and others

From his descriptions, the ideal transducer has to be robust and easy to install. Besides, a direct and integral water cooling system is necessary. The details from his suggestion can be found in Table 2-1.

Lancaster and co-workers [26] presented a detailed procedure for using it, ranging from instrument preparation to the pressure data analysis method used. According to their study, the main problems of using piezoelectric transducers are the lack of linearity and the susceptibility to thermal and mounting strains. To minimize the measurement error, they also suggested using a large and water-cooled transducer with a careful calibration beforehand.

Flush mounting of the pressure transducer is suggested by conventional wisdom. However,

this method will magnify the consequences of thermal shock. The temperature variations will change the resonant frequency and the Young's modulus of the quartz crystal, the other effect is the material expansion/contraction phenomena happening on the diaphragm and mount of the transducer's external parts. The thermal shock problem becomes more serious when the engine is firing, because the temperature variation can be in the range of two thousand Celsius degrees difference and several times per second.

Some researchers applied coating on the diaphragm and effectively damped the quick heat flux change, but the thermal stress on the mounting area will still exist. Randolph [27] was concerned about the thermal shock effects at the transducer surface, he said the raw data errors caused by this phenomenon are severe. Moreover, because of the variability, it becomes even harder to detect. He suggested a proper mounting for the transducer can resolve the problem. Three different mounting methods were then compared by him, and the benefits of using a connecting passage for the mounting were clearly shown in his results.

2.1.3. Ionisation Sensor

Another tool that needs to be illustrated for pressure data acquization in SI engines is using the spark plug as an ionization sensor. The spark plug is normally used to ignite the inlet mixture, but it can also work as a sensor for detecting the in-cylinder properties of the

combustion. The duration of the spark operating time needs only a very short period compared with one engine revolution, that means the spark plug is available for measurement during nearly the whole part of the combustion. The use of such a device can be more economic and easy to install than a piezoelectric pressure transducer, but the spark plug circuit has to be modified for electrode polarization and current measurement.

The formation of ions in the engine combustion relies on the gas temperature, chemical compositions and geometry of engine chamber. This provides the hope of using the ions for an assessment of the quality of combustion. By applying a constant DC voltage across the electrode gap of a spark plug during combustion, a current, which reflects the presence of ions as well as other local conditions near the electrode gap, can be generated.

The current signal that induced during combustion often consists of two discrete peaks. The first peak is usually explained because of chemi-ionisation, and occurs when the flame front passes the electrodes. Until the flame kernel grows further, pressure and temperature in the burned gas around the electrodes increase rapidly, and the process of thermal-ionisation becomes measurable. When the pressure reaches a maximum value, the large quantity of nitric oxide (NO) will increase the conductivity within the spark plug, a second current peak can then be observed.

Ionisation sensors have been used to detect flame propagation in engine combustion for a long

time. Some researchers have used this technology to detect knocking problem [28, 29], some have used it to identify the coefficient of variation of IMEP [30, 31].

Apart from the former functions, it can also be used for heat release rate calculation by introducing a Wiebe function.

$$x_b = 1 - \exp\left[-a\left(\frac{\theta - \theta_0}{\Delta\theta} \right)^{m+1} \right] \qquad \text{Eq. 2-1}$$

where

x_b is the mass fraction burned, the value varies from 0 to 1.

θ is the crank angle, subscript 0 indicates the start of ignition

$\Delta\theta$ is the total burn duration.

a and m are adjustable duration and shape parameters respectively.

Values of parameters a and m can be decided by correlating Eq. 2-1 with the peak pressure derived from ion current signals, consequently the mass fraction burned trace can be obtained once a and m have been settled [24, 32].

2.1.4. Estimation of Pressure Data

Apart from using instruments installed on engine cylinder, a new method is growing up, based on a statistical method, called chaos or deterministic chaos theory, which intends to use suitable perspective to investigate random-like behaviour and estimate it accurately through

calculated results. Daw and Kahl [33] concentrated their study on peak pressure of cycle-by-cycle variation in four stroke SI engines and in their conclusions the chaotic time series analysis on this topic is viable if more engine types and more engine cycles can be analysed.

Advantages of this method are that the cost will be reduced and real-time analysis becomes more efficient because the time necessary for acquiring data has been shortened by the computer calculation. Guezennec and Gyan [34] proposed a stochastic estimation approach to produce pressure data by just simply using the crankshaft velocity, different operating conditions like engine speed, load, EGR content and spark timing are all considered in their method.

By this method, estimated pressure can be obtained through the following low-order and non-linear equation:

$$P_{est} = a_{00} + a_{10} f_\theta + a_{12} f_\theta \dot{\tilde{\theta}} + a_{13} f_\theta \ddot{\theta} + a_{23} \dot{\tilde{\theta}} \ddot{\theta} \qquad \text{Eq. 2-2}$$

where a polytropic process was assumed and pressure variation follows pV^k=C, subscript k is decided by individual engine characteristic.

f_θ : a position function proportional to V^{-k} during compression and expansion strokes and constant otherwise.

$\dot{\tilde{\theta}}$: crank shaft velocity

$\ddot{\theta}$: crank shaft acceleration

Coefficients a_{00}, a_{10}, a_{12}, a_{13}, a_{23} are solved by a covariance matrix which introduced the

cross-correlation relations between pressure and the five basis functions (1, f_θ, $f_\theta\dot{\tilde{\theta}}$, $f_\theta\ddot{\theta}$, $\dot{\tilde{\theta}}\ddot{\theta}$).

To take account of different operating conditions, some linear equations need to be added. By referencing real engine running conditions, all coefficients of Eq. 2-2 can be derived by curve fitting.

Although this mechanism seems economic and efficient, there are some notions that need to be borne in mind when used:

(1) It is still necessary to estimate the polytropic index beforehand.

(2) The order of error will be increased because of curve fitting the coefficients.

(3) For those conditions which different engine operations are required all the time, this method might not be adequate due to the pre-calculation necessity of coefficients.

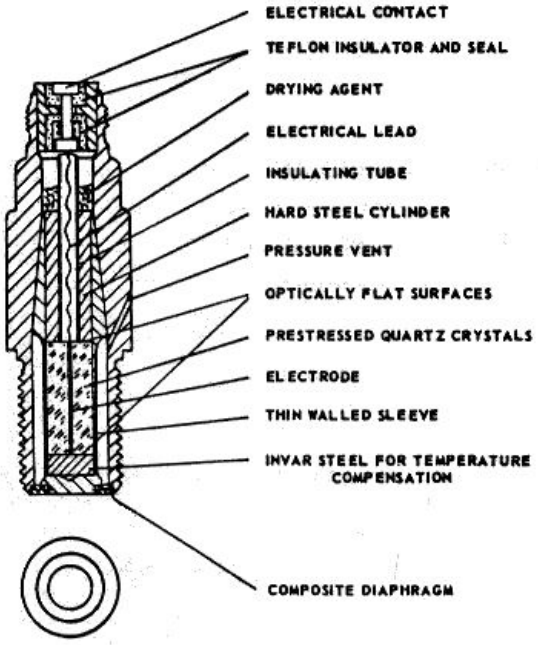

Figure 2-1 Details of piezoelectric pressure transducer [25].

1. Linearity	Better than 1%
2. Change of Pressure Sensitivity with Pressure	Less than 1% up to 400 psi, less than 3% up to maximum pressure
3. Repeatability	0.1% from room temperature to operating temperature
4. Frequency Response	DC to 50,000 cps
5. Thermal Strain Sensitivity	Less than 0.01 psi/F at 5cps
6. Acceleration Sensitivity	Less than 0.01psi/g to 20,000 cps
7. Signal to Noise Ratio	Better than 3000:1
8. Hysteresis	Less than 0.1% up to 100 cps

Table 2-1 Specification of ideal transducer by [25].

2.2. Some Aspects of Acquiring Accurate Pressure vs. Volume Data

To obtain reliable results, the quality of signals or data acquired from engine becomes very important. It is the fundamental requirement of analysis, the accuracy of data will affect further analysis substantially. Chapter 2.1.2 has drawn some attention to the use of piezoelectric transducer. An integral consideration of data acquisition/processing system will be discussed in this section for providing qualified information about engine performance.

There is a large amount of literature relating to engine combustion parameters, nevertheless, we can still roughly distinguish those available approaches into two basic types: direct and indirect ways [35]. Direct methods are much more about the optical engine data acquisition, which is not practical for most researchers. Therefore, the indirect method, since the end of eighteenth century Watt had developed the P-V indicator, the mechanism to obtain pressure-volume information simultaneously from a running engine will be investigated intensively here. The method of acquiring pressure data in terms of crank angle is one of the key points to gain heat release information from engine cylinder by most of the combustion analysing models.

2.2.1. Choosing the Number of Cycles to Analyse

This issue mostly depends on the operation conditions, data analysis method and data storage ability of equipment. Most researchers have their own point of view of how many cycles they should take for analysis. The most important thing needs to be considered here is the objectivity of the data. In general, the more the data the better for analysis, but meanwhile the time consumption will increase and the data storage space becomes unacceptable huge. When higher crank angle resolution is necessary, it becomes even worse. The data processing and calculation will be very inefficient if too many cycles are chosen, which could also be fruitless. Moreover, in some circumstances, when real time data analysis is required, it will make the response on the transient conditions very difficult. A general survey on the choice of range is given below aiming to outline the effects, a further investigation is needed if the application of data is specialized.

Lancaster and co-workers [26] suggested that, to obtain reliable results with engine pressure data, at least 40 cycles is needed, and 300 cycles is considered for high variability conditions. In the study of heat release analysis, Gatowski and co-workers [36] used 44 cycles data per condition to produce their results, following on from their work Chun and Heywood [6] only used 39 cycles to compare heat-release and mass-of-mixture burned estimations. The subsequent investigation from the Sloan Automotive laboratory at MIT by Cheung and

Heywood [37] recommended more than 100 cycles of data needed for confirming the statistical validation of a one-zone burn-rate analysis.

Cartwright and Fleck [38] said because of WOT condition applied in all cases of their study, 35–40 cycles were sufficient for their engine performance analysis on a two-stroke engine. Jensen and Schramm [39] used 50 cycles measured pressure data as the analysis source of their three-zone heat release model. Hayes and co-workers [5] said that in most engine heat-release programs, 100 to 300 continued engine cycles are traditionally used as input data. Hassaneen and co-workers [40] acquired 300 consecutive in-cylinder pressure cycles for the calculation of initial flame development time and the rapid burn duration. Each application has been considered by the researchers on their own opinions, however, the results shown in Figure 2-2 by Brunt and Emtage [41] clearly presents the effect of number of cycles on IMEP analysis. By using 100-cycles signals, less than 1% error of IMEP can be achieved, but when the amount is increased to more than 100 cycles, and up to 300 cycles, it does not make a big difference. They concluded that 150 cycles is needed to gain a reasonable accuracy but 300 or more cycles should be used ideally.

If the performance indicators of combustion need to be deduced from mean (averaged) pressure data, in some particular events, i.e. knocking, surface ignition, etc, such abnormal information will be smoothed out through averaging by a large amount of cycles. However, if

the real time analysis is not very important, in the author's opinion, keeping more than 100 cycles of raw data is always recommended.

2.2.2. Phasing of TDC

Phasing is the term used to associate TDC with the traces of pressure signals, thus the pressure vs. volume relation of engine cylinder can be known. Rocco [42] emphasized the importance of correctly identifying the position of TDC, he said that a wrong datum point could cause major errors in the calculation of parameters of engine performance, such as IMEP, thermal efficiency and heat release curves in the engine thermodynamic cycle. A linear relationship between IMEP error and TDC error can be seen in Figure 2-3, the acceptable range of faulty position for TDC is within 0.1° CA.

Two major mechanisms can locate TDC. Nevertheless the difference is up to 0.5° CA in some cases. The first method uses a dial–gauge to point out the TDC position when engine is constructed. The other way, which is more precise, needs to trace the pressure data when the engine is motoring, two crank angles with the same pressure (inflexion point) can be found on both compression and expansion strokes, the TDC is supposed to be right in the middle between them.

The above assumption is an ideal condition, it is obvious that during the motoring cycles,

because of heat transfer, the peak pressure will occur before TDC. The real TDC position needs to be obtained by calculation, therefore up to 0.7° crank angle difference might happen by applying different formulas of heat transfer coefficient. Considering such phenomenon, Staś [43] referred to the concept of "loss angle", which is the deviation of crank angle from the peak pressure to the minimum volume. Motoring pressure data and an estimated constant polytropic index are used to obtain a ratio value. By adjusting the TDC position to keep this value within a certain range (from 2.2 to 2.3 in his study), the phasing within 0.1° CA accuracy can be kept. Morishita and Kushiyama [44, 45] proposed an equation to combine the effects of four major errors from P-V diagrams on polytropic index, the deviation of TDC position is one of them. They also pointed out that the gas leakage is the reason why the mid-point of two inflexion points will moves slightly backward when pressure decreases. Besides, their deductions also establish the existence of polytropic processes within compression and expansion strokes apart from combustion period.

Tazerout and co-workers [46] revealed a new method to locate TDC. Uunder motoring conditions, compression and expansion strokes are symmetrical with respect to the peak temperature in the Temperature-Entropy diagram. From Figure 2-4, a loop within maximum temperature region can be found if there is a TDC phase lag. This method will need more information about fuel composition and cylinder temperature.

Lancaster and co-workers [26] presented two methods to examine the TDC phasing, which are feasible to be implemented as checking mechanisms to see if re-calibration is necessary before starting the collection of firing data, or used as routine check tools for experimental accuracy. The first method examines motored P-V diagrams, the peak pressure should occur before TDC because of heat transfer. On the other hand, if peak pressure occurs more than 2° CA before TDC, the pressure data is considered as advanced with respect to volume. The other method is to analyse the logarithmic P-V diagram. Due to the polytropic process mentioned previously, the relation

$$PV^n = \text{constant} \qquad \text{Eq. 2-3}$$

n is the polytropic index

can be applied and two straight lines before and after TDC will be found in the motored cycle if the phasing is correct, otherwise, curve or crossed lines will appear instead. Figure 2-5 shows a normal logarithmic P-V diagram with proper TDC phasing.

41% change of IMEP was reported when the pressure has one crank angle degree advanced or retarded difference in respect to volume, hence the calibration is very important.

2.2.3. A Reference Datum for Piezoelectric Transducer Signals

As described in Section 2.1.2, the main problem in using piezoelectric transducers to acquire

pressure data is that only the reference (or dynamic) pressure can be obtained. To make it relevant, an already known pressure datum needs to be referred (known as pegging).

Brown [25] said absolute pressure is not important for determining IMEP, because the work is done on a cycle basis, and the difference will be eliminated at the end of integration. However, absolute pressure is important for engine performance analysis. Brunt and Emtage [47] said that in calculating MFB and burn angles, the referencing offset is the biggest source of error. At bottom dead centre (BDC), the inlet manifold pressure is close to the cylinder pressure, probably within the range between 70 and 140 mbar, therefore it is acceptable and convenient method to use it for pressure referencing. Amann [3] said the error might be in the order of 10 kPa, which is acceptable for IMEP calculation. Brunt and Pond [48] proposed that more than 20% error might be experienced due to the pressure pegging offset. They also suggested using the inlet manifold pressure as a reference pressure for better results.

Randolph [49] provided nine different pegging methods and compared the effects of each. He concluded that setting the bottom dead centre pressure of the inlet stroke to be equal to the intake manifold absolute pressure was a better method when only one pressure transducer is used. A different reference datum was described by Stone and co-workers [1], two pressure transducers were fitted on the cylinder barrel of K4 optical engine, they said when the piston was about 20° CA or further from BDC both barrel transducers record the atmospheric

pressure.

2.2.4. Crank Angle Resolution

This is an important variable for the accuracy of pressure data acquisition, although not much literature has so far mentioned this subject. The resolution of crank angle is the interval between each pressure signal being measured. Most researchers suggested that 1° CA resolution is more suitable for nearly all kinds of engine studies. On the other hand, it is the most common resolution on the market. Brunt and Emtage [47] said one-degree crank angle resolution is adequate for the calculation of burn angle statistical data.

Brunt and Lucas [50] pointed out three advantages of increasing CA resolution in the measurement of engine pressure data and performance analysis. They are:

(1) Increased sensitivity to pressure variation,

(2) More precisely identification of a certain change,

(3) Improved crank angle phasing.

The first one is obviously the effect of physical change. However, higher resolution causes the increasing requirement of data storage space, it is a disadvantage of real time data logging, therefore finding the balance in this trade-off becomes a challenge for researchers.

Karim and Khan [51] presented a variable CA resolution method that can remove the noise by

frequency changed, in their method the CA resolution used for the calculation of engine performance parameters is a function of the rate of change of pressure. Therefore, during the compression before combustion and the latter part of expansion after firing, a coarse CA resolution will be used because of lower pressure rise rate. This method reduces the space necessary for data storage and maintains the accuracy of the heat release rate calculation to a certain degree, the effect can be clearly found after TDC. One unwanted condition might occur at the peak pressure when the pressure change rate becomes zero, the attempt of using a large resolution will cause calculation errors, and therefore a limit to the maximum CA interval during the peak pressure area needs to be arranged to solve this problem.

2.2.5. Finding the End of Combustion through Pressure Traces

It is very difficult to decide when the end of combustion (EOC) will be inside a working engine cylinder. Observations from an optical engine show that even once combustion has completed the flame will remain luminous. However, EOC is very important in the calculation of either mass fraction burned or heat release. It is necessary to find out when the combustion reaches its end.

To determine the expansion polytropic index through a logarithmic P-V diagram, EOC needs to be known as well. In the method of calculating mass fraction burned proposed by

Rassweiler and Withrow (R&W) [14], an estimated EOC has been used and checked with the calculation result to see if it is right at the position when pressure change by combustion turns to zero or negative.

Shayler and co-workers [52] compared three different methods of finding EOC, Ball and co-workers [53] discussed similar methods few years later. Based on detecting the first calculated negative value of combustion pressure, these three methods are:

(1) First negative – combustion completes immediately after the calculated pressure value caused by combustion becomes negative.

(2) Sum negative – combustion completes after three consecutive negative calculated pressure values caused by combustion.

(3) Standard error – combustion completes when the calculated pressure caused by combustion has settled to certain range of standard error.

Although the last method seemed most accurate in their test, doubt still remained because of seeing different EOC points and burn rate profile were produced by each method, they alternatively suggested that for the burn rate calculation the whole procedure can be continued until exhaust valve opens (EVO).

Homsy and Atreya [54] used the same idea, they chose from the start of injection to EVO as a whole heat released process, thus the 5% and 95% of the cumulated heat released stand as

start of combustion (SOC) and EOC respectively. The basic idea of this method bases on no combustion pressure being produced after EOC, therefore even if the calculation continues to the EVO, it will not affect the cumulated heat released result at all.

Reddy and co-workers [35] did not adopt the polytropic index to find EOC, instead they used the differentiated pressure signal versus time as a tool to locate it. The diagram of second derivative pressure data vs. time is more precise, and less personal judgement needed when determining the combustion condition/performance in a diesel engine.

2.2.6. Raw Data Smoothing

This is a controversial issue, different circumstances and operating conditions will require different considerations. Collecting pressure data from an engine through a piezoelectric transducer will suffer noise pick-up from many interference sources. The cables used to transmit signals are suggested to be well shielded and as short as possible. However, unavoidable vibration can still cause noise.

A signal conditioner containing filters can reject unwanted noise within a certain frequency range. Approximately all DAQ applications are subject to some level of 50 or 60 Hz noise picked up from power lines or machinery. Therefore, most conditioners also include a low-pass filter designed specifically to provide maximum rejection of 50 to 60 Hz noise.

For the purpose of reducing noise level, Brunt and Lucas [50] applied a nine point weighted function to smooth unwanted signals, this mechanism can be presented by this eqaution:

$$P_s(\theta) = \frac{\left[\begin{array}{l} -21P(\theta-4\Delta\theta)+14P(\theta-3\Delta\theta)+39P(\theta-2\Delta\theta)+54P(\theta-\Delta\theta)+59P(\theta) \\ +54P(\theta+\Delta\theta)+39P(\theta+2\Delta\theta)+14P(\theta+3\Delta\theta)-21P(\theta+4\Delta\theta) \end{array}\right]}{231}$$

Eq. 2-4

where

P_s = the smoothed cylinder pressure

P = the unsmoothed cylinder pressure

θ = crank angle

$\Delta\theta$ = the resolution of CA

To level the pressure signals after averaged by 80 cycles, Homsy and Atreya [54] used the same method mentioned as “lightly smoothed” in their papers.

A similar method but with different equation was used by both Checkel [8] and May [10] called “low pass filter”:

$$F(\theta) = \frac{\left\{\begin{array}{l} 2*\left[P(\theta-4)+P(\theta+4)\right]+3*\left[P(\theta-3)+P(\theta+3)\right] \\ +4*\left[P(\theta-2)+P(\theta+2)\right]+5*\left[P(\theta-1)+P(\theta)+P(\theta+1)\right] \end{array}\right\}}{133}$$

Eq. 2-5

where

F = the filtered pressure data

P = the unfiltered pressure data

θ = crank angle

It can eliminate those insignificant and minor trends from the second derivative pressure data and separate the high frequency fluctuations from the original pressure signals too.

Rauckis and McLean [55] mentioned that they averaged their pressure signals then accomplished a seven point least squares best fitting cubic with point-by-point smoothing to derive better accuracy of results.

Grimm and Johnson [56] presented another three methods to smooth the raw pressure data:

(1) linear least squares method of the form:

$y = c_1 + c_2 x$

(2) quadratic least squares method of the form:

$y = c_1 + c_2 x^2$

(3) third order least squares with seven points method of the form:

$$y(\theta) = \frac{\left\{\begin{array}{l} -2*\left[x(\theta-3)+x(\theta+3)\right]+3*\left[x(\theta-2)+x(\theta+2)\right] \\ +6*\left[x(\theta-1)+x(\theta+1)\right]+7x(\theta) \end{array}\right\}}{21} \qquad \text{Eq. 2-6}$$

different forms are needed for the first and last three pressure data.

They suggested using the third method because it provided a smooth differentiation and the most consistent heat-release rate result in all cases they discussed.

Apparently, averaging the cyclic data can also smooth the random noise, Morishita and Kushiyama [45] suggested three main average methods:

(1) arithmetical mean

(2) least squares

(3) the quadratic curve fitting

The effects of choosing these three different methods were examined at different crank angle positions, and the arithmetical mean method was then excluded from their further discussions because of the fluctuation tendency, although it is very common to be used by many researchers.

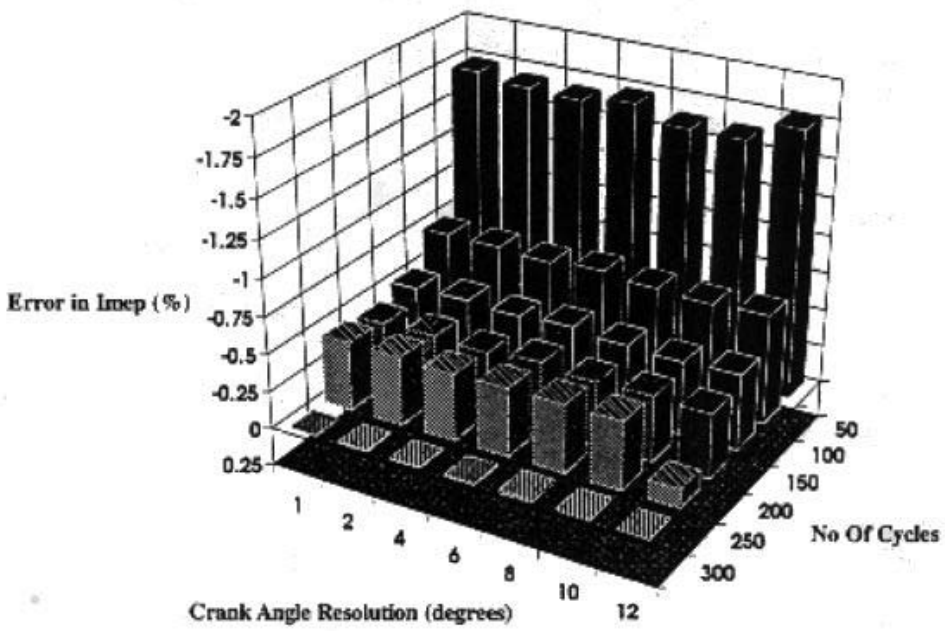

Figure 2-2 Effect of crank angle resolution and number of cycles on mean IMEP error in low load low speed [41].

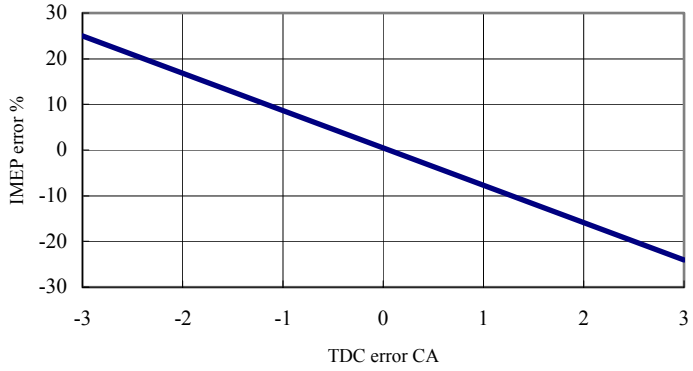

Figure 2-3 IMEP error as a function of a TDC error [57].

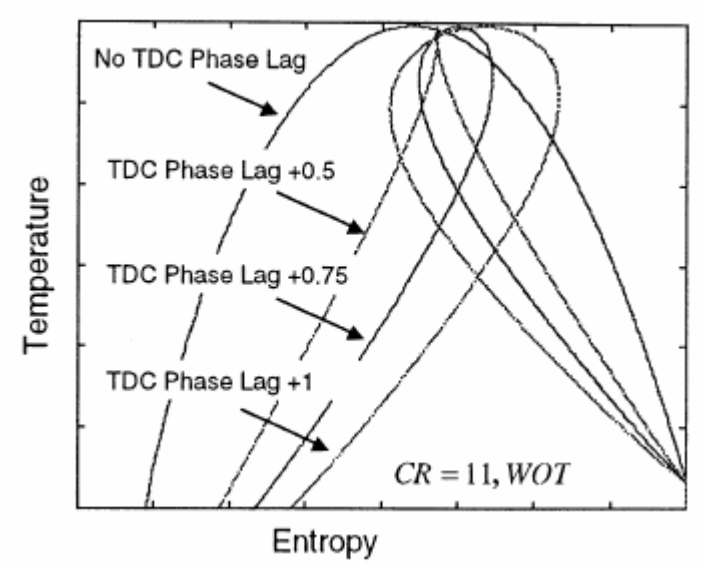

Figure 2-4 T-S diagram with different TDC phase lags [46].

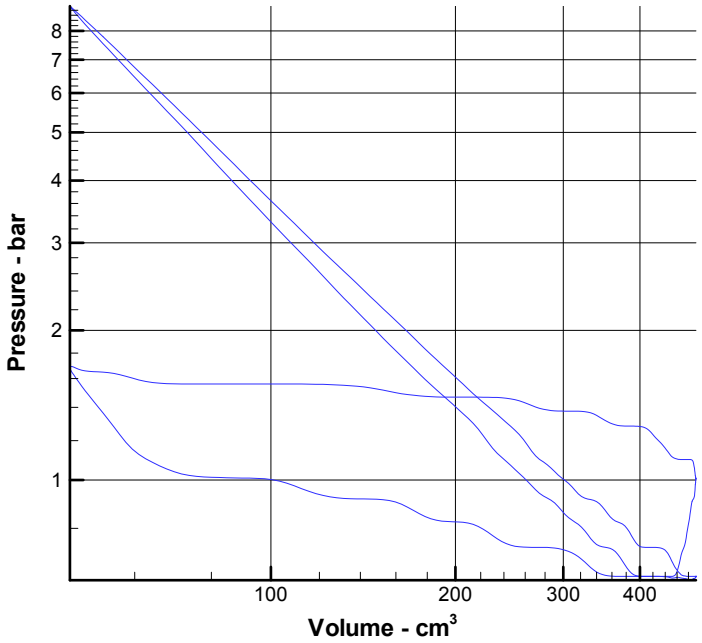

Figure 2-5 log P – log V diagram with properly phased TDC at motoring condition.

2.3. Generating Information from Acquired Data

2.3.1. Indicated Mean Effective Pressure (Gross and Net IMEP)

To obtain this characteristic value of an engine, the measured work output needs to be divided by displaced volume in cycle base. There is no universal characterization with this engine performance parameter for four strokes engines. Two widely used definitions are well known by researchers as gross and net IMEP. Their difference is whether pumping mean effective pressure (PMEP) is incorporated, and the relation can be expressed by the following equation:

$$IMEP_g = IMEP_n + PMEP \qquad \text{Eq. 2-7}$$

the subscript *g* and *n* mean gross and net respectively.

Stone [58] used net IMEP as a characteristic of engine type, Heywood [11] preferred to use gross IMEP and believed it was more proper to specify the impact of compression, combustion and expansion processes on engine performance.

There are several approximate integration ways to compute IMEP, Brunt and Emitage [41] proposed five altered equations for gross IMEP and compare their differences. Only small variations in result were detected and no remarkable effects were found, they recommended using the consumption of computation time to judge the priority. In their discussion the following equation needs the minimum processing effort:

$$IMEP = \frac{\Delta\theta}{V_s} \sum_{i=\theta_0}^{\theta_n} p(i) \frac{dV(i)}{d\theta} \quad \text{Eq. 2-8}$$

where

$p(i)$ = cylinder pressure at crank angle position i (Pa)

$V(i)$ = cylinder volume at crank angle position i (m^3)

V_s = cylinder swept volume (m^3)

θ_0 = BDC induction integer crank angle position (CA deg.)

θ_n = BDC exhaust integer crank angle position -1 (CA deg.)

Calculation methods for cylinder volume and volume change rate can both be easily found from many engine textbooks [11, 58, 59].

2.3.1.1. Coefficient of Variation of IMEP (COV_{IMEP})

Standard deviation is usually normalized with an averaged value to give a coefficient of variation (COV), which can be used to reveal the cyclic variability of engine. When studying the cycle-by-cycle variations in spark ignition engine, Stone [60] chose COV_{IMEP} as a comparison parameter because it is the most relevant to the engine output. Cartwright and Fleck [38] elucidated the definition of COV:

$$COV = \frac{s}{\overline{p}} \times 100\% \quad \text{Eq. 2-9}$$

s – is the standard deviation and can be calculated by:

$$s = \sqrt{\frac{\sum (p - \bar{p})^2}{x - 1}} \qquad \text{Eq. 2-10}$$

where

x = number of samples

$\bar{p}$ = average value of relevant parameter p

Five different pressure-related identifier, i.e. P_{max}, θp_{max}, IMEP, $(dp/d\theta)_{\max}$ and $\theta(dp/d\theta)_{max}$ were discussed by Ozdor and co-workers [61], they used derived COV values to compare the sensitivity in different operating condition. According to the normalized condition, the variations of IMEP are usually essentially less than the variations of P_{max}. However, COV_{IMEP} is still an important indicator of engine performance, Johansson [62] emphasized that it is a good parameter to be used for a transmission design and a general indicator of engine behaviour. Previous study has suggested less than 10% of value is acceptable and will not cause drivability problems [11].

2.3.2. Mass Fraction Burned Calculation

An engine combustion model was presented in 1938 by Rasseweiler and Withrow [14], which simply just used engine pressure in terms of volume history data to apply to their calculation. Until now, it is still widely adopted by many engine researchers. After comparing with other

complex models, e.g. two-zone combustion model, the first law thermodynamic model, etc, researchers [7, 47, 52, 53] concluded that even very complicated models will not produce more accurate results than R&W's method.

Mass Fraction Burned (MFB), determined from the analysis of measured cylinder pressure, is an evaluation of the fraction of the energy released from the fuel combustion to the total energy produced at the end of the combustion process. Firing cylinder pressure consists of two main sources, one is caused by the combustion, the other one is from the piston movement, and Figure 2-6 shows the relationship. The pressure produced from combustion is functional to the mass burned of the charge. In the motoring condition, polytropic processes are observed during the compression and expansion strokes. Therefore, by observing the polytropic processes during compression and expansion strokes (except the combustion period) when engine is firing, one can easily estimate the pressure produced by piston movements; consequently, the pressure formed by combustion can be deduced from subtraction. Adding up all the derived pressure value and divide it into each value to derive the fraction, which is correspondent to the percentage of mass fraction burned, the value should be unity at the end of combustion.

Many researchers [38, 47, 52] used the following form of R&W's model and have produced very good results.

$$\Delta P_{cn} = \left[P_{i+1} - P_i \left(\frac{V_i}{V_{i+1}} \right)^n \right] \frac{V_i}{V_r} \qquad \text{Eq. 2-11}$$

$$x = \frac{mb_i}{mb_e} = \frac{\sum_s^i \Delta P_{cn}}{\sum_s^e \Delta P_{cn}} \qquad \text{Eq. 2-12}$$

where

ΔP_{cn} = the normalized pressure rise due to combustion

V = Volume

P = Pressure

n = polytropic index

V_r = the referenced volume

mb = accumulated mass burned from start to crank angle θ_i.

x = mass fraction burned

θ_i is the crank angle position, s indicates the start of ignition or injection, e means EOC.

There is only one single polytropic index needed in the calculation, EOC is derived by guessing at the beginning of the calculation and is then checked for accuracy with the results. The original method used the volume at the start of ignition or end of combustion as a reference volume to normalize the percentage of mass burned. Shayler and co-workers [52] pointed out several uncertainties from those assumptions made in this method, they suggested not using the start of ignition or end of combustion volumes as a reference datum, but choosing TDC volume instead to enlarge the pressure scale for easier calculation.

At least three other derivation methods of using polytropic index can be found in the

application of R&W's models. The first one uses an average value of expansion and compression indices during the whole combustion process [7]. The second one chose compression index in calculation until user-defined point (TDC, normally) then switch to expansion index for the rest of calculation [38, 52, 63]. The third one applied compression index value throughout the whole combustion process [32, 49], Ball and co-workers [53] said when the expansion index is lower than the compression index, if the compression index is still used throughout the whole combustion process in R&W's model, it will underestimate the burn rate during the later stages of combustion.

The ratios of mass fraction burned have been used as indicators for different combustion phenomena, which can be classified in Table 2-2. Another commonly used definition, which is similar to the combustion duration, is the "main combustion duration". Instead of using ignition or injection as a start point, the position right after ignition delay is referred to, the intention being to focus on the rapid burning period. To locate the peak pressure at a specific crank angle is important in order to obtain maximum engine efficiency, and the optimum position is approximately at 15° or 16° ATDC [11, 24], which can be approached by maintain 50% MFB at 10° ATDC. (where maximum thermal efficiency or MBT generally occurs).

MFB can be correlated with other parameters to investigate engine combustion, Ishii and co-workers [64] examined the cycle-by-cycle variations of IMEP in a lean burn spark ignition

engine, they pointed out three reasons that caused this phenomenon and the variation of total mass fraction burned is one of them. Figure 2-7 clearly shows when 5% mass fraction burned (θ_{xb5}) increased, the normalized IMEP (which is IMEP value divided by Max. IMEP value in the sampled cycles) will decrease. This result indicated the longer ignition delay of combustion should take the responsibility of lower efficiency.

2.3.3. Heat Release Rate

During the firing process, as crank angle changes, the main effects with the cylinder pressure are the variation of cylinder volume, combustion of charge, heat transfer to the wall and gas blow by through the crevices. Considering the heat release rate of engine combustion, the R&W's model, in which the heat transfer and mass variation are ignored, this method will be more complicated but accurate. To describe the combustion condition inside the engine cylinder, an open system based on the first law of thermodynamics was provided by Cheung and Heywood [37]:

$$\delta Q_{ch} = dU_s + \delta W + \sum h_i dm_i + \delta Q_{ht} \qquad \text{Eq. 2-13}$$

This equation includes the internal energy change of the intake charge, the output work done by the engine, the crevices blow by effect and heat transfer to the wall as the result of

chemistry equilibrium with mixture charge burned.

For better understanding of whether an engine is under optimum design or operating condition, Austen and Lyn [65] tried to characterize the ideal shape of the heat release diagram, which could be used to provide the best compromise between peak pressure, cycle efficiency and rate of pressure rise (noise). Their attempt shed the light on using heat release data to correlate with engine performance, if the operation conditions can be specified precisely, the basic engine working theory: the conversion of the chemical energy of a fuel into mechanical work, might be tractable simply by checking the pressure-volume diagram.

The first method for calculating apparent heat release from engine cylinder was introduced by Krieger and Borman [66], they deduced the internal energy and gas constant values of olefin series fuel (C_nH_{2n}) from temperature, pressure and equivalence ratio data. A few assumptions were made in their study, i.e. the engine cylinder is in thermodynamic equilibrium, no dissociation occurs and the cylinder chamber is divided into burned and unburned portions by an infinitesimally thin flame front during combustion.

To investigate the combustion condition, heat release rate is more precise and practical than R&W's model, because it takes account of the heat transfer effects. The simplicity might be remained and no detailed knowledge of the combustion is necessary. Unfortunately, high accuracy of the pressure data is required for this method, normally a 0.25° crank angle

resolution will be considered as adequacy [67].

Krieger and Borman's method [66] is widely mentioned in many heat-released models, it can be classified as a two zones model or zero-dimensional thermodynamic model because no spatial parameter is used. Opposite to the two zones model there is one zone model, which intends to be simpler but still maintain the accuracy. For example, the following equation presented originally by Gatowski and co-workers [36], based on the first thermodynamics law, considers all sorts of the related effects on the heat release rate:

$$\frac{dQ_{ch}}{d\theta}=\frac{\gamma}{\gamma-1}p\frac{dV}{d\theta}+\frac{1}{\gamma-1}V\frac{dp}{d\theta}+V_{cr}\left[\frac{T'}{T_w}+\frac{T}{T_w(\gamma-1)}+\frac{1}{bT_w}\ln\left(\frac{\gamma-1}{\gamma'-1}\right)\right]\frac{dp}{d\theta}+\frac{dQ_{ht}}{d\theta} \quad \text{Eq. 2-14}$$

where

Q_{ch} = combustion energy release,

V_{cr} = crevice volume,

T' = cylinder gas temperature when flow is into the crevice, and crevice gas temperature when flow is out of the crevice,

T_w = wall temperature,

γ = ratio of specific heats for cylinder gas,

γ' = ratio of specific heats for crevice gas,

Q_{ht} = heat transfer to the combustion chamber walls.

They adopted thermodynamic properties by using the linear relation with temperature for the ratio of specific heats (γ) into their calculation.

$$\gamma(T) = a + bT \qquad \text{Eq. 2-15}$$

This relationship is well known but the values of *a* and *b* varied by different operating condition and fuel type, the range of *a* is within 1.33 ~ 1.4, and *b* varied between $6x10^{-5}$ and $8.5x10^{-5}$ [36, 37, 59, 63]. Heat transfer calculation was based on the form proposed by Woschni [68], other definition [69-73] for engine heat transfer can also be considered in this form, and basically the differences are the use of Reynolds and Nusselt numbers.

2.3.4. Emissions Prediction

Since the pressure data can represent the combustion condition inside cylinder, it is reasonable to assume that through some correlation we should be able to find out the emission behaviours, because both emissions and fuel consumption are explicitly dependent on combustion process.

May and Gyorog [10] tried to use three different approaches: the closed loop methodology, the first derivative and the second derivative of pressure data to achieve the object of using one single value to predict exhaust emissions. Their results did show some interesting topics for future development, especial in CO and NO. They said the carbon monoxide could be related with the integral of the second derivative of the pressure data by a logarithmic function of the form:

$$y = A + B\ln(x)$$ Eq. 2-16

and the nitric oxide can be represented with the integral of the second derivative of the pressure data by an exponential function of the form:

$$y = Ae^{Bx}$$ Eq. 2-17

In their calculation, only the pressure data between ignition and the maximum peak of the first derivative were chosen, and the most suitable integral curve for predicting the emission behaviours is the second derivative of pressure data.

2.3.5. Studies of Combustion Behaviour

The derivative of pressure data in terms of time can not only be used to predict the engine pollutant, but can also be found from some investigations on abnormal combustion behaviours. Studying a direct injection diesel engine, Reddy and co-workers [35] characterized ignition delay and combustion duration by just using diagram of the second derivative of pressure data. At about the same time, Patro [74] used similar method and confirmed it is also suitable for hydrogen enriched diesel engine observation.

The third derivative pressure data are well used for detecting knock in engines. Checkl and Dale [8] said a large negative value of the third differential of pressure data indicates the

abrupt pressure rise and narrow pressure peak commonly associated with gas auto-ignition. Rosseel and Sierens [9] used the same mechanism in a hydrogen engine to detect the knock at the end of combustion, because of the fast flame speed, they said that introducing a knock index to retain the accuracy, minimized period of detection and remove the necessity for high crank angle resolution were all necessary.

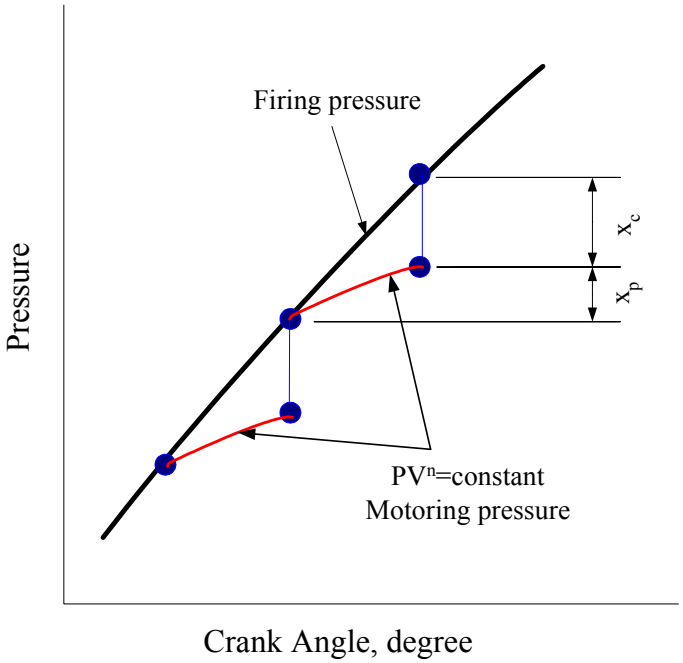

Figure 2-6 The pressure inside cylinder during combustion can be divided to two sources: combustion (x_c) and piston movement (x_p).

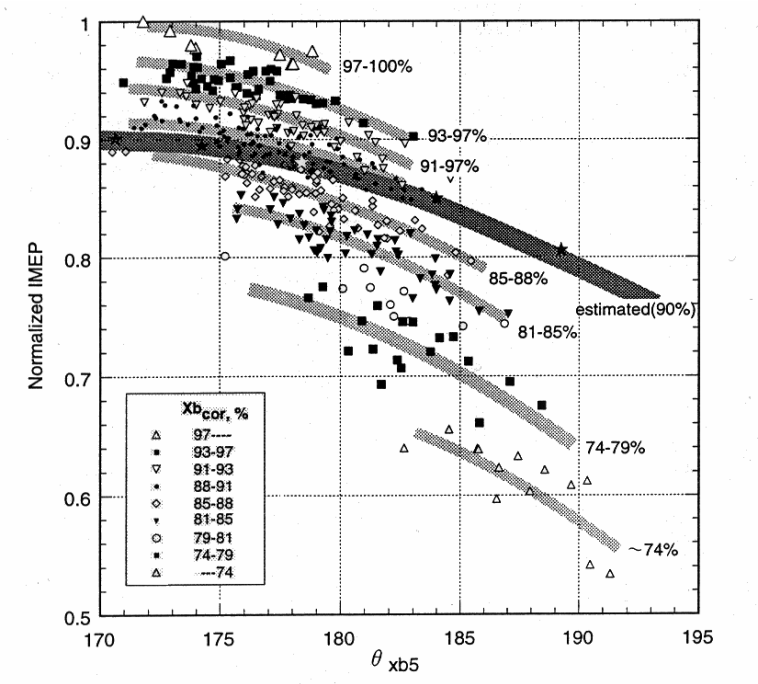

Figure 2-7 Cyclic variations of normalized IMEP with θ_{xb5} and Xb_{cor}. [64].

Term	Description	Definition
Ignition delay	the detectable pressure rise after ignition or injection	2%, 5%, 10%
Maximum thermal efficiency	half of the MFB, believed to have the maximum thermal efficiency if it is located at 10° CA ATDC	50%
Combustion duration	from the ignition or injection to a defined point as a whole combustion period	0 ~ 90%, 0 ~ 95%

Table 2-2 The definitions of percentages of mass fraction burned.

2.4. Natural Gas as an Alternative Fuel for SI Engine

Since the oil crisis of the 1970s, a lot of efforts have been made to find some alternative fuels which can replace petroleum and diesel as a main fuel for automobiles. Therefore, many alternative fuels have been investigated by researchers [75-77], a wide range of fuels which could not be derived from non-crude oil resources were reviewed to substitute the vehicular fuels such as gasoline and diesel. Natural gas becomes a candidate mainly because of the low emissions ability and abundance in the world.

In reality, not many alternative fuels have been commercialised on a large scale. One of the problems is the infrastructure system of supplying and refuelling, the other one is the cost. Compared with traditional fossil fuels, these two aspects are hard to be equal with alternative fuels. Natural gas and electricity could be, but few of them have production facilities and distribution networks available in most advanced countries. Nevertheless, it would still be necessary to build up extra refuelling stations and increase the distribution capacity for vehicular use.

To convert a petrol engine into a gas fuelled one, changing the fuel distribution system is the only thing has to do apart from fitting a suitable natural gas fuel tank. By simply using a gas carburettor, a natural gas fuelled sparking ignition engine can be easily obtained.

The main constituent of natural gas is methane (CH_4) generally within 80% to 95% by volume,

Table 2-3 shows typical components of natural gas by volume and mass percentage. Unburned methane is the main pollutant from the natural gas fuelled engine, it is less reactive than the unburned hydrocarbon emissions produced from traditional liquid fuel and will not cause too serious smog problem. However, NG fuelled vehicles still suffer from NO_x emission, (mainly is NO), and have to be overcome to cope with the growing rigorous environmental legislation. Natural gas has a high octane rating, which make it possible to use it in high compression ratio engines and increase the thermal efficiency, the warm-up efficiency can also be improved. It will not mix nor dilute the lubricating oil and does not cause deposits on spark plugs and in the combustion chamber, consequently, it extends the life of spark plug and piston ring. However, although the low-density characteristic can be used in high pressure compressed storage, compared with gasoline, vehicles fuelled by natural gas still suffer the problem of a short driving range. The lower volume calorific value and less volumetric efficiency will make the performances even worse. Table 2-4 show the properties of three different fuels.

To compensate the drawbacks of using natural gas in converted spark ignition engine, special modifications to the engine are needed, Kato [78] in Toyota transferred a 2.2 litre gasoline engine to a dedicated CNG engine, results show better power output because of utilizing a higher compression ratio, but still not enough to reach the original gasoline engine

performance. Use of additives to natural gas could be another way to improve its combustion performance. Swain and co-workers [79] used 20% hydrogen (by volume) to replace the charge fuel and successfully decreased both the ignition delay and combustion duration periods in a methane engine. It shows the potential for improving the combustion performance, therefore further investigation on the effects of adding additives to a natural gas fuelled SI engine is necessary.

Component	Volume percent (%)	Mass Percent (%)
Methane	92.29	84.37
Ethane	3.60	6.23
Propane	0.80	2.06
Butanes	0.29	0.99
Pentanes	0.13	0.53
Hexanes	0.08	0.39
Carbon dioxide	1.00	2.52
Nitrogen	1.80	2.89
Water	0.01	0.01
Total	100	100

Table 2-3 Typical composition of natural gas [80].

(A)

Thermodynamic Property	Hydrogen	Methane	Gasoline
Molecular weight (kg/kmole)	2.016	16.043	107.0
Density of gas at NTP (g m^{-3})	83.764	651.19	4400
Heat of combustion (low) (kJ g^{-1})	119.93	50.02	44.5
Heat of combustion (high) (kJ g^{-1})	141.86	55.53	48
Specific heat (c_p) of NTP gas (J g^{-1} K^{-1})	14.89	2.22	1.62
Viscosity of NTP gas (g cm^{-1} s^{-1})	0.0000875	0.000110	0.000052
Specific heat ratio (γ) of NTP gas	1.383	1.308	1.05
Gas constant (R) (cm^2 atm g^{-1} K^{-1})	40.7030	5.11477	0.77
Diffusion coefficient in NTP‡ air (cm^2 s^{-1})	0.61	0.16	0.005

(B)

Combustion Property	Hydrogen	Methane	Gasoline
Limits of flammability in air (vol %)	4.0-75.0	5.3-15.0	1.0-7.6
Stoichiometric composition in air (vol %)	29.53	9.48	1.76
Minimum energy for ignition in air (MJ)	0.02	0.29	0.24
Autoignition temperature (°K)	858	813	501-744
Flame temperature in air (°K)	2318	2148	2470
Burning velocity in NTP‡ air (cm s^{-1})	265-325	37-45	37-43
Quenching gap in NTP‡ air (cm)	0.064	0.203	0.2
Percentage of thermal energy radiated from flame to surrounding (%)	17-25	23-32	30-42
Diffusivity in air (cm^2 s^{-1})	0.63	0.2	0.08
Normalized flame emissivity (2000K, 1atm)	1.00	1.7	1.7
Limits of flammability (equivalence ratio)	0.1-7.1	0.53-1.7	0.7-3.8

‡ NTP: Standard Temperature and Pressure (25°C and 1 bar)

Table 2-4 (A) Thermodynamic and (B) combustion properties of hydrogen, methane and gasoline [81].

2.5. Effects of EGR and Hydrogen as Additives on Engine Combustion

2.5.1. Exhaust Gas Recirculation (EGR)

EGR has been considered as a strategy to achieve extremely low nitric oxide and carbon monoxide. Adding EGR is also an alternative method to dilute the premixed air-fuel charge. Comparing the effects on emission results with lean burn, it shows lower NO_x, better HC control and more stable combustion [82]. However, the flame speed will be decreased and combustion duration will be delayed consequently resulting in low thermal efficiency. Another disadvantage of using EGR is the effect of higher cycle-by-cycle variations, which causes drivability problem and limits its use.

With three-way catalyst as an emission after treatment measure, it is necessary to run the engine under stoichiometric conditions. The main problem accompanied with stoichiometric combustion is knocking, the engine needs to keep the inlet manifold pressure low and maintain the same compression ratio to prevent knocking, and thereby high fuel consumption and low BMEP result. EGR can improve the anti-knock characteristics for an engine, when EGR mixes with combustion air the inert components like CO_2 and N_2 will lengthen the combustion reaction, reduce the flame speed and decrease the temperature of the end gas. Considering the lowest C/H ratio of hydrocarbon fuel, natural gas will produce the largest

water content in the exhaust gas, Sakonji and Shoji [83] recommended using dry EGR to improve the maximum mean effective pressure and fuel consumption.

Heywood [11] said the amount of EGR an engine can tolerate is dependent on its combustion characteristics, the speed and load, and the equivalence ratio. From 15 to 30 percentage of EGR will be the maximum amount for a spark-ignition engine under normal part-throttle condition.

2.5.2. Hydrogen (H_2)

Hydrogen has been considered as the future fuel for a long time, it is possible to generate hydrogen from non-fossil sources, so it is a potential fuel to escape from the crisis of oil exhaustion. In addition, the heat of combustion (the amount of heat that a standard amount of substance releases on combustion) of hydrogen is two to three times higher than other fuels. Hydrogen has a wide extent of flammability from 4% to 75%, which means the lean-burn limit of combustion inside engines can be extended by adding hydrogen as a supplement. The flame speed of natural gas is lower than the traditional fuels, consequently it is necessary to increase the rate of combustion to retain thermal efficiency such as keeping 50% mass fraction burned at 10° CA ATDC, and adding hydrogen can just fulfil the requirement. Hydrogen as an additive can efficiently increase the burning velocity of the charge [55, 84].

Although Swain and co-workers [79] acquired very good combustion improvements by adding 20% hydrogen in volume to natural gas fuel, most of the research was concentrated on small amount of hydrogen addition due to the difficulty of mass storage.

To cross this storage barrier, Stocky and co-workers [85] proposed an on-board hydrogen generator by a partial oxidation reaction to supply a hydrogen rich gas, by such mechanism a 25% improvement of fuel economy and NO_x reduction were achieved. Shrestha and Karim [86] applied small amount of hydrogen to a methane fuelled spark ignition engine, they suggested optimum concentration of hydrogen in the fuel mixture for producing a power gain and avoiding knock is about 20-25% by volume. They also tried the on-board hydrogen producing technology by applying engine-produced energy to electrolyse water, but did not succeed because of the inefficiency.

2.5.3. Trade-off Effects of EGR and H_2

According to previous discussions, the benefits and disadvantages of adding hydrogen and EGR are clear. Nevertheless, it is interesting to consider the condition when they are added together, which is similar with the condition under the on-board exhaust gas fuel reforming. This technology has often been well studied at the University of Birmingham [87-91], hydrogen is produced after reforming then applied back to the inlet manifold with exhaust gas,

therefore, a hydrogen enriched fuelling condition can be formed.

Wyszynski and Wanger [92] proved that up to 32% of hydrogen in volume could be produced from exhaust reforming method. Theoretically, up to 75% of hydrogen can be obtained from the product gas by a similar technology of mini-reactor [92]. The results shed light on on-board hydrogen generation, and also solve the inherent storage problem, the latter was always thought of as a big obstruction of hydrogen-related engine development.

Since hydrogen can extend the lean-burn limit of combustion inside engines, the amount of EGR possible into an engine will increase considerably, besides compensating for the instability by fast flame speed. Das and Mathur [81] discussed the conditions when EGR applied to hydrogen-supplemented multi-cylinder spark ignition engine, NO_x level has been observed to decrease dramatically, and this effect of a certain quantity of EGR is clearly reflected with various levels of hydrogen substitution. Smith and Bartley [93] ran a natural gas fuelled SI engine with EGR under stoichiometric operation, an in-house mixture gas (29.7% H_2 by volume) was applied to the engine, 44.4% mass based rise of EGR tolerance and 77% reduction in raw NO_x were reported. In certain EGR fraction, the ignition delay and 10 to 90 percent mass fraction burned duration decreased relative to the increased of the mixture gas ratio. This work encourages the study of exhaust gas fuel reforming method in NG fuelled SI engine, which has very similar content in the inlet charge.

3. IMPROVED METHODS OF CALCULATION OF THE MASS FRACTION BURNED RESULT

Previous investigations have generally shown the merits of the R&W model [14]. Consequently it has become the best choice for studying engine combustion performance when a real time analysis is necessary. Reaching better accuracy is imperative for data analysis and can save experimental time and lower running cost indirectly. Therefore, efforts have focused on how to clarify the nebulous definitions from the R&W's original assumptions, using better data processing method and a more precise correlation between pressure and volume data. An in-house program based on the graphical software LabVIEW has been developed to fulfil these requirements, and the detail of each improved approach will be explained with the relevant part in the program.

3.1. Deduction from the Classic Mass Fraction Burned Method

3.1.1. R&W's Model

In the literature survey, a common form (Eq. 2-12) original from R&W's model has been outlined, nevertheless it is just a simplified model under the assumption of equivalence of

compression and expansion indices, the selections of polytropic index value and the end of combustion position are varied by different researchers, consequently the results may conclude in very different direction. According to the presumption in this model, the cylinder pressure is constituted by two sources, combustion and piston movement. The polytropic behaviour of compression and expansion strokes under "firing compression" condition (ignition suspended right after normal firing condition) can be used to deduce the pressure caused by piston movement, subsequently the combustion pressure can be known. If the amount of non-inflamed charge during the combustion is of interest, information about the burned charge can be known firstly through correlations between combustion pressure and burned charge mass, and then the unburned charge. Alternative measure uses a polytropic process observed right after EOC to explain the burned charge behaviour during combustion and subsequently obtain the fraction of inflamed charge.

Two contrasting assumptions were then made to confirm if the mass burned in the varied volume can be correlated with observed pressure. Table 3-1 illustrates all the parameters used in the R&W's deduction, and they will remain the same in the following content.

Assumption 1

Under firing condition, non-inflamed charge keeps the same polytropic behaviour (polytropic index n') as during the firing compression condition throughout the whole

combustion period, and the charge density is uniform at the moment of ignition thus volume is proportional to the mass. Therefore, the mass fraction of in-flamed charge at a certain crank angle during combustion can be obtained by this equation:

$$\text{MFB}=1-\left(\frac{\mathrm{V_t}-V_t''}{V_{ti}}\right)\left(\frac{P_t}{P_{ti}}\right)^{\frac{1}{n'}} \qquad \text{Eq. 3-1}$$

Assumption 2

The behaviour of burned charge during the whole combustion period can be represented by the polytropic trend observed during the early part of expansion stroke in the firing condition (ploytropic index n'') and the density is uniform at EOC, therefore the mass fraction of burned charge can be gained by this equation:

$$\text{MFB}=\frac{V_t''}{V_{tf}}\left(\frac{P_t}{P_{tf}}\right)^{\frac{1}{n''}} \qquad \text{Eq. 3-2}$$

The equations derived from the above need either the volume percentage of unburned or burned charges observed from motion pictures, both of which are not available in this study. Fortunately, a further assumption made by them just eliminates all those motion pictures related terms and makes this method very simple. These two approaches have reached similar results to confirm the assumption of polytropic behaviour, and because the difference between two polytropic indices is within 0.06 (1.36 and 1.30), it is acceptable to presume n' and n'' are the same as n for simplicity. By equating Eq. 3-1 and Eq. 3-2, the following equation can be

obtained:

$$\mathrm{MFB} = \frac{P_t^{\frac{1}{n}} V_t - P_{ti}^{\frac{1}{n}} V_{ti}}{P_{tf}^{\frac{1}{n}} V_{tf} - P_{ti}^{\frac{1}{n}} V_{ti}} \qquad \text{Eq. 3-3}$$

Both volumes at ignition and end of combustion are required in this equation. The ignition timing is decided before testing, so the volume can be known beforehand. Therefore, an approach to find the correct EOC is necessary for obtaining a more precise result.

Since the firing pressure is the accumulation of pressure caused by combustion and piston movement, it appears very straightforward if one can acquire a combustion pressure value by just simply subtracting the piston movement pressure from the pressure amount, because the pressure due to piston movement can be measured directly from a motoring engine. The reason why it is incorrect to do so is because even if one can collect the motoring pressure at the same speed as firing condition, the different operating circumstances between motoring (where the engine is driven by a motor normally under lower temperature and pressure) and firing (which apparently is much hotter and features high-pressure) conditions, consequently, the heat transfer and crevice blow-by problems are severe in the latter case. Rassweiler and Withrow interrupted the ignition promptly when engine was firing and recording the pressure traces to gain motoring pressure, which can be considered as the same condition as firing. Nevertheless, this method is not very convenient to use as promptly interrupting the engine ignition will cause many troubles to the modern engine control system.

3.1.2. The Novel r-R&W Model Proposed in this Thesis

When the gaseous fuel is used in an SI engine, the difference between two polytropic processes (compression and expansion) becomes bigger than the traditional hydrocarbon liquid fuels, Figure 3-1 shows the difference between natural gas and petrol fuel when used in K4 engine for this thesis, and consequently the assumption of constant polytropic index becomes improper. Under such circumstance, it is not adequate to keep using a constant polytropic index for the mass fraction burned calculation, no matter by which of the methods that have been mentioned above in Section 2.3.2. Ball and co-workers [53] considered the condition when two polytropic indices are different and presented a revised mathematic equation of R&W's model:

$$\mathrm{MFB} = \frac{P_t^{\frac{1}{n_e}}\left(V_t P_t^{\frac{1}{n_c}} - V_{tf} P_{tf}^{\frac{1}{n_c}}\right)}{V_{tf} P_{tf}^{\frac{1}{n_e}} P^{\frac{1}{n_c}} - V_{ti} P_{ti}^{\frac{1}{n_c}} P^{\frac{1}{n_e}}} \qquad \text{Eq. 3-4}$$

where

subscript *c* and *e* represent compression and expansion process respectively.

Two different polytropic indices are adopted in this equation, and the volume and pressure data at ignition and EOC are both needed as well. The difficulty of finding EOC has been mentioned in Section 2.2.5, icccf this point is chosen wrongly, three parameters will be

affected in the equation, i.e. P_{tf}, V_{tf} and n_e. However, this method uses two different polytropic indices in the calculation without compromise, which seems more suitable to apply to the gaseous fuelled engines. If the EOC point can be located carefully and subsequently acquire these two polytropic indices, the mass fraction burned profile and other relevant performance indicators will be able to present the combustion condition inside engine cylinder more accurately.

Time	At Ignition	During Combustion	At End of Combustion
Observed Pressure	P_{ti}	P_t	P_{tf}
Total Volume of Combustion Chamber	V_{ti}	V_t	V_{tf}
Volume of Non-inflamed Charge	V'_{ti}	V'_t	
Volume of Inflamed Charge	V''_{ti}	V''_t	V''_{tf}

Table 3-1 Definitions of Parameters in R&W's assumptions [14].

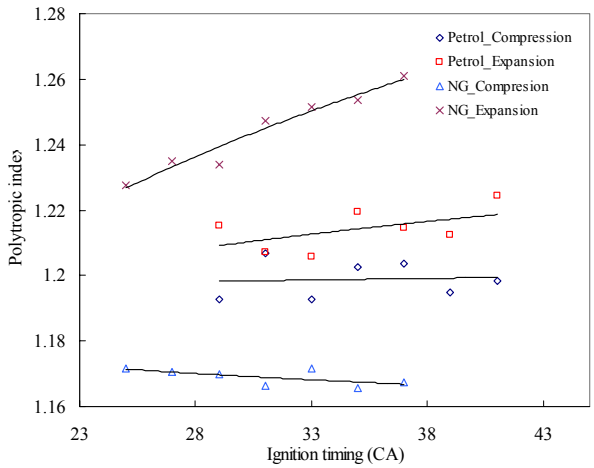

Figure 3-1 The comparison of Polytropic indices between petrol and natural gas fuel at 2000 rpm, 2 bar IMEP, produced from K4 engine for this thesis.

3.2. Method of Linear Changes of Polytropic Indices

An alternative method to continuing the use of the common R&W model when compression and expansion polytropic indices are very different, i.e. more than 0.1 in this study, is the introduction of a non-constant linear polytropic indices method. Since the compression polytropic index is based on unburned charge and the expansion polytropic index is based on burned mixture, the value of the polytropic index during the period between ignition timing and EOC position, it seems reasonable to assume that the polytropic index value $n(\theta_i)$ varies linearly from compression index (general 1.15) to expansion index (general 1.25) with increasing crank angle. The application is outlined below:

$$n(\theta_i) = n_c + (\theta_i - \theta_s) \times \left(\frac{n_e - n_c}{\theta_e - \theta_s} \right) \quad \text{Eq. 3-5}$$

$$\Delta P_c = P(\theta_{i+1}) - P(\theta_i) \left[\frac{V(\theta_i)}{V(\theta_{i+1})} \right]^{n(\theta_i)} \quad \text{Eq. 3-6}$$

$$\Delta P_c' = \Delta P_c \left[\frac{V(\theta_i)}{V_c} \right] \quad \text{Eq. 3-7}$$

$$x(\theta_i) = \sum_{\theta_s}^{\theta_i} \Delta P_c' \Big/ \sum_{\theta_s}^{\theta_e} \Delta P_c' \quad \text{Eq. 3-8}$$

n_c and n_e are obtained directly from the log P-log V diagram which are the slopes of polytropic processes in the compression and expansion processes respectively. Subscript *s* and *e* denote the start and end of combustion, θ_i is the crank angle during combustion. ΔP_c

is the pressure increment due to combustion in each crank angle interval. P, V are the measured pressure and volume at crank angle θ_i, V_c is the clearance volume.

The basic thinking behind this method is trying to smooth the variation of polytropic index during the combustion period. The commonly used polytropic index methods either underestimate or overestimate the result in the ignition delay or burn duration periods, therefore this blended method gradually simulates the performance of combustion from unburned charge behaviour toward the burned charge behaviour according to the progress of combustion (not practical). It might be able to improve the accuracy of results.

3.3. Finding the End of Combustion

Eq. 3-3 and Eq. 3-4 both reveal the necessity of an accurate EOC point. However, in R&W's method there is no detailed explanation of finding it, because the flame progress is monitored by motion pictures, hence such information was obtained entirely from observation. Therefore, the method of try and error is needed for locating the EOC point, at least for the initial position. The calculation result has to be examined following the initial supposition, which means a check on the last increment of pressure produced by combustion if it turns to zero or negative value. In real time analysis, this method might be not practical and the iterations of

calculation will occasionally take a very long time to reach convergence. Instead of blindly guessing the EOC, Reddy and co-worker [35] suggested using differential pressure data to decide the end of combustion for a diesel engine, which seems to be a good method to provide a proper starting point for approaching the correct EOC position. Nevertheless, the suggested criterion for determining its location does not seem to be suitable for the natural gas fuelled engine.

Eq. 3-4 does not calculate the pressure increment at each crank angle, so the method of examining the final pressure increment cannot be applied. However, the common R&W form Eq. 2-12 can be considered as a reference method to obtain the correct EOC and then provide the result to Eq. 3-4 for final calculation. Because the measured pressure traces, 100 cycles in most cases of this study, will be smoothed and then averaged into only one single cycle for further calculation the consideration of noise and interference can be ignored. Consequently, for those three methods for deciding EOC mentioned in Section 2.2.5, the first negative one is adopted on the basis of time saving. The in-house program uses one crank angle increment to approach the EOC, it starts with the initial value derived from the aforementioned differential method until the preset criterion, which is the first pressure increment equal to or less than zero has been met. Figure 3-2 shows the approaching traces in a normal engine operating condition arbitrarily selected from tests conducted for this thesis. From the left to the right, the

upper part of the MFB curve gradually becomes an asymptote toward unity, which means the EOC point has been progressively reached. A flow diagram of this method is presented in Figure 3-3.

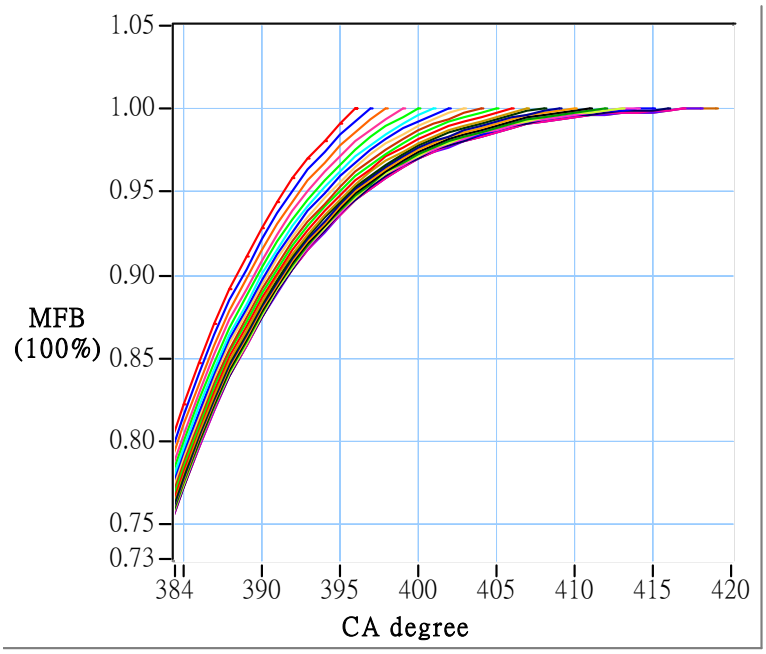

Figure 3-2 The upper part of mass fraction burned profile, the traces fro the left to the right gradually approach to the final EOC position with one crank angle degree increment.

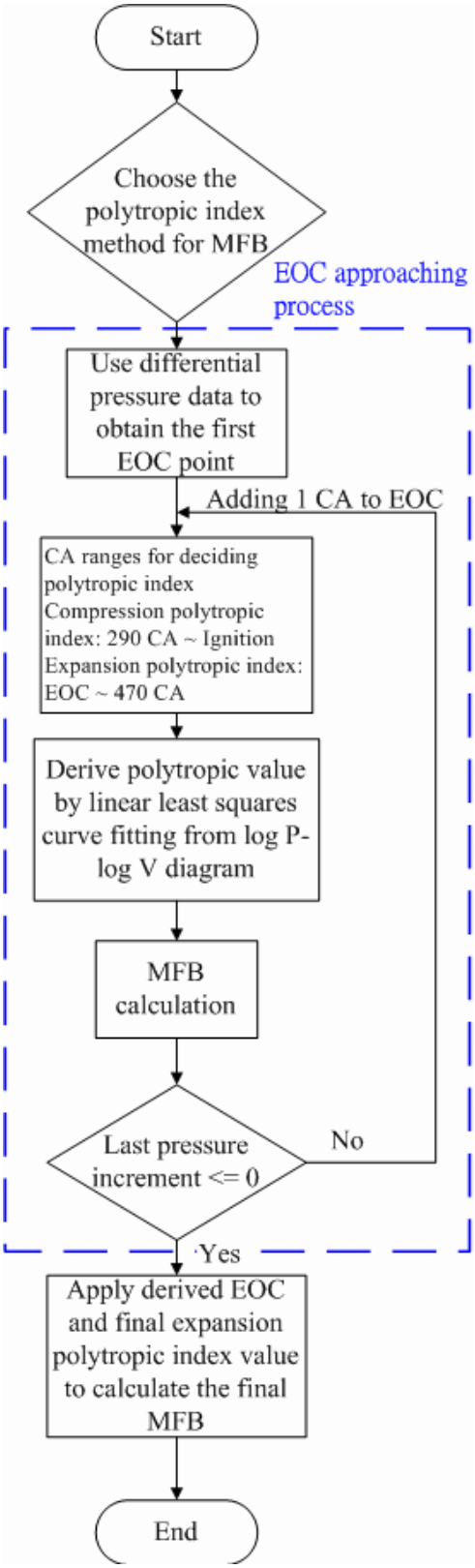

Figure 3-3 Flow diagram of the EOC approaching process.

3.4. Determination of the Polytropic Index

According to the discussion in the literature survey, there are many polytropic index methods that have been used by researchers to calculate the mass fraction burned. The program provides a selection knob for choosing between different polytropic index methods, five options are available to choose.

(1) Compression –use compression index for the whole combustion period

(2) Linear – the index value varies from compression index to expansion index linearly

(3) Averaged – use the averaged value of two indices for calculation

(4) Switching – compression index is used before TDC, then switches to expansion index for the remainder

(5) R&W method – both indices are used in calculation

Option 5 uses Eq. 3-4 and option 2 uses Eq. 3-5 ~ Eq. 3-8, the rest of methods use Eq. 2-12 to calculate the MFB.

The most right term $\left[V\left(\theta_i\right)/V\left(\theta_i+1\right)\right]^{n(\theta_i)}$ in Eq. 3-6 determines the pressure increment of each interval. When different polytropic index methods are applied on the same data, at the same crank angle, the larger the value of this term, the smaller the increment will be. Figure 3-4 presents the effects of different polytropic index values on the results. Except the compression index method, the effects are similar for the other three methods before TDC.

Differences begin from 5° CA ATDC, the value deduced by the linear index method varies from averaged to switching index method. This phenomenon can be explained by characteristic of the linear index method, which gradually increases the polytropic index from compression to expansion value (same value used after TDC with the switching index method).

It is known that under a polytropic process, a straight line should be found from a logarithmic P-V diagram, however, the pressure data collected from engine are discrete points between each resolution interval, a trend line needs to be found to represent the polytropic curve. Because of the variations of combustion and random noises, even after data smoothing and averaging, some points might still be apart from the trend line, hence it is necessary to use a curve fitting method to obtain the regression line and slope, e.g. polytropic index. Previous discussion has suggested that the linear least squares method is the most suitable strategy to use, therefore, a best fit mechanism is adopted in the program to obtain the regression line from those discrete data.

Since the slope is derived from the regression line, choosing the proper crank angle range becomes critical. Normally, from the intake valve close (IVC) to ignition and from the end of combustion to exhaust valve open (EVO) are both thought as appropriate periods of examining the polytropic processes [26]. However, owing to the engine running condition

continually varying, shorter periods will be considered as more suitable.

3.4.1. Compression and Expansion Polytropic Index

The intake valve of the K4 engine closes at 52° CA after bottom dead centre, therefore, 290° CA is chosen arbitrarily as a start point for calculating the compression polytropic index. From the start point to ignition, i.e. MBT timing (31° CA BTDC for 2000 rpm, 2 bar IMEP condition in this study), is about 40° CA, therefore it should be able to produce an adequate trend line to predict the polytropic behaviour during the compression stroke.

The exhaust valve open at 52° CA BBDC, hence the end of examining period for the expansion polytropic index is arbitrary set at 470° CA, about 20° CA before the valve opens. The start position is from the calculated end of combustion point by the aforementioned method. Owing to the temperature in the expansion stroke being higher than in the compression stroke, causing greater heat transfer, the expansion polytropic index value is normally larger than the compression value. Figure 3-5 shows how the program derives polytropic indices from those four relevant points. Through this method, consequently, the mass fraction burned calculation can now be conducted even more precisely.

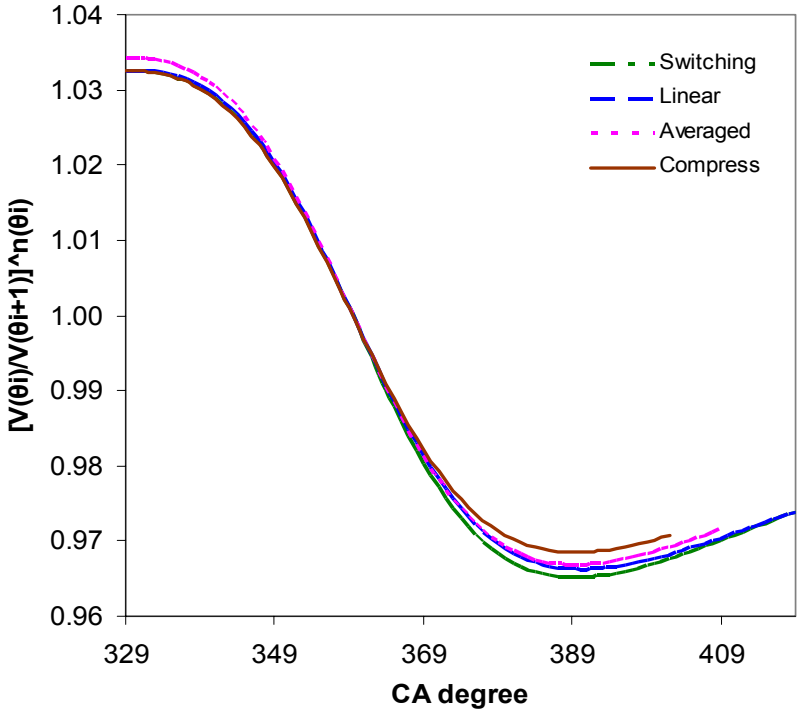

Figure 3-4 **Effects of different polytropic index methods on deciding the pressure increment of K4 engine**

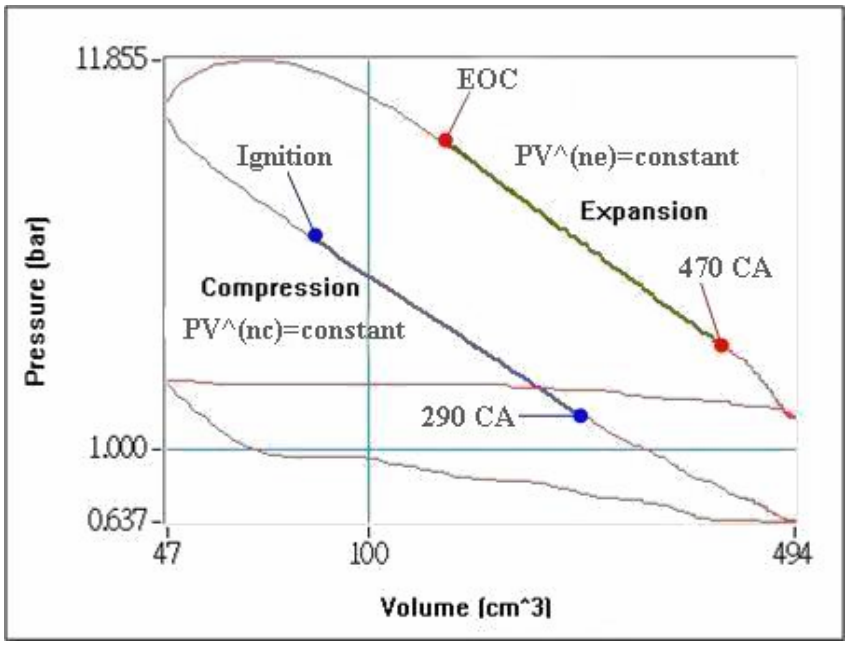

Figure 3-5 **log P – log V diagram in normal firing condition; the polytropic indices *nc* and *ne* in compression and expansion strokes respectively are derived by the best fit curve fitting.**

3.5. Ignition Delay and Burn Duration

3.5.1. Ignition Delay

Some researchers investigated the diverge point from the pressure trace and defined the period from the ignition to this diverge point as a delay period. In Heywood's book [11], ignition delay of spark ignition engine is called 'flame-development angle', it is the crank angle interval between the spark ignition and a small amount of fuel energy having been released, or a small but significant fraction of charge mass having been burned. For the mass fraction burned, from 1% ~ 5% and 10% have all at times been used to define the ignition delay, 5% is chosen arbitrarily in this study for convenience.

The ignition delay changes with equivalence ratio, spark timing and residual fraction. Sher and Hacohen [94] defined the aforementioned departure point by $d^2p/d\theta^2 = 0$ and said this point normally corresponds to 2% MFB for a gasoline SI engine, this value will be examined with regard to experimental results to see if it is still adequate when applied to natural gas fuel. The 'Turbulent entrainment model' presented by Tabaczynski and co-workers [95] correlates the ignition delay to the laminar flame speed, which is one of the disadvantages of using natural gas fuel, therefore the ignition delay of a natural gas fuelled engine is supposed to be longer than the traditional fuelled engine. Fortunately, this can be improved by adding

additives, e.g. hydrogen. The burning velocity of hydrogen is about 300 cm/s, which is eight times more than normal hydrocarbon fuel. A more chemical way to illustrate the improvement of ignition delay by the adding hydrogen was presented by Hassaneen and co-workers [40], they concluded the ignition delay time depends on the rate of chemical processes in the expanding flame kernel, adding hydrogen will accelerate the early stage of the combustion by the rapid chain branching oxidation characteristics of hydrogen. Again, this accelerating phenomenon will be examined by the durations of 5% MFB with different amount of hydrogen additive.

3.5.2. Burn Duration

The rapid-burning angle, again by Heywood's definition, of the SI engine is between the ignition delay and 90% or 95% MFB empirically. The reason for not choosing the EOC as a finish point is because of the difficulty of finding it, and the error can be minimized if one overestimates this point (after real EOC CA, the increment of pressure by combustion should be zero to the next combustion). Most researchers believe this period is controlled by the turbulent transport, and the flame speed is increased approximately linearly with the engine speed.

There are two alternative opinions with regard to the effect of hydrogen on this interval. Hires

and co-workers [96] said it will be reduced because of the faster laminar flame speed of hydrogen. Blizard and Keck [97] proposed that the rate of turbulent flame propagation is primarily governed by hydrodynamic processes during intake, compression and combustion, therefore the addition of hydrogen is not very significant to the burn duration. The observation here will focus on the interval change after adding hydrogen, and on examining the accuracy of the proposed method of finding the EOC point by inspecting the trend consistence of 95% MFB and the total combustion duration.

3.5.3. MFB Definitions Used in the Program

5% and 95% of MFB have been chosen in the program as end points of ignition delay and burn duration respectively. The definitions of both terms are:

Ignition delay: ignition point ~ 5% MFB

Burn duration: 5 ~ 95% MFB

4. DESCRIPTION OF EXPERIMENTAL METHOD AND PROCEDURE

4.1. Hardware Arrangement

4.1.1. Engine

The single cylinder engine, called "K4 Medusa", used in this study was effectively one quartered from a Rover K16 1.8 litre 4 cylinder gasoline engine. Stone's group [1, 53] has used a similar design but with optical access at the University of Oxford for combustion and cycle-by-cycle variation studies. Table 4-1 shows the specifications of the K4 engine.

Bore	80 mm
Stroke	88.9 mm
Displacement	446.86 cm^3
Connecting-rod Length	160 mm
Compression Ratio	10.5 : 1
Inlet Valve Opens	12 ° BTDC
Inlet Valve Closes	52 ° ABDC
Exhaust Valve Opens	52 ° BBDC
Exhaust Valve Closes	12 ° ATDC

Table 4-1 Specifications of the K4 Medusa engine.

The original fuel injector is replaced by a gas carburettor so the gaseous fuels can be used. Considering the high variation of intake air flow in single cylinder engine, the inlet air flow rate is evaluated by a positive displacement rotary flow meter (Romet G40). After the flow meter is a mixture throttle, which produces vacuum pressure in the mixture section to suck in

air and EGR. The other throttle is inside the carburettor, which controls the inlet mixture into the engine by varying the throttle open area to adjust the inlet manifold pressure and create a further vacuum in the mixture section. The amount of inlet air and fuel can be changed by tuning these two throttles.

The spark plug is controlled by an engine control system IC5460 according with the TDC signal from an optical shaft encoder (type: RS 341-581), which is coupled with the crank shaft of the engine, detail specifications can be found in Table 4-2. The shaft encoder also supplies degree signals (360 pulses per revolution) to trigger the data acquiring mechanism on a multi I/O data acquisition card.

RS Stock Number		341-581
Pulses per revolution		360 Pulses
Phase shift between A and B outputs		90 Degrees
Output signal A & B	High level	2.4 V
	Low level	0.4 V
Synch. Pulse output	High level	2.4 V
	Low level	0.4 V
Operation frequency		50 kHz
Equivalent disc speed		8333 rpm

Table 4-2 Specification of optical shaft encoder.

4.1.2. Fuel Supply

Natural gas fuel came directly from the mains gas, a pressure regulator reduced the pressure to about 16 ~ 20 mbar and an automatic cut-off solenoid valve was installed for safety, controlled by a tachometer set to monitor engine speed. A mains gas sample was sent to the laboratory of Scienco Ltd. Birmingham for major components analysis in the early stage of tests, the following compositions result was from their analysis report:

CH_4	C_2H_6	C_3H_8	CO_2	N_2
84.5%	6.0%	1.5%	2.0%	6.0%

Table 4-3 Main compositions of natural gas used in the tests.

Consequently the molar weight of natural gas used in this study is 18.583 (kg/kmol). In stoichiometric condition without considering dissociation, the chemical equilibrium equation can be presented as

$$0.845CH_4 + 0.06C_2H_6 + 0.015C_3H_8 + 0.02CO_2 + 0.06N_2 + 1.975\left(O_2 + 3.76N_2\right) \rightarrow 1.93H_2O + 1.03CO_2 + 7.49N_2 \quad \text{Eq. 4-1}$$

The stoichiometric air/fuel ratio (λ) is 14.59 and CO_2 is about 10 (wet) or 12 (dry) volume percent in the exhaust. Except the nearly zero content of oxygen in the exhaust, the average CO_2 percentage (11%) in the emissions was occasionally adopted as an alternative criterion of stoichiometric when the λ value indicated by the Horiba did not work properly.

An EGR loop was taken from the exhaust pipe 10 cm after the outlet port of engine, the amount of EGR returning back to the engine intake system was controlled by a globe valve sitting in the downstream section of the loop. The loop pipe, without any covering of insulation material, will naturally cool down the temperature of exhaust gas before it joining the inlet air. Hydrogen was stored in a high pressure vessel and mixed with natural gas fuel before feeding into the gas carburettor. Figure 4-1 shows the detail intake piping system arrangement.

4.1.3. Temperature Monitoring

Seven positions around the engine system have been monitored by K type thermocouples, all the wires are connected to a multifunction meter, so the temperature of each position can be read from the indicator by choosing the corresponding connection port. Table 4-4 lists the relevant information.

Mark	T1	T2	T3	T4	T5	T6	T7
Correspondent connection port	10	2	3	4	5	6	7
Description	coolant in	coolant out	oil in	oil out	inlet manifold	exhaust out	air in

Table 4-4 List of temperature monitoring points.

The coolant and oil temperatures were kept at 90°C and 80°C respectively throughout the

engine testing period. All temperatures were recorded by the end of each test for future analysis.

4.1.4. Emissions Measurement

An emissions analysis kit built up previously was used to examine the exhaust results during the experiments. Three main emission items, i.e. CO, UHC, NO, and two combustion related gases, e.g. CO_2 and O_2, were monitored and recorded for each test. The employed instruments include:

Instrument Name	Maker / Model	Analysed Gas
Emission Analyser	Horiba / MEXA-574GE	O_2, CO_2, CO, UHC
Infrared Analyser	Beckman / 864	CO_2
NO/NO_x Analyser	Beckman / 951A	NO/NO_x

Table 4-5 Instruments list of emissions analysis.

To make sure a stable condition can be reached, all equipments were warmed-up at least one hour before testing and the cooling system has to reach the default temperature, the calibrations of emissions analysis kit by zero and span gases were done before the very first test in every testing day. Exhaust gas was collected through an insulated pipe, which was taken from the exhaust pipe about 30cm from the engine exhaust port, then passed into a conditioning unit. After water separating procedure, dry exhaust gas was then analysed by

those instruments. The definition of EGR% adopted in this study is by the volumetric change of carbon dioxide:

$$\mathrm{EGR}\% = \frac{(CO_2)_{inlet}}{(CO_2)_{exhaust}} \times 100 \qquad \text{Eq. 4-2}$$

$(CO_2)_{exhaust}$ measured the content of CO_2 from the exhaust pipe when EGR was applying; $(CO_2)_{inlet}$ was obtained from the inlet manifold as switching off EGR supply. Both values were taken from the Horiba.

4.1.5. Data Acquisition Rig

The schematic arrangement of the integral data acquisition system is presented by Figure 4-2, the details of each item are explained below.

4.1.5.1. Data Acquisition Board

To acquire the pressure against volume signals from K4 engine at high speed and in real time, a multifunction I/O board from National Instruments was chosen. This PCI-MIO-16E-4 card is suitable for PCI bus computers with analog input, analog output, digital I/O and timing I/O functions. Those specifications related to test settings are listed below:

Model	PCI-MIO-16E-4
Analog input	
Number of channels	16 single-ended or 8 differential
Resolution	12 bits
Max. sampling rate	500 kS/s
Input coupling	DC
Max working voltage	Bipolar input range of ±5V
Digital trigger	
Compatibility	TTL
Response	Rising or falling edge
Pulse width	10 ns Min.

Table 4-6 Relevant specifications of data acquisition board: NI PCI-MIO-16E-4.

This card was installed in a personal computer with an AMD K6-333 processor and Windows 98 platform. The data acquiring functions were software controlled by NI DAQ 6.6 software together with the LabVIEW program.

4.1.5.2. Pressure and Crank Angle Acquiring Instruments

A Kistler quartz pressure sensor (Model 6125A) with T_iN coating was flush mounted in the cylinder head, signals were then sent to a Kistler Charge Amplifier (Model 5011) to convert the charge yielded from the piezoelectric effect into a proportional voltage signal. There are four settings on the charge amplifier that needed to be set:

Charge Amplifier	T (**T**ransducer sensitivity)	S (mechanical **S**cale)	LP (**L**ow **P**ass filter)	TC (**T**ime **C**onstant)
Kistler 5011	15	20	3 k H_Z	Short

Table 4-7 Settings for charge amplifier.

A dead weight calibration is needed for using the combination set-up of a pressure transducer and a charge amplifier. Except the time constant being set to “long” for calibration, which is suggested by the user’s manual, the parameters were kept the same. Four calibrations were conducted before installing the pressure transducer into the cylinder head, calibration results are presented in Figure 4-3 and an average value is adopted for ongoing using. A detailed calibration spreadsheet can be found in Appendix A. Deposits were found on the piezoelectric surface of transducer after a numbers of tests, therefore a regular check and re-calibration (probably every 20 working hours) is recommended for reasons of accuracy.

The first two charge amplifier settings decide the range of output signal, which has to be smaller than the limit of the input signal of the data acquisition board. Since the signal is of a differential type, according to Table 4-6, the safe working range is within ±5V. Figure 4-3 shows the chosen settings have restricted the output voltage less than 2V when the estimated maximum pressure (35 bars) was reached, this will protect the data acquisition system from overloading.

A shaft encoder, as mentioned earlier, was securely coupled with the engine spindle. TDC

position is supposed to be consistent with the synchronous pulse signal (1pulse/revolution) in order to identify each revolution of crank shaft. By dividing each two TDC period into 360 intervals and correlating them with relative pressure signals acquired by one crank angle base, the data of pressure traces versus cylinder volume can be derived. For convenience sake, the TDC signal has been set up as 70° before real TDC position in the control system, on the flywheel there is a TDC mark used for calibration, the TDC signal of the shaft encoder was synchronized with this point, consequently all the stored pressure data have to be shifted -70° CA in terms of cylinder volume.

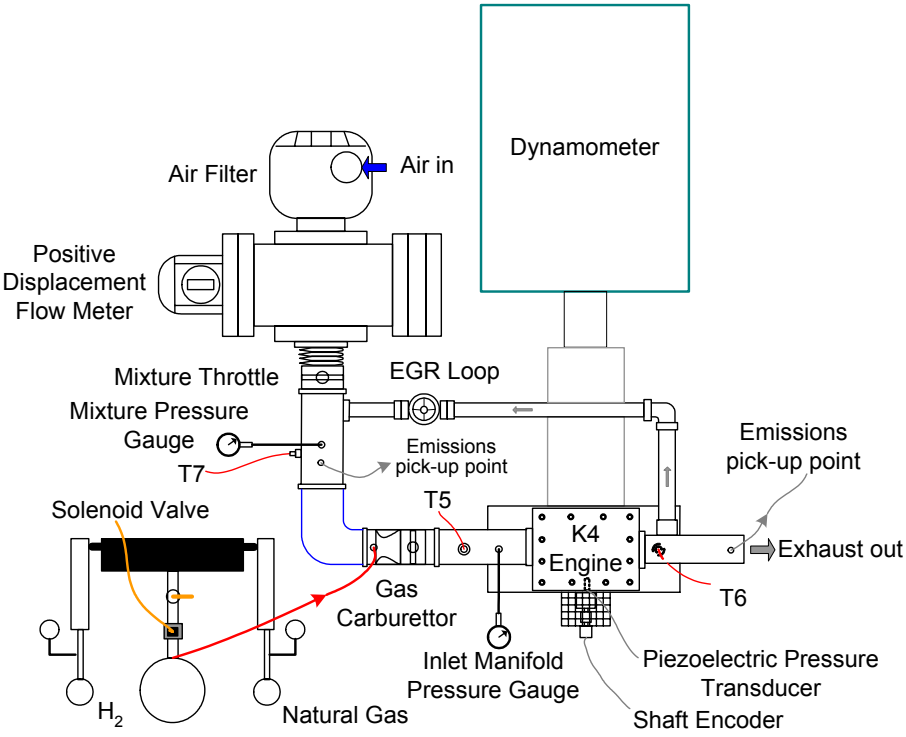

Figure 4-1 Intake piping arrangement of K4 engine.

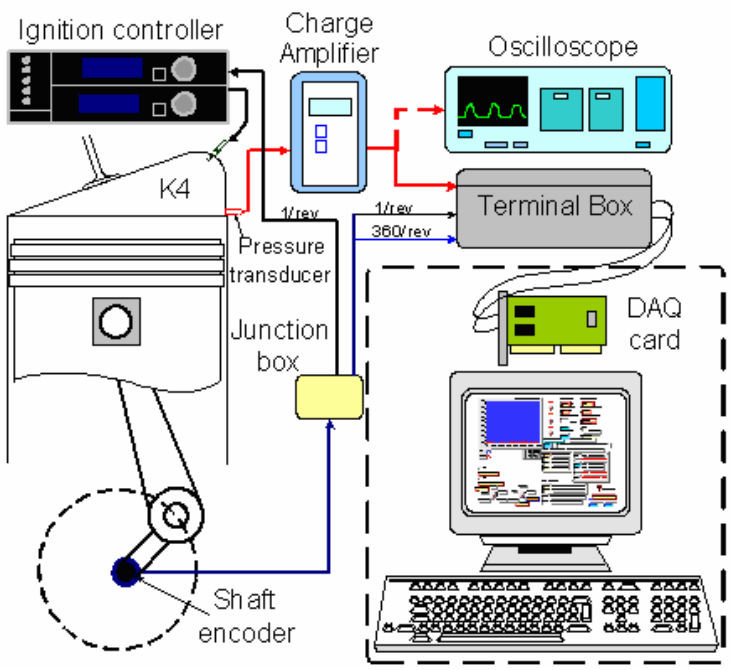

Figure 4-2 Schematic diagram of data acquisition rig.

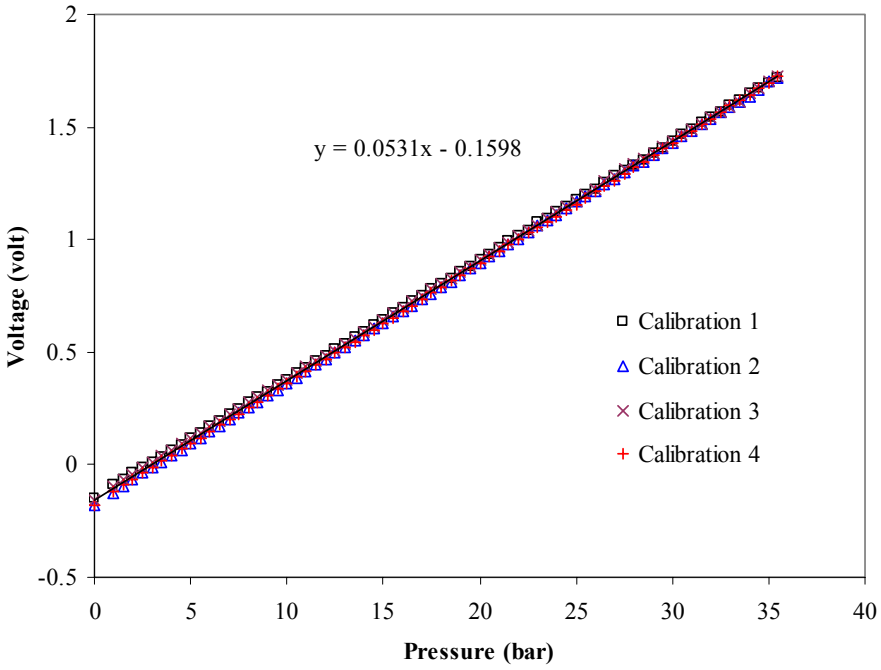

Figure 4-3 Dead weight calibration results of pressure transducer and charge amplifier set with the similar setting of charge amplifier in the tests.

4.2. Program Description

In this study, an in-house program has been developed with the purposes of acquiring and processing engine pressure and volume data in real-time. This program is written using the graphic language software LabVIEW 5.1, three main functions are included: data acquisition, IMEP and mass fraction burned calculations. Each function can be performed alone or cooperation with one or two other functions to obtain the desired results. Figure 4-4 shows the links and purposes of these functions. Figure 4-5 presents a partial view of the program and highlights some relevant items with simple explanations.

4.2.1. Data Acquisition

Signals from shaft encoder and pressure transducer are connected to the connectors of the data acquisition board. The scanning frequency of the board was chosen to use degree signals from the shaft encoder, thus at each degree the TTL pulse (output signal A or B) from the shaft encoder will trigger the data acquisition board to acquire the incoming signals once. Item 2 in Figure 4-5 will display the signals condition, a simple examination of acquired data can be done by checking this window.

Engine speed and desired cycle number have to be input before starting, the program will stop

the acquiring procedure and move on to the next step when the required number of signal has been reached.

4.2.2. IMEP Calculation

The desired value of IMEP needs to be input before starting, when the result falls within the chosen range, the value of COV_{IMEP} will show up and pause the program, this step will give the tester a chance to decide whether to store the data and move to IMEP function or not. For calculating the IMEP, the following procedures are then conducted in order:

(1) Verify the TDC signals from data to divide pressure signals into cycles

(2) Examine each set of cycle data and eliminate bad cycle(s) by judging whether there are 720 signals in the cycle

(3) Correlate the pressure data with crank angle

(4) Smooth pressure data by chosen method. See item 5 in Figure 4-5

(5) Average all good cycles and convert pressure to absolute value by referring the inlet manifold pressure as BDC pressure. See item 9 in Figure 4-5

(6) Correlate the average pressure with the cylinder volume

(7) Calculate the IMEP, COV_{IMEP} and find out the maximum pressure in each cycle

The cylinder volume at crank angle θ is calculated by the following equations [11]:

$$V = V_c + \frac{\pi B^2}{4}\left(l + \frac{L}{2} - s\right) \quad \text{Eq. 4-3}$$

$$s = \frac{L}{2}\cos\theta + \left(l^2 - \frac{L^2}{4}\sin^2\theta\right)^{\frac{1}{2}} \quad \text{Eq. 4-4}$$

where V_c is the clearance volume, B is the cylinder bore diameter, l is the length of connecting-rod and L is the stroke.

In this study, the compression ratio r_c is 10.5, therefore V_c can be obtained by the following equation:

$$V_c = \frac{V_s}{r_c - 1} \quad \text{Eq. 4-5}$$

where V_s is the swept volume of engine.

IMEP is calculated by Eq. 2-8 and COV is by Eq. 2-9. The detail calculation of IMEP can be found in Appendix B.

4.2.3. Mass Fraction Burned

To investigate the combustion conditions, the results of mass fraction burned were used. Through comparisons, a process obtained from selected methods mentioned in Chapter 3 will be verified in Chapter 5 and adopted for further discussions. Both methods of finding the initial EOC position and deriving the polytropic index value have to be chosen before starting, they are item 7 and 4 respectively in Figure 4-5. The ignition timing of item 3 needs to be

input as well. The first and second differential pressure traces will not only be used to estimate the initial EOC position, but also to predict the emissions behaviour, the detail will be described in Chapter 7.

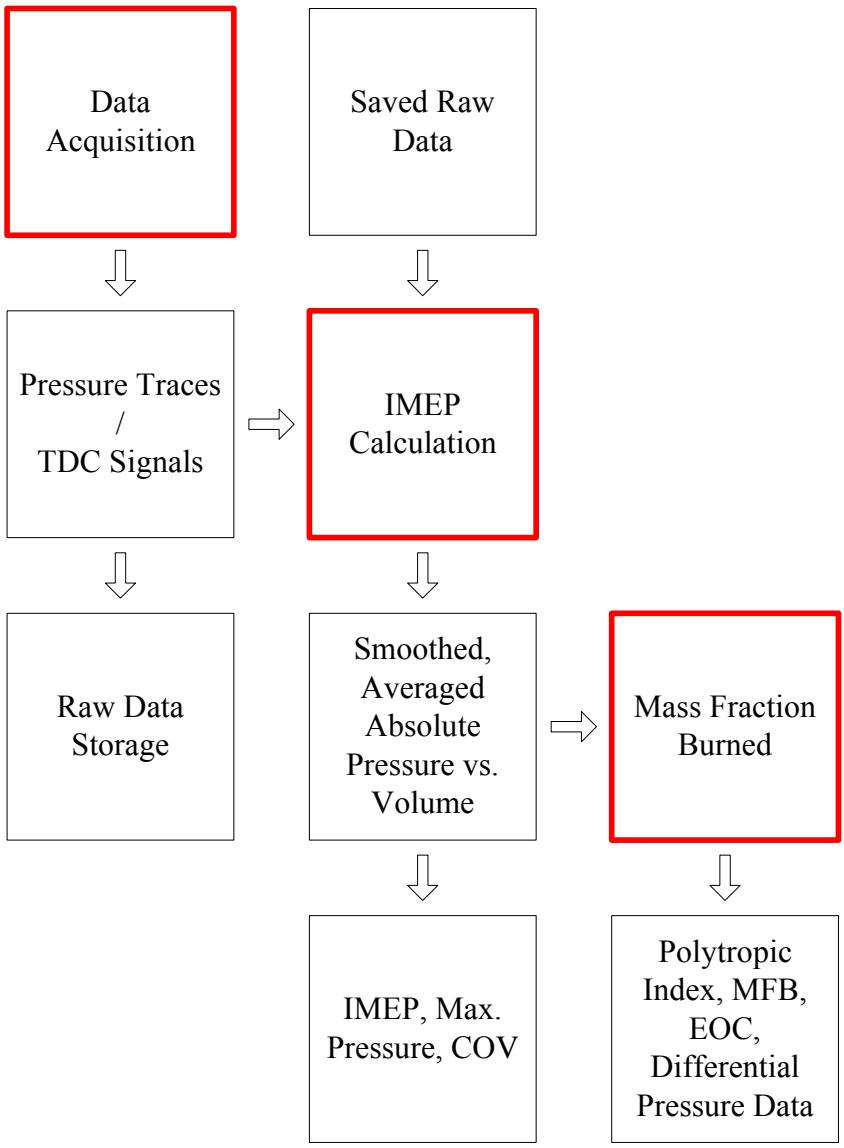

Figure 4-4 Block diagram of three main functions in the program.

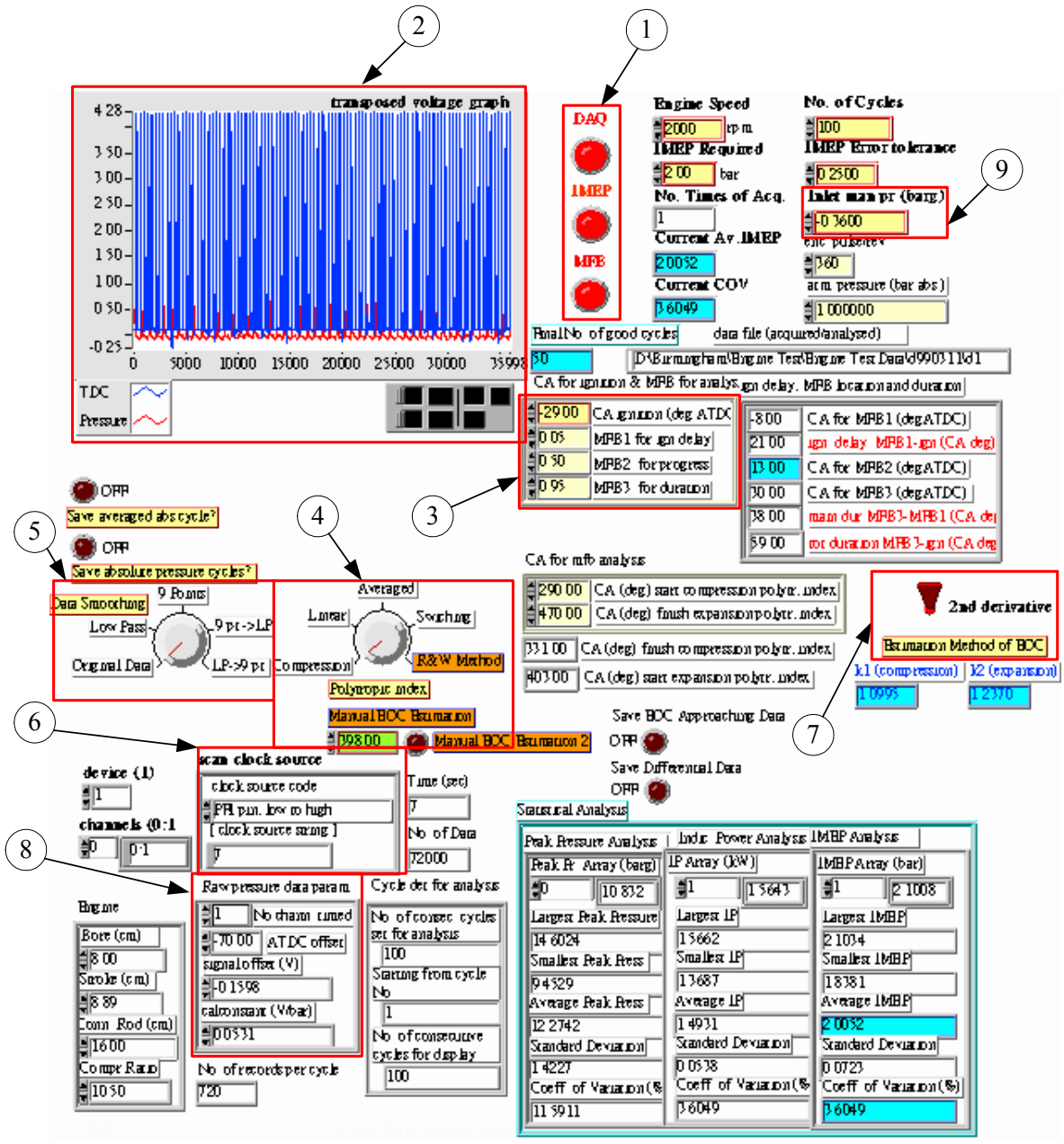

1. Main functions choosing buttons
2. Incoming signals monitoring window
3. Mass fraction burned set-up
4. Polytropic index method choosing knob
5. Data smoothing method
6. Scanning clock set-up
7. First EOC estimation method
8. Pressure signals calibration
9. Inlet manifold pressure

Figure 4-5 A partial front panel of the in-house program.

4.3. Test Procedure

Stoichiometric combustion is required to work successfully with a three-way catalyst in the after-treatment of engine exhaust, typically the air/fuel ratio needs to be within 1% of the stoichiometric value to protect the precious metals, hence such requirement will be adopted in this study too. The drivability is another concern, to fulfil the stability requirement, $COV_{IMEP} \leq 5\%$ has been set as a basic criterion to make sure the cycle by cycle variations of IMEP will not change too much.

Engine tests were conducted mainly by three base line operating conditions[†], these tests include some basic operating adjustments, i.e. engine speed, load and ignition timing, and will establish a set of reference data for better understanding of some complex problems.

(1) Standard condition: 2000 rpm, 2 bar IMEP, -31° ATDC ignition timing[‡], stoichiometric condition and $COV_{IMEP} \leq 5\%$.

(2) Higher load condition: 2000 rpm, 4bar IMEP, -31° ATDC ignition timing[‡], stoichiometric condition and $COV_{IMEP} \leq 5\%$.

(3) Lower speed condition: 1500 rpm, 2 bar IMEP, -29° ATDC ignition timing[‡], stoichiometric condition and $COV_{IMEP} \leq 5\%$.

[†] S, H and L may occasionally apply on some figures or captions to stand for above three operating conditions according to the order.

[‡] Base line (MBT) timing, change of timing may be applied as condition required.

The following three investigations will be carried out and discussed individually.

(1) Since the revised r-R&W model has been selected for the MFB calculation, consequently locating the EOC point and deducing two polytropic indices correctly become significant. The most suitable data processing method for the present study will be examined according to the results from above three operating conditions (except the spark timing in lower speed condition has been advanced to 31° CA BTDC for easy comparing). The chosen mechanism will then be secured and applied on all the tests.

(2) Effects of additives on the combustion duration of a natural gas fuelled engine, especially for adding EGR and hydrogen, will be investigated in terms of the combustion indicators. A combined effect of EGR and hydrogen, based on the benefit of exhaust gas reforming method, will then be examined and compared with the individual effect. According to previous study, the volume percentage of EGR in the inlet charge can be increased up to 25% with hydrogen as a supplement, the variations of combustion durations during the change will be investigated by a gradually increasing method, i.e. adding two additives alternately to extend the limit of EGR content and still retain the COV_{IMEP} under 5%.

(3) Taking emissions readings normally takes a number of actions to derive the results,

these have been found probably the most time consuming procedures in this study. Therefore a simple measure that can reveal the tendency of the relevant emissions, i.e. NO, CO, will be very efficient and attractive. The derivative of pressure data have been found very useful in diagnosis of engine combustion, the first and second derivative of pressure data will then be used as tools to investigate the relationships with MFB profile and emissions behaviour. The object of this part is trying to predict the required CA for each stage of MFB and the tendency of emissions within a relevant window by using the differential pressure.

5. EFFECTS OF IMPROVED APPROACHES ON COMBUSTION DURATION CALCULATION

Since the calculation of combustion duration in the present study is based on the incoming signals indicating pressure and volume, the impacts on the result due to the data modifications have to be examined before the further step of investigation the additives' effects. However, the combustion behaviours changes with changing engine operation, i.e. different ignition timing, speeds and loads etc., have to be known in advance. Moreover, the phasing of pressure in terms of crank angle needs to be accurate enough to calculate the IMEP and the data smoothing methods should still retain the characteristics of combustion. This chapter will explore the above issues and compare their effects using the MFB results calculated by the revised R&W method (r-R&W), and then a decision should be made to select a more suitable data processing method for natural gas fuelled engine. For the convenience of discussion, the order of the following topics may not be consistent with the order of the program procedures. However, the procedures of data analysis have already been outlined in Chapter 4.2.2.

5.1. Effects of Basic Operating Conditions

Cylinder combustion can be affected by many operating parameters, therefore this

investigation will only concentrate on these items related to the effects of adding EGR and (or) hydrogen additive(s), they include engine speed, load (IMEP) and ignition timing.

5.1.1. Engine Speed

Two different speeds, i.e. 1500 and 2000 rpm were compared under similar operating conditions. Data had not been modified by any smoothing methods (raw data), and the switching polytropic index method was chosen arbitrarily to decide the EOC points. By using the above data, the MFB results were then obtained using the r-R&W model.

Figure 5-1 shows MFB profiles of two different speeds at the same IMEP. The comparison, on the basis of crank angles, reveals 25% more crank angle degrees are required to reach the first 5% MFB (ignition delay), however the time required at 2000 rpm is 6.3% less than at 1500 rpm. Higher speed takes less time and CA degrees during the burn duration (5% ~ 95% MFB), which agrees with the explanation that the turbulence dominates the combustion speed during this period and the engine speed has a direct link with the turbulence inside a cylinder.

Another phenomenon that should be noted is the proportion of combustion occurring prior to TDC. To reach the same IMEP, with the same ignition timing, the lower speed condition requires a greater percentage of mixture burned before 360° CA, thus more combustion conducted in compression stroke. In this case, when the mass fraction burned was 12.3%

more conducted before TDC, it will cause a 40% higher average peak pressure in the combustion.

5.1.2. Gross IMEP

According to Eq. 2-8, under a similar operating condition, higher IMEP requires higher pressure to be produced inside the cylinder. The average peak pressures are 12 and 29.5 bar with respect to 2 and 4 bars IMEP as shown in Figure 5-2 (A), this figure also shows the pronounced pressure difference in terms of cylinder volume. In the 4 bar IMEP case, a steeper pressure rise in the compression stroke after the ignition can be seen, probably because the energy was released from more fuel mixture (76% more in this case), the other reason is the percentage of burned gas occurring before TDC, 15% MFB difference has been observed. Besides, in the 4 bars IMEP case, a longer total combustion period was needed, although the 95% MFB were indicating approximately the same in both tests.

5.1.3. Ignition Timing

Results in this section are derived from the data smoothed by the nine points weighted method, EOC points were calculated through the switching polytropic index method and consequently

adopted for the revised R&W model in the MFB calculation.

Figure 5-3 shows the correlation between IMEP and ignition timing in three different operating conditions. The MBT timing can be roughly located by finding the point on the IMEP curve corresponding to the minimum point of the COV_{IMEP} curve [98, Ch. 4], as a result -31°, -29° and -31° are MBT timing for standard, lower speed and higher load conditions respectively, ±1° tolerance should be considered because the test interval is 2° CA. Average peak pressure decreased when the ignition timing moved toward TDC, there is no direct link between peak pressure and IMEP value, although higher peak pressure do produce higher IMEP, Figure 5-4 presents a linear-like relationship between average peak pressure and ignition timing. Similar behaviour of NO in terms of ignition timing is also showing in this diagram, such phenomena can be explained by the quantity of combustion occurring before TDC. A retarded ignition will shorten the combustion time before TDC, therefore the pressure and temperature inside cylinder decreases, and subsequently less NO will be produced in the exhaust.

In standard condition, varying the ignition timing has been found to be irrelevant with regard to the MFB profile, Figure 5-5 illustrates this phenomenon. It also provides a simple solution to retaining a significant MFB value at a certain position without too much effort. Except in the case of ignition timing 29° CA BTDC, an increasing combustion duration was concurrent

with advanced ignition timing at each MFB stage (5%, 50%, 95% and EOC), Figure 5-6 illustrates plainly this unique behaviour. The other two operating conditions show different types of tendency in Figure 5-5, there are remarkable offsets at 95% MFB between 33° ~ 31° BTDC for both cases, nevertheless, the other two combustion stages 5% and 50% MFB remain at nearly the same levels throughout all the variations. Figure 5-7 presents this behaviour at the lower speed condition, the reason for those two peculiar profiles can be found from Figure 5-8, showing the expansion polytropic index has a similar trend line with 95% MFB and EOC. Unfortunately, the MFB calculation was not conducted by switching index method but by the r-R&W model. If the switching index was applied, it will be very easy to explain why the profiles change suddenly after 50% MFB (around TDC in this case, the same position for switching the polytropic index in MFB calculation from compression to expansion value). However, this phenomenon reveals the consistency in MFB calculation of switching polytropic index method and r-R&W model, and the strong effect of the polytropic index on the MFB result. These relationships will be investigated in the next section.

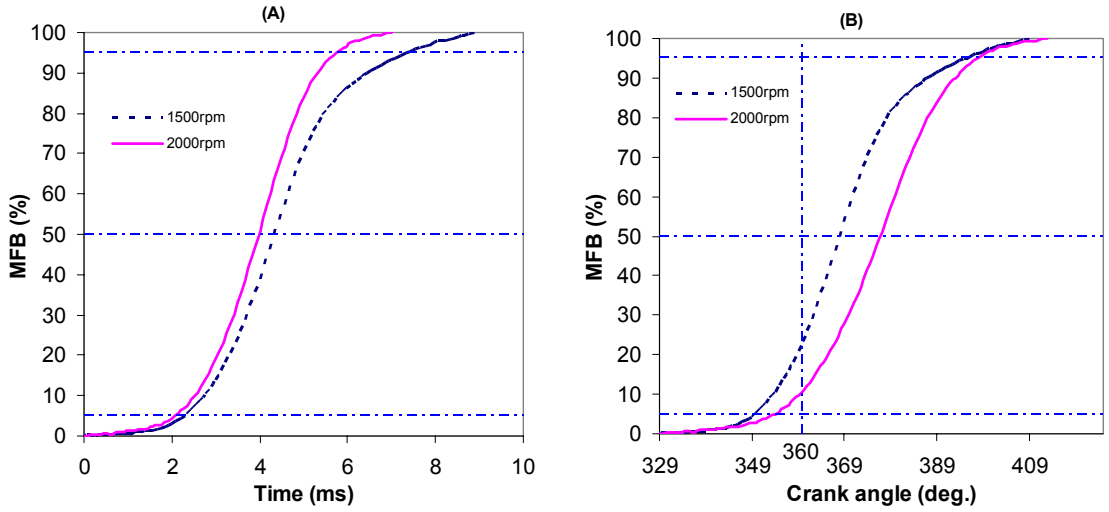

Figure 5-1 **The variation of MFB between two speeds at two different comparison bases, i.e. time and crank angle. Operating conditions: 2 bar IMEP, IG timing: -31° ATDC, $COV_{IMEP} \leq 5$ %.**

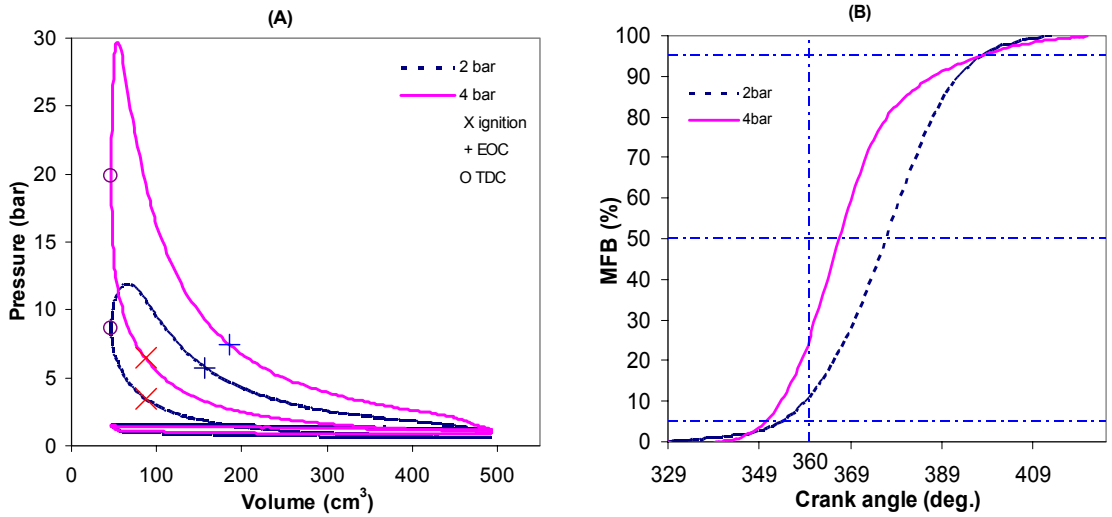

Figure 5-2 **Comparison between two different IMEP at 2000 rpm, IG timing: -31° ATDC. (A) P-V diagram (B) MFB.**

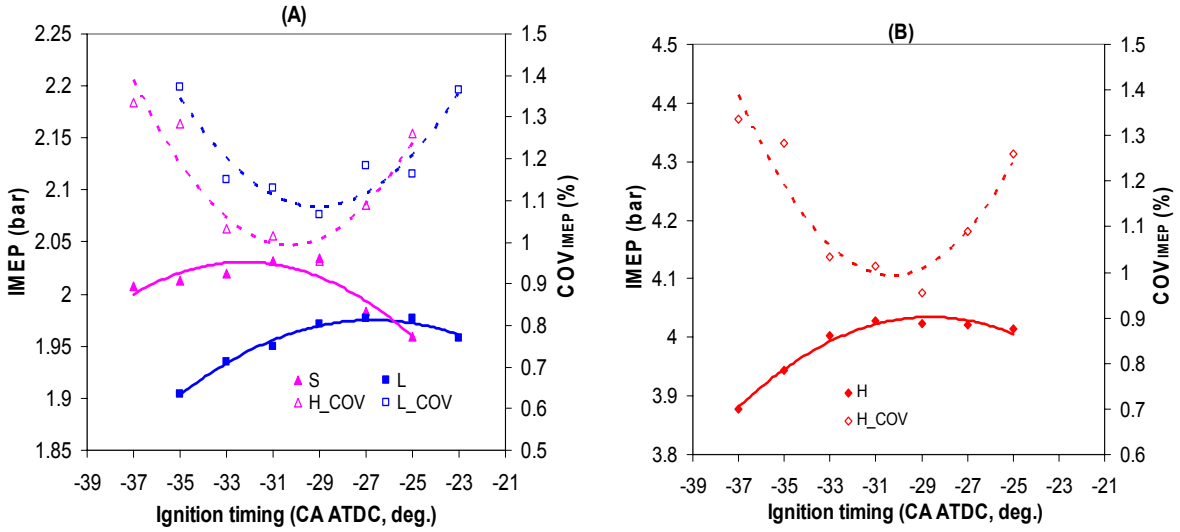

Figure 5-3 **Correlations between ignition timing, IMEP and COV_{IMEP} (A) Standard and Lower speed conditions, (B) Higher load condition.**

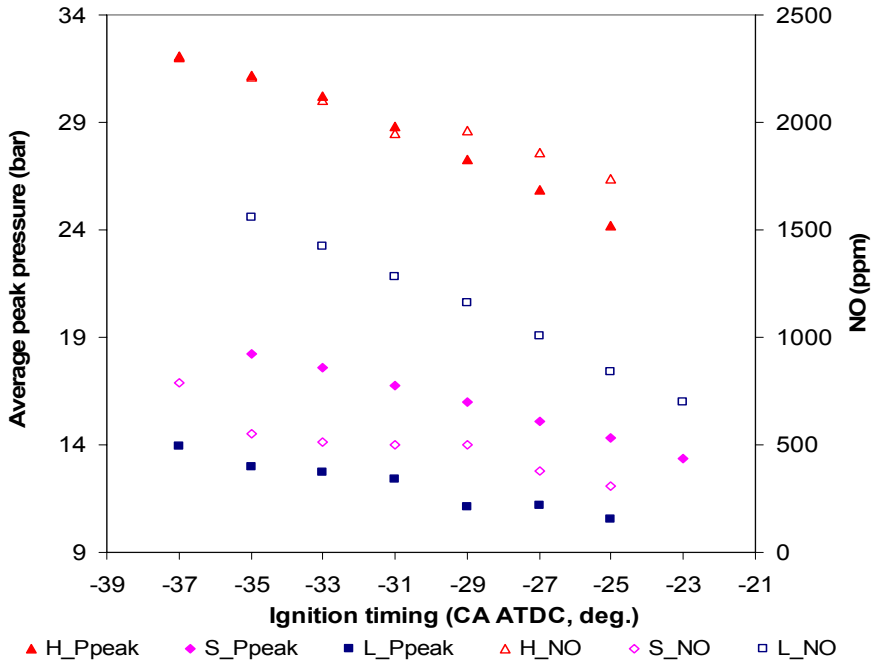

Figure 5-4 **Correlation between ignition timing and average peak pressure in three different operating conditions; the related NO content in exhaust is showing the same tendency.**

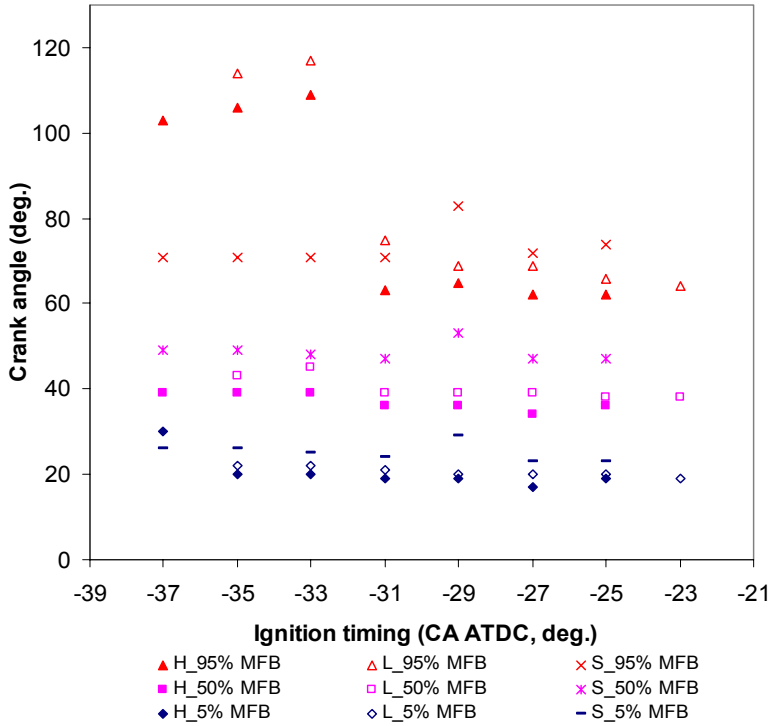

Figure 5-5 Comparison of 5%, 50% and 95% MFB in three different conditions.

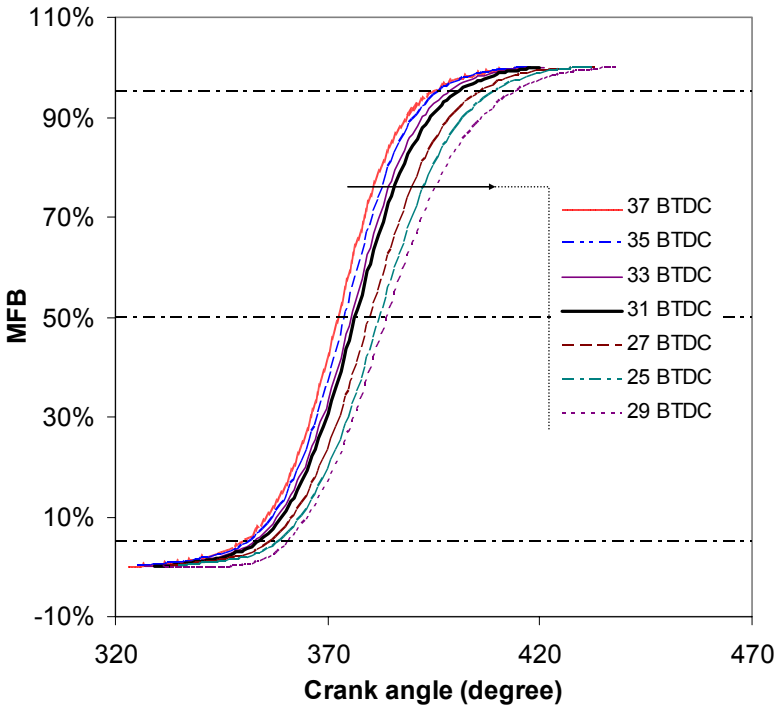

Figure 5-6 MFB profile vs. ignition timing in standard condition.

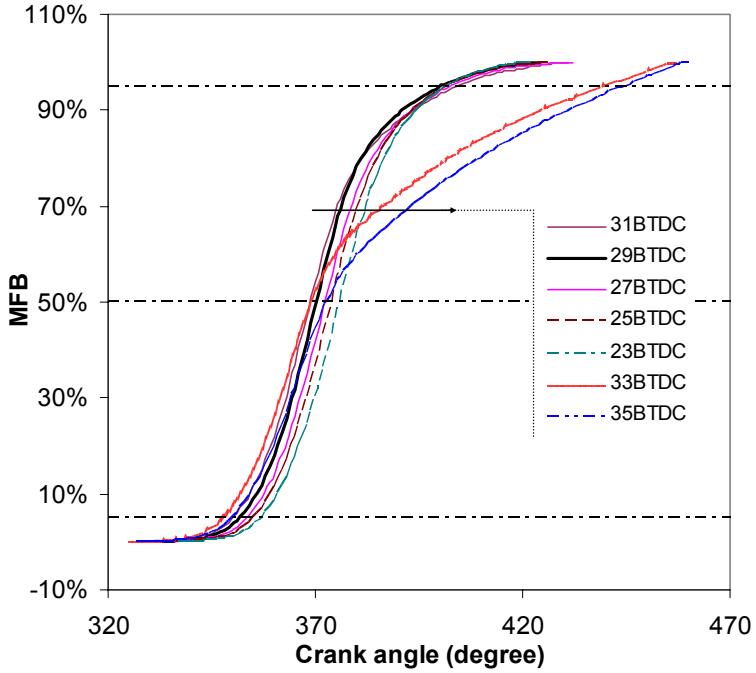

Figure 5-7 **MFB profile vs. ignition timing in lower speed condition.**

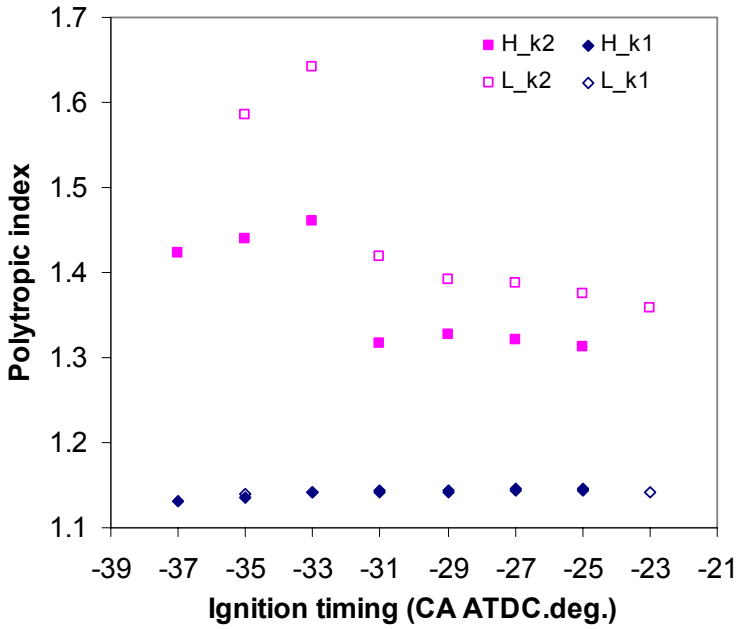

Figure 5-8 **The variation of Polytropic index against ignition timing in two different operating conditions. k1 - compression polytropic index, k2 – expansion polytropic index.**

5.2. Effects of Data Processing and Analysis Methods

Data processing is necessary for data analysing, Figure 5-9 (A) illustrates one of the examples. The diagram shows the improvement in the second derivative pressure data produced by applying the low pass filter to the data. The derived data can then be used much more easily to decide the initial EOC point and predict the emissions trend later. The disadvantage of smoothing data is that the result may not be able to present the real condition if some occasional abnormal phenomena are smoothed out. In this study, most of the data were taken under acceptable drivability, i.e. $COV_{IMEP} \leq 5\%$, which means that these unusual events had already been exempted from the tests. Moreover, the stored computer files of satisfactory raw data signals and piles of data sheets recorded with operating condition and emissions result make it easy to reinvestigate.

Once engine speed, ignition timing and desired IMEP are decided, the calculation of duration of combustion is determined by the accuracy of the data and the computation mechanism. If any alteration has been done on raw data, the effect on the result needs to be evaluated and borne in mind during the analysis. The in-house program introduces raw pressure signals into the steps of phasing, pegging, smoothing and averaging before conducting the MFB calculation, and the first three processing effects were investigated to help understand the behaviour of the result.

5.2.1. Data Smoothing Methods

Due to unavoidable noise pickup and electronic interaction, data smoothing is necessary. Two different methods were suggested above, they are the nine points weighted smoothing method (9PWT, hereafter) as Eq. 2-4 and the low pass filter method (LPF, hereafter) as Eq. 2-5. Both of them are believed to have superior performance for eliminating noise, and the latter has also been claimed to show good performance on the second derivative of pressure data. Figure 5-9 (B) compares the second derivative of pressure data smoothed by the LPF and the 9PWS methods; the former method does, in fact, present a better result. The average pressure cycle is produced after the data smoothing procedure and used in MFB calculation to shorten the time. The comparisons of MFB results between raw and smoothed data, which include the individual and combined effects of these two smoothing methods, are discussed below.

5.2.2. Polytropic Index Method

There are many different polytropic index methods for mass fraction burned calculation. The single value methods, it has been argued, tend to underestimate the results because a lower index value is chosen in the expansion process. Therefore, the switching and linear methods will be examined to see if they can provide more accurate results. The r-R&W method was set

up as a standard reference model to compare these differences.

Figure 5-10 to Figure 5-12 illustrate the MFB calculation results with different polytropic index values when different smoothing methods were applied. Except in the Standard condition, single index methods, i.e. compression and averaged polytropic index values, do show shorter periods of combustion than the other two methods.

Four types of data condition were compared:

(A) Raw data – data derived from the data acquisition rig without a signal smoothing procedure

(B) The LPF method

(C) The 9PWS method

(D) The combined method – signals smoothed by both LPF and 9PWS methods

In some cases, mostly when linear or switching polytropic index values were used, the total combustion duration became very long. Therefore, the EOC point was too short to derive a proper regression line, e.g. it was less than 10 CA degrees to the default end point (470 CA degree) for deriving the expansion polytropic index value, so a further retarding action was taken to extend the end point toward the exhaust valve opening crank angle (488 CA degree). Those marked with the symbol * were in this condition.

Table 5-1 is related to Figure 5-10 ~ Figure 5-12 showing the differences in MFB results as

percentages under three engine operating conditions and using four different polytropic index methods. There is no doubt that all the smoothed data delayed the calculation results of the duration of total combustion. The worst cases happened when the LPF method was chosen, whether it worked alone or was combined with the 9PWS method. A 65% increment (5.778 ms or 52° CA) of the total duration was found when either the linear or switching polytropic index method was applied. An alternative method suggested by other researchers, which decided the end of combustion by choosing a smaller value (95% in this study) of MFB was found to make little improvement to the difference. However, up to 46.87% increment still occurred when the switching method was used with LPF modified data. The nine points weighted smoothing method worked adequately in all cases, especially in standard conditions, and nearly the same results were found at 5%, 50% and 95% MFB calculations.

The compression polytropic index method produced very similar results with raw data no matter what kind of smoothing mechanism was applied, which consequently makes the linear and switching methods appear to overestimate the combustion duration, contradicting previous research results. Nevertheless, a similar result with raw data does not guarantee the accuracy, because the calculation according to the raw data could be wrong since it is unfiltered, hence comparisons were made between different approaches and the reference method, the r-R&W model.

Matrix structure comparisons originally stemming from Figure 5-10 ~ Figure 5-12 were conducted and the results can be divided into three corresponding groups of diagrams: Figure 5-13 ~ Figure 5-16, Figure 5-17 ~ Figure 5-20 and Figure 5-21 ~ Figure 5-24. Each diagram presents the difference in MFB profiles between the applied polytropic index method and the r-R&W model, a table under the diagrams gives the percentage deviation at three combustion stages. To use the r-R&W model for the MFB calculation, the EOC point has to be known in advance; therefore in each comparison the EOC point derived from the other method was used; thus both methods employ the same polytropic index value(s) and the combustion finishes at the same point.

Figure 5-13 ~ Figure 5-16 illustrate the results originally from Figure 5-10 in the standard operating condition. The switching index method has the best agreement with the r-R&W model in all kinds of data, but the linear polytropic index method performed well too. A slightly lower result from both single index methods was observed, as expected.

Figure 5-17 ~ Figure 5-20 are results initially from tests of Figure 5-11 in the higher load condition. Pronounced deviations after 50% MFB happened in all cases; the low pass filter smoothing worsens the results, as shown in Figure 5-18 and Figure 5-20. The nine points weighted smoothing with the switching polytropic index method (9PWS-SW, hereafter) is competent to produce a very similar profile to the r-R&W model; that is in response to the

previous discussion of data smoothing methods, which shows the potential of reliable application.

Figure 5-21 ~ Figure 5-24 present comparisons in the lower speed condition than Figure 5-12. Very similar comparison results were produced to the higher load condition, which encourages the use of the 9PWS-SW mechanism. The linear polytropic index method does not seem to be suitable for reconciling with those data smoothed by the lower pass filter method; a gap during 60% ~ 90% MFB is obviously seen, and the deviation starts earlier than other cases from TDC (about 30% MFB).

Compared with the other two operating conditions, the standard one shows less affected by the chosen polytropic index method. Both dual index methods worked compatibly with each other and show very close results to the r-R&W model, which encourages a further investigation of the linear polytropic index method, because to the author's knowledge, this method has not been adopted by any other researcher. Since the 9PWS-SW mechanism has shown potential for future use, the investigation of the effect of additives in the next chapter will use this method for data processing in all cases.

5.2.3. Pressure Phasing

Although the TDC signal can be roughly calibrated before the experiment by observing the

motoring signals every time, there is still some possibility of phasing deviation, especially when the engine is firing. During the experiments, the aluminium coupling connecting the engine spindle and shaft encoder broke several times, due to the misalignment or high torque rotation. When the fault occurred, the figure in the diagrams were twisted and deformed to begin with, and then the data acquisition ceased to function because the checking mechanism of the signal number could not reach the criteria in the program. Another defective condition was that the TDC position deflected a few degrees away and the changes were hardly noticed.

Comparisons between correct phasing and degree offset error are discussed here. To simulate the faulty condition, phasing from 1° CA to 5° CA and 10° CA advanced and retarded errors are shown in Figure 5-25. In this test, the engine was run in standard operating condition, the nine points weighted smoothing method was chosen to process the pressure data, the linear polytropic index method was applied to decide the EOC point, and the MFB was derived by the r-R&W model. Diagram (A) presents the MFB profile variations according to the phasing errors; diagram (B) shows the trend lines of four combustion stages: 5%, 50%, 95% MFB and EOC. The advanced and retarded phasing errors affected the 5% MFB calculation linearly; an inclined tendency was observed from -10° CA to +10° CA. A dip area similar to the normal heat transfer effect can be seen, owing to the retarded phasing; this phenomenon is exaggerated when the phasing error increases. Conversely, the trends of 50%, 95% MFB and

EOC all incline from the advanced side down toward the retarded side. Such a result shortens the period of burn duration but with a longer ignition delay, thus 12% increment of ignition delay and a 22.7% reduction in burn duration were produced at a +5° CA phasing error. Figure 5-26 presents the way in which the polytropic index values are affected by phasing errors, the increasing compression index value k1 and the decreasing expansion index value k2 correspond to the ignition delay and burn duration tendencies respectively.

In Figure 5-27, diagram (A), showing the effects on the IMEP and COV_{IMEP} calculation, very similar tendencies can be observed. The reason why the IMEP changes when the pressure suffers phasing error can be easily explained by reference to diagram (B); that the deformed compression and expansion strokes affect the IMEP calculation area can be seen.

There is a linear relationship between the percentage of IMEP inaccuracy and the phasing error; only 5% IMEP deflection is observed in Figure 5-28 when the pressure with respect to volume has 1° CA error; therefore, for the 2 bar IMEP test, setting up ± 0.1 bar as tolerance value is within 1° CA phasing error. This result agrees with Figure 2-3 presented by Hribernik [57].

5.2.4. Pressure Pegging

A piezoelectric transducer can only produce dynamic pressure data, but an absolute pressure

reference is needed for using such an instrument. According to the conclusions by [47-49], the inlet manifold pressure was chosen because of its relevance. Pegging error normally occurs when the reference datum is decided wrongly; such as when a wrong absolute pressure value is given or the reference point is misplaced. The latter has been generally discussed in the scope of phasing error; therefore the focus will be on the accuracy of the reference pressure. Nevertheless, one should know that the pegging error will not affect either the IMEP result or the COV_{IMEP}, because the curve on the P-V diagram will simply be shifted vertically without any deformation.

In the present test, the inlet manifold pressure value was obtained through a Bourdon gauge and a sintered filter was fitted before the gauge in an attempt to attenuate the fluctuation problem of the indicator. The reading was taken by eye measure and most of the readings were decided by choosing the value from the middle of the variation range in a consequence of the severe fluctuation. With increasing pegging value (absolute pressure of inlet manifold), Figure 5-29 (A) shows that the MFB results gradually decreased, except that the 50% MFB remained at the same level. 16% ignition delay reduction was caused by referencing a datum with +0.2 bar absolute pressure error. Polytropic index values were affected, the compression polytropic index k1 had similar behaviour as the ignition delay; this tendency is illustrated in diagram (B).

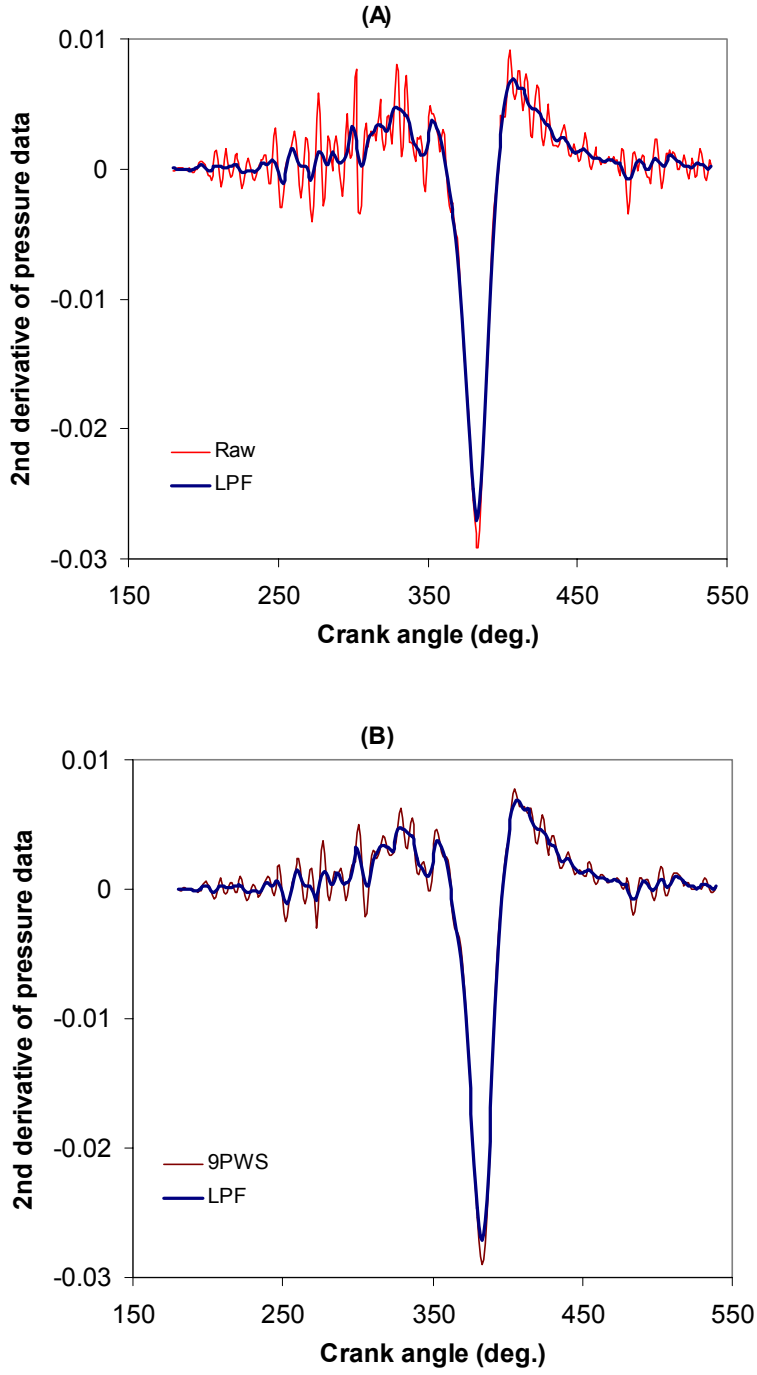

Figure 5-9 **The difference between raw data and smoothed data methods in 2nd derivative of pressure data in the standard operating condition. (A) Raw data vs. LPF, (B) 9PWS vs. LPF.**

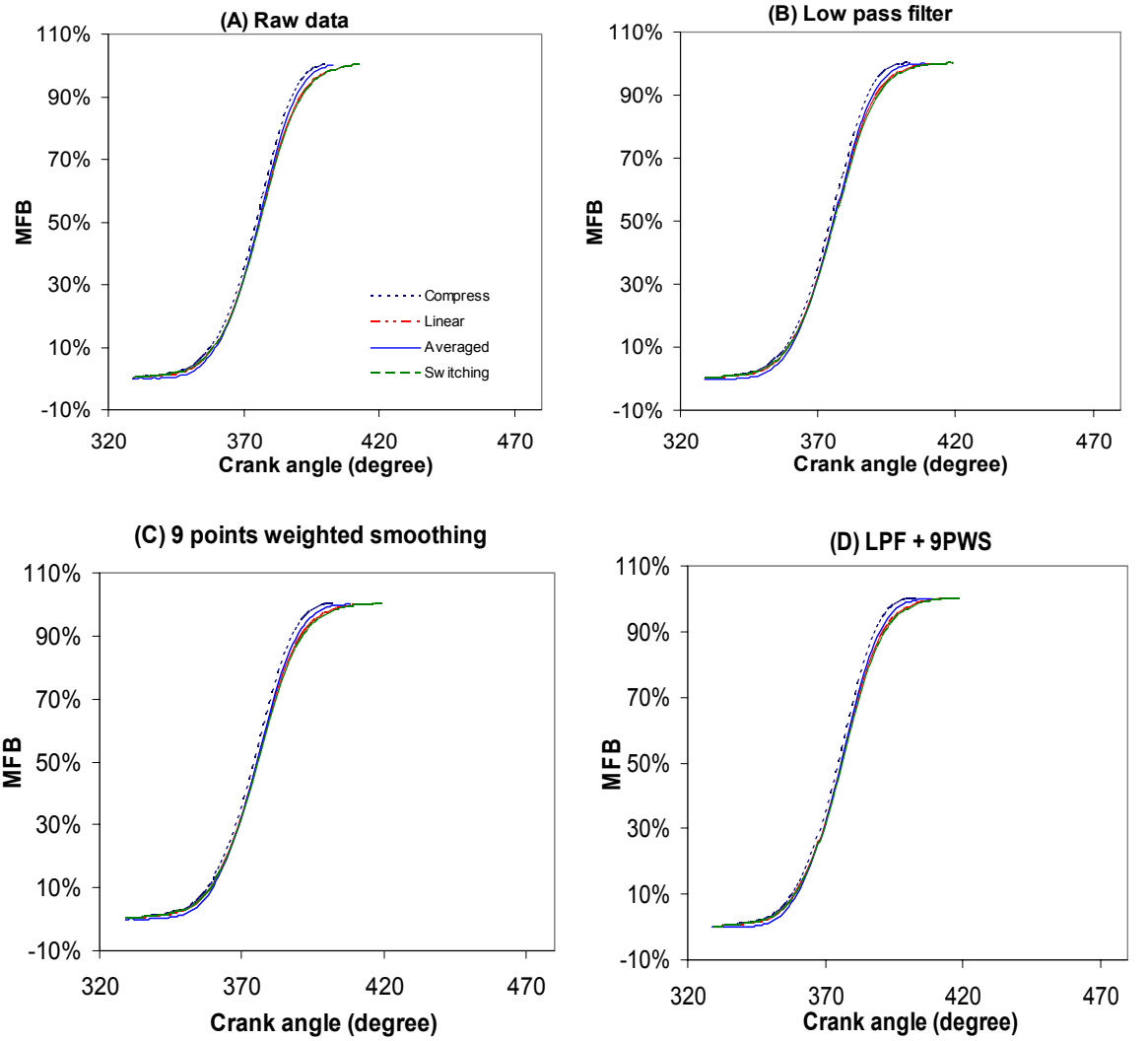

(A)	5%MFB ms (CA)	50%MFB ms (CA)	95%MFB ms (CA)	Total ms (CA)
Compress	2.000 (24)	3.750 (45)	5.167 (62)	5.917 (71)
Linear	2.083 (25)	3.833 (46)	5.500 (66)	7.000 (84)
Averaged	2.167 (26)	3.833 (46)	5.250 (63)	6.167 (74)
Switching	2.083 (25)	3.917 (47)	5.583 (67)	7.000 (84)

(B)	5%MFB ms (CA)	50%MFB ms (CA)	95%MFB ms (CA)	Total ms (CA)
Compress	2.000 (24)	3.750 (45)	5.167 (62)	6.167 (74)
Linear	2.083 (25)	3.917 (47)	5.583 (67)	7.500 (90)
Averaged	2.167 (26)	3.833 (46)	5.333 (64)	6.667 (80)
Switching	2.083 (25)	3.917 (47)	5.667 (68)	7.500 (90)

(C)	5%MFB ms (CA)	50%MFB ms (CA)	95%MFB ms (CA)	Total ms (CA)
Compress	2.000 (24)	3.750 (45)	5.167 (62)	6.083 (73)
Linear	2.083 (25)	3.833 (46)	5.500 (66)	7.500 (90)
Averaged	2.167 (26)	3.833 (46)	5.333 (64)	6.583 (79)
Switching	2.083 (25)	3.917 (47)	5.583 (67)	7.500 (90)

(D)	5%MFB ms (CA)	50%MFB ms (CA)	95%MFB ms (CA)	Total ms (CA)
Compress	2.000 (24)	3.750 (45)	5.167 (62)	6.167 (74)
Linear	2.083 (25)	3.917 (47)	5.583 (67)	7.500 (90)
Averaged	2.167 (26)	3.833 (46)	5.333 (64)	6.667 (80)
Switching	2.083 (25)	3.917 (47)	5.667 (68)	7.500 (90)

Figure 5-10 The effects of data smoothing on MFB calculation results with different polytropic index methods. Engine operated in the standard condition.

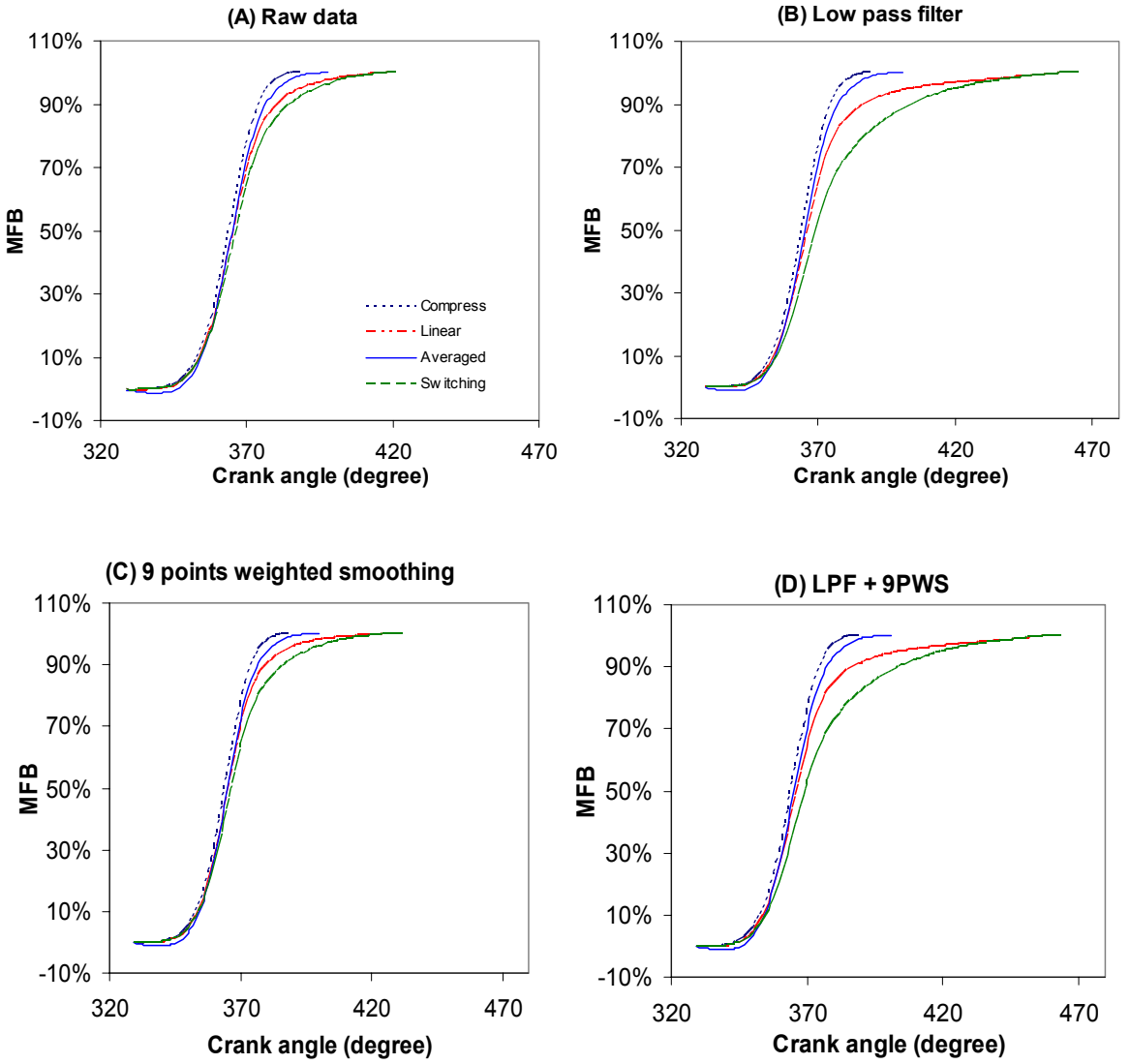

(A)	5%MFB ms (CA)	50%MFB ms (CA)	95%MFB ms (CA)	Total ms (CA)
Compress	1.667 (20)	2.917 (35)	3.917 (47)	4.917 (59)
Linear	1.750 (21)	3.000 (36)	4.917 (59)	7.667 (92)
Averaged	1.833 (22)	3.000 (36)	4.250 (51)	5.750 (69)
Switching	1.750 (21)	3.083 (37)	5.417 (65)	7.667 (92)

(B)	5%MFB ms (CA)	50%MFB ms (CA)	95%MFB ms (CA)	Total ms (CA)
Compress	1.667 (20)	2.917 (35)	4.000 (48)	5.000 (60)
Linear*	1.750 (21)	3.083 (37)	7.083 (85)	11.333 (136)
Averaged	1.833 (22)	3.000 (36)	4.333 (52)	6.000 (72)
Switching*	1.833 (22)	3.333 (40)	7.583 (91)	11.333 (136)

(C)	5%MFB ms (CA)	50%MFB ms (CA)	95%MFB ms (CA)	Total ms (CA)
Compress	1.667 (20)	2.917 (35)	3.917 (47)	4.917 (59)
Linear	1.750 (21)	3.000 (36)	4.833 (58)	8.583 (103)
Averaged	1.833 (22)	3.000 (36)	4.250 (51)	5.917 (71)
Switching	1.750 (21)	3.083 (37)	6.000 (68)	8.583 (103)

(D)	5%MFB ms (CA)	50%MFB ms (CA)	95%MFB ms (CA)	Total ms (CA)
Compress	1.667 (20)	2.917 (35)	4.000 (48)	5.000 (60)
Linear*	1.750 (21)	3.083 (37)	6.333 (76)	11.250 (135)
Averaged	1.833 (22)	3.000 (36)	4.333 (52)	6.000 (72)
Switching*	1.833 (22)	3.333 (40)	7.583 (91)	11.250 (135)

Figure 5-11 The effects of data smoothing on MFB calculation results with different polytropic index methods. Engine operated in higher load condition.

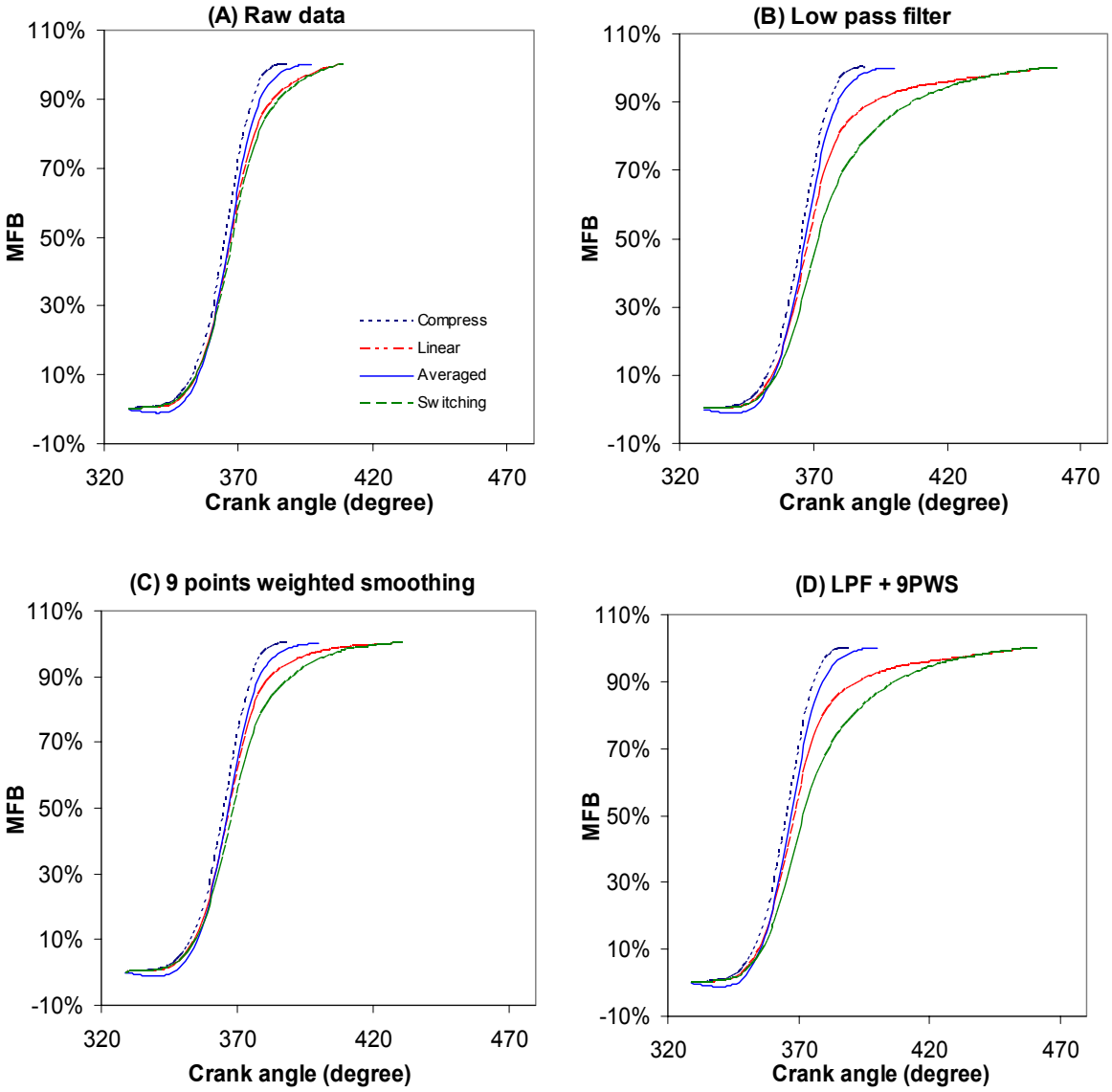

(A)	5%MFB ms (CA)	50%MFB ms (CA)	95%MFB ms (CA)	Total ms (CA)
Compress	2.222 (20)	4.000 (36)	5.333 (48)	6.556 (59)
Linear	2.333 (21)	4.222 (38)	6.889 (62)	8.889 (80)
Averaged	2.556 (23)	4.111 (37)	5.889 (53)	7.556 (68)
Switching	2.333 (21)	4.333 (39)	7.111 (64)	8.889 (80)

(B)	5%MFB ms (CA)	50%MFB ms (CA)	95%MFB ms (CA)	Total ms (CA)
Compress	2.222 (20)	4.000 (36)	5.444 (49)	6.667 (60)
Linear*	2.444 (22)	4.333 (39)	9.333 (84)	14.667 (132)
Averaged	2.556 (23)	4.222 (38)	6.000 (54)	7.889 (71)
Switching*	2.444 (22)	4.667 (42)	10.444 (94)	14.667 (132)

(C)	5%MFB ms (CA)	50%MFB ms (CA)	95%MFB ms (CA)	Total ms (CA)
Compress	2.222 (20)	4.000 (36)	5.333 (48)	6.556 (59)
Linear	2.333 (21)	4.222 (38)	6.889 (62)	11.333 (102)
Averaged	2.556 (23)	4.111 (37)	5.889 (53)	7.889 (71)
Switching	2.333 (21)	4.333 (39)	7.778 (70)	11.333 (102)

(D)	5%MFB ms (CA)	50%MFB ms (CA)	95%MFB ms (CA)	Total ms (CA)
Compress	2.222 (20)	4.000 (36)	5.444 (49)	6.667 (60)
Linear*	2.444 (22)	4.333 (39)	9.333 (84)	14.667 (132)
Averaged	2.556 (23)	4.222 (38)	6.000 (54)	7.889 (71)
Switching*	2.444 (22)	4.667 (42)	10.444 (94)	14.667 (132)

Figure 5-12 The effects of data smoothing on MFB results with different polytropic index methods. Engine operated in lower speed condition (IG timing: -31° CA ATDC).

(1) Standard condition

(A)	5%MFB ms (CA)	50%MFB ms (CA)	95%MFB ms(CA)	Total ms (CA)
Compress	2.000 (24)	3.750 (45)	5.167 (62)	5.917 (71)
Linear	2.083 (25)	3.833 (46)	5.500 (66)	7.000 (84)
Averaged	2.167 (26)	3.833 (46)	5.250 (63)	6.167 (74)
Switching	2.083 (25)	3.917 (47)	5.583 (67)	7.000 (84)

[(B) - (A)] / (A)	5%MFB	50%MFB	95%MFB	Total
Compress	0.00%	0.00%	0.00%	4.23%
Linear	0.00%	2.19%	1.51%	7.14%
Averaged	0.00%	0.00%	1.58%	8.11%
Switching	0.00%	0.00%	1.50%	7.14%

[(C) - (A)] / (A)	5%MFB	50%MFB	95%MFB	Total
Compress	0.00%	0.00%	0.00%	2.81%
Linear	0.00%	0.00%	0.00%	7.14%
Averaged	0.00%	0.00%	1.58%	6.75%
Switching	0.00%	0.00%	0.00%	7.14%

[(D) - (A)] / (A)	5%MFB	50%MFB	95%MFB	Total
Compress	0.00%	0.00%	0.00%	4.23%
Linear	0.00%	2.19%	1.51%	7.14%
Averaged	0.00%	0.00%	1.58%	8.11%
Switching	0.00%	0.00%	1.50%	7.14%

(2) Higher Load condition

(A)	5%MFB ms (CA)	50%MFB ms (CA)	95%MFB ms(CA)	Total ms (CA)
Compress	1.667 (20)	2.917 (35)	3.917 (47)	4.917 (59)
Linear	1.750 (21)	3.000 (36)	4.917 (59)	7.667 (92)
Averaged	1.833 (22)	3.000 (36)	4.250 (51)	5.750 (69)
Switching	1.750 (21)	3.083 (37)	5.417 (65)	7.667 (92)

[(B) - (A)] / (A)	5%MFB	50%MFB	95%MFB	Total
Compress	0.00%	0.00%	2.12%	1.69%
Linear*	0.00%	2.77%	44.05%	47.82%
Averaged	0.00%	0.00%	1.95%	4.35%
Switching*	4.74%	8.11%	39.99%	47.82%

[(C) - (A)] / (A)	5%MFB	50%MFB	95%MFB	Total
Compress	0.00%	0.00%	0.00%	0.00%
Linear	0.00%	0.00%	-1.71%	11.95%
Averaged	0.00%	0.00%	0.00%	2.90%
Switching	0.00%	0.00%	10.76%	11.95%

[(D) - (A)] / (A)	5%MFB	50%MFB	95%MFB	Total
Compress	0.00%	0.00%	2.12%	1.69%
Linear*	0.00%	2.77%	28.80%	46.73%
Averaged	0.00%	0.00%	1.95%	4.35%
Switching*	4.74%	8.11%	39.99%	46.73%

(3) Lower Speed condition (IG timing: -31° CA ATDC)

(A)	5%MFB ms (CA)	50%MFB ms (CA)	95%MFB ms(CA)	Total ms (CA)
Compress	2.222 (20)	4.000 (36)	5.333 (48)	6.556 (59)
Linear	2.333 (21)	4.222 (38)	6.889 (62)	8.889 (80)
Averaged	2.556 (23)	4.111 (37)	5.889 (53)	7.556 (68)
Switching	2.333 (21)	4.333 (39)	7.111 (64)	8.889 (80)

[(B) - (A)] / (A)	5%MFB	50%MFB	95%MFB	Total
Compress	0.00%	0.00%	2.08%	1.69%
Linear*	4.76%	2.63%	35.48%	65.00%
Averaged	0.00%	2.70%	1.88%	4.41%
Switching*	4.76%	7.71%	46.87%	65.00%

[(C) - (A)] / (A)	5%MFB	50%MFB	95%MFB	Total
Compress	0.00%	0.00%	0.00%	0.00%
Linear	0.00%	0.00%	0.00%	27.49%
Averaged	0.00%	0.00%	0.00%	4.41%
Switching	0.00%	0.00%	9.38%	27.49%

[(D) - (A)] / (A)	5%MFB	50%MFB	95%MFB	Total
Compress	0.00%	0.00%	2.08%	1.69%
Linear*	4.76%	2.63%	35.48%	65.00%
Averaged	0.00%	2.70%	1.88%	4.41%
Switching*	4.76%	7.71%	46.87%	65.00%

Table 5-1 The differences of MFB calculation between raw and smoothed data under diferent operating conditions and polytropic index values.

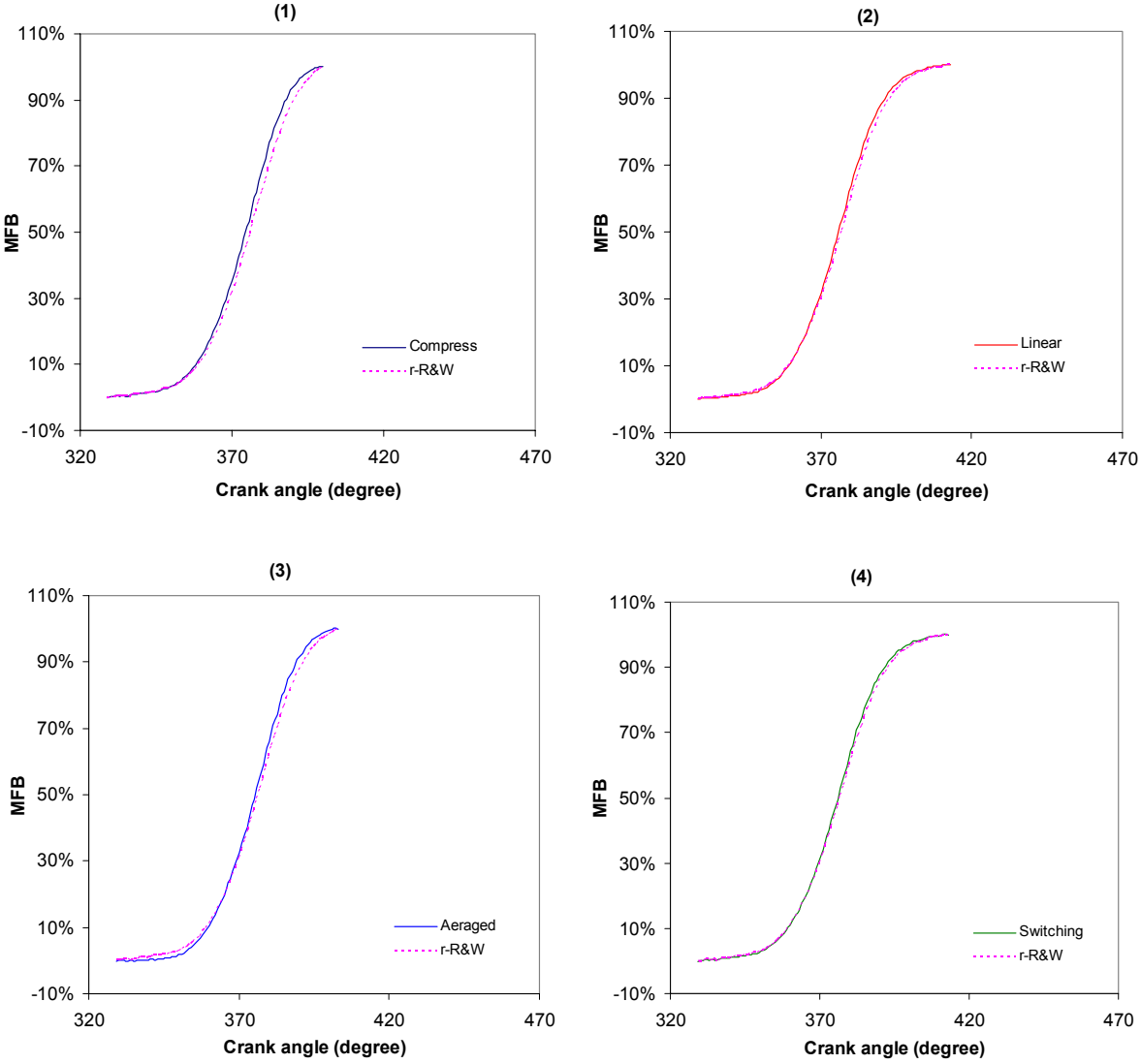

(1)	5%MFB ms (CA)	50%MFB ms (CA)	95%MFB ms (CA)	Total ms (CA)
Compress	0.00%	-4.26%	-4.62%	5.917 (71)
r-R&W	2.000 (24)	3.917 (47)	5.417 (65)	

(2)	5%MFB ms (CA)	50%MFB ms (CA)	95%MFB ms (CA)	Total ms (CA)
Linear	0.00%	-2.13%	-2.94%	7.000 (84)
r-R&W	2.083 (25)	3.917 (47)	5.667 (68)	

(3)	5%MFB ms (CA)	50%MFB ms (CA)	95%MFB ms (CA)	Total ms (CA)
Averaged	8.33%	-2.13%	-4.55%	6.167 (74)
r-R&W	2.000 (24)	3.917 (47)	5.500 (66)	

(4)	5%MFB ms (CA)	50%MFB ms (CA)	95%MFB ms (CA)	Total ms (CA)
Switching	0.00%	0.00%	-1.47%	7.000 (84)
r-R&W	2.083 (25)	3.917 (47)	5.667 (68)	

Figure 5-13 The comparison of MFB results between different polytropic index methods and revised R&W model. Data smoothing method: raw data; engine operated in standard condition. Percentages stand for the deviation from the r-R&W model.

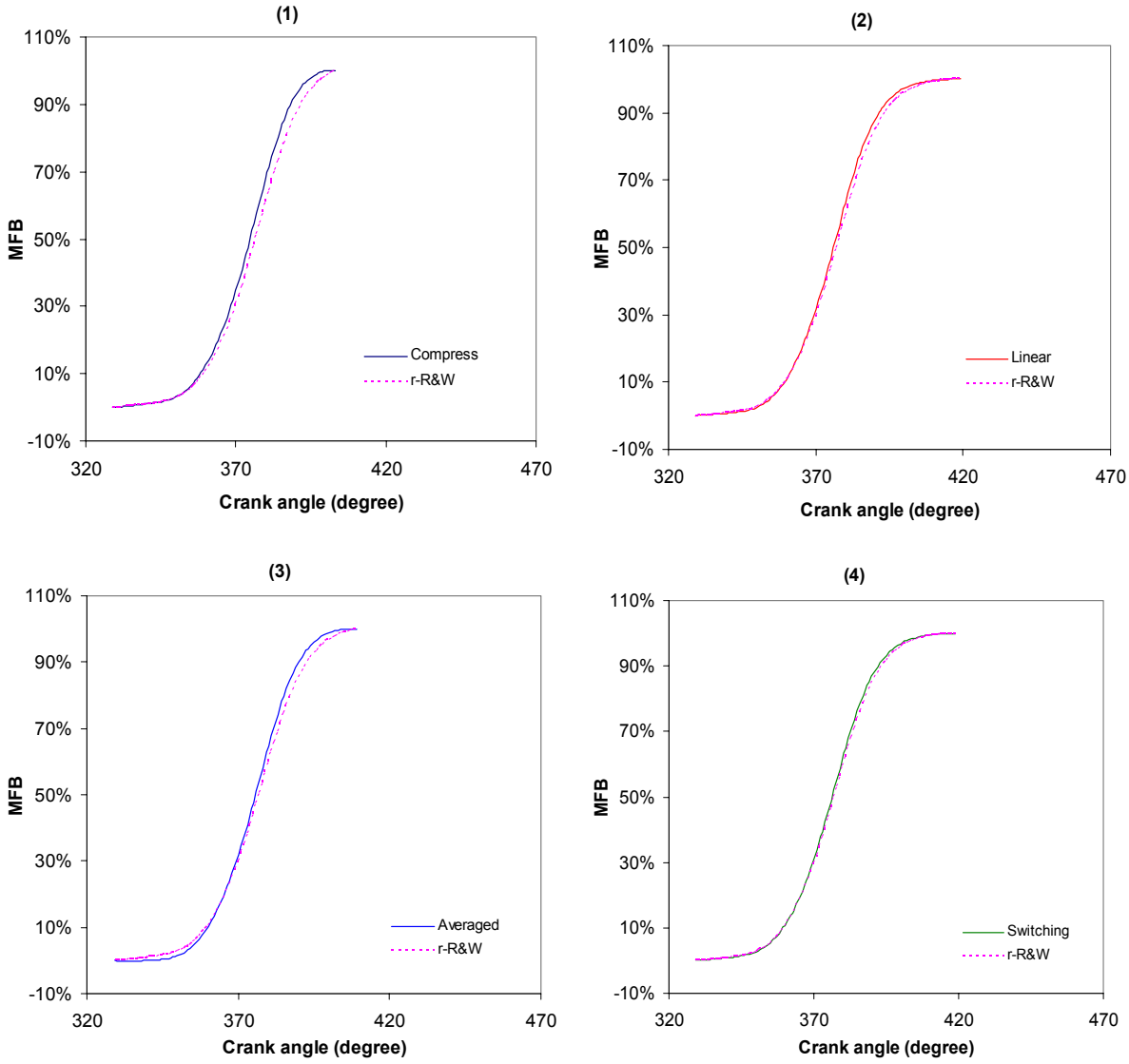

(1)	5%MFB ms (CA)	50%MFB ms (CA)	95%MFB ms (CA)	Total ms (CA)
Compress	-4.00%	-4.26%	-6.06%	6.167 (74)
r-R&W	2.083 (25)	3.917 (47)	5.500 (66)	

(2)	5%MFB ms (CA)	50%MFB ms (CA)	95%MFB ms (CA)	Total ms (CA)
Linear	0.00%	0.00%	-2.90%	7.500 (90)
r-R&W	2.083 (25)	3.917 (47)	5.750 (69)	

(3)	5%MFB ms (CA)	50%MFB ms (CA)	95%MFB ms (CA)	Total ms (CA)
Averaged	4.00%	-2.13%	-5.88%	6.667 (80)
r-R&W	2.083 (25)	3.917 (47)	5.667(68)	

(4)	5%MFB ms (CA)	50%MFB ms (CA)	95%MFB ms (CA)	Total ms (CA)
Switching	0.00%	0.00%	-1.45%	7.500 (90)
r-R&W	2.083 (25)	3.917 (47)	5.750 (69)	

Figure 5-14 The comparison of MFB results between different polytropic index methods and revised R&W model. Data smoothing method: low pass filter; engine operated in standard condition. Percentages stand for the deviation from the r-R&W model.

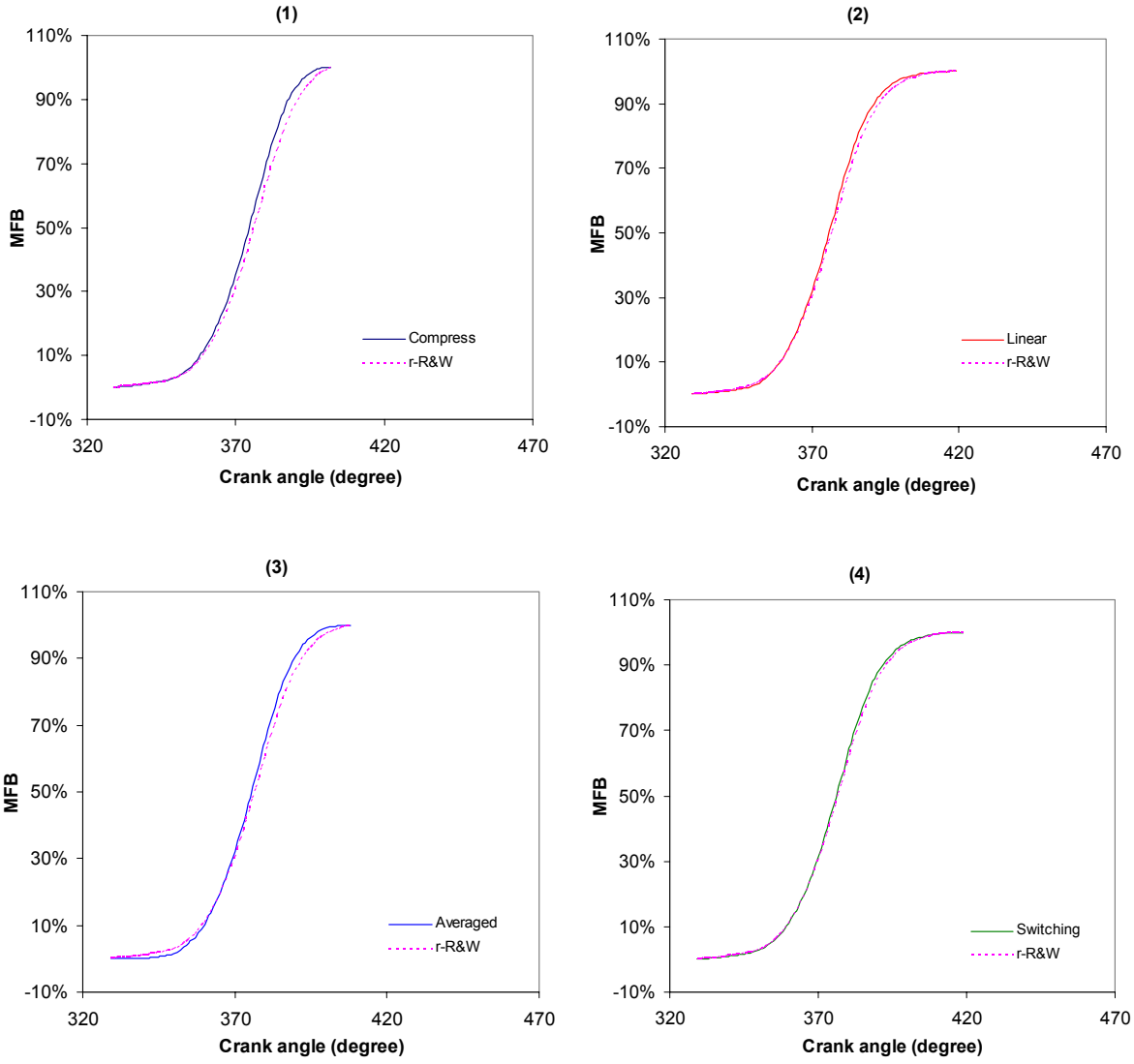

(1)	5%MFB ms (CA)	50%MFB ms (CA)	95%MFB ms (CA)	Total ms (CA)
Compress	0.00%	-4.26%	-4.62%	6.083 (73)
r-R&W	2.000 (24)	3.917 (47)	5.417 (65)	

(2)	5%MFB ms (CA)	50%MFB ms (CA)	95%MFB ms (CA)	Total ms (CA)
Linear	0.00%	-2.13%	-4.35%)	7.500 (90)
r-R&W	2.083 (25)	3.917 (47)	5.750 (69)	

(3)	5%MFB ms (CA)	50%MFB ms (CA)	95%MFB ms (CA)	Total ms (CA)
Averaged	8.33%	-2.13%	-4.48%	6.583 (79)
r-R&W	2.000 (24)	3.917 (47)	5.583 (67)	

(4)	5%MFB ms (CA)	50%MFB ms (CA)	95%MFB ms (CA)	Total ms (CA)
Switching	0.00%	0.00%	-2.90%	7.500 (90)
r-R&W	2.083 (25)	3.917 (47)	5.750 (69)	

Figure 5-15 The comparison of MFB results between different polytropic index methods and revised R&W model. Data smoothing method: 9 points weighted smoothing; engine operated in standard condition. Percentages stand for the deviation from the r-R&W model.

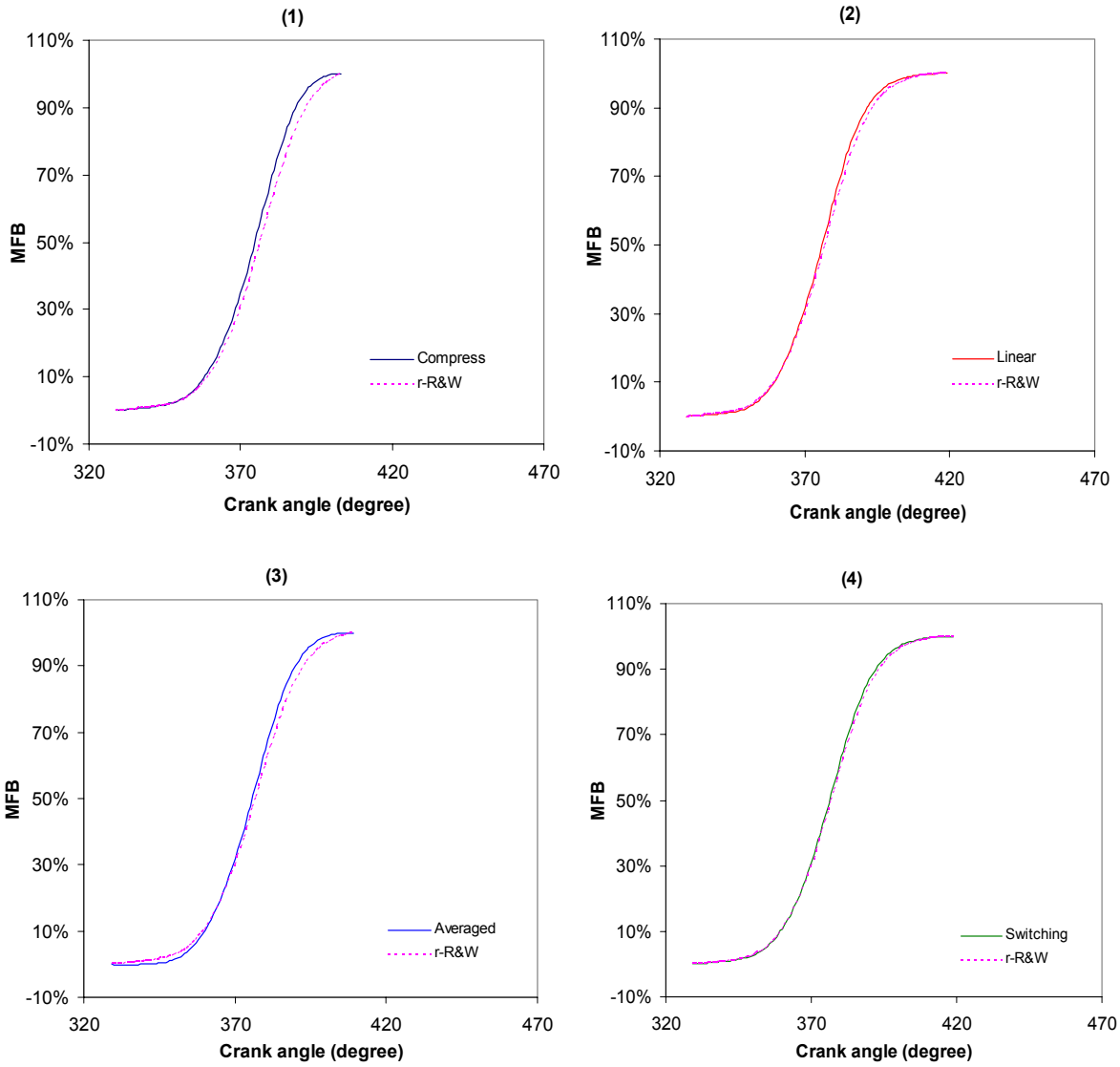

(1)	5%MFB ms (CA)	50%MFB ms (CA)	95%MFB ms (CA)	Total ms (CA)
Compress	-4.00%	-4.26%	-6.06%	6.167 (74)
r-R&W	2.083 (25)	3.917 (47)	5.500 (66)	

(2)	5%MFB ms (CA)	50%MFB ms (CA)	95%MFB ms (CA)	Total ms (CA)
Linear	0.00%	0.00%	-2.90%	7.500 (90)
r-R&W	2.083 (25)	3.917 (47)	5.750 (69)	

(3)	5%MFB ms (CA)	50%MFB ms (CA)	95%MFB ms (CA)	Total ms (CA)
Averaged	4.00%	-2.13%	-5.88%	6.667 (80)
r-R&W	2.083 (25)	3.917 (47)	5.667 (68)	

(4)	5%MFB ms (CA)	50%MFB ms (CA)	95%MFB ms (CA)	Total ms (CA)
Switching	0.00%	0.00%	-1.45%	7.500 (90)
r-R&W	2.083 (25)	3.917 (47)	5.750 (69)	

Figure 5-16 The comparison of MFB results between different polytropic index methods and revised R&W model. Data smoothing method: LPF + 9PWS; engine operated in standard condition. Percentages stand for the deviation from the r-R&W model.

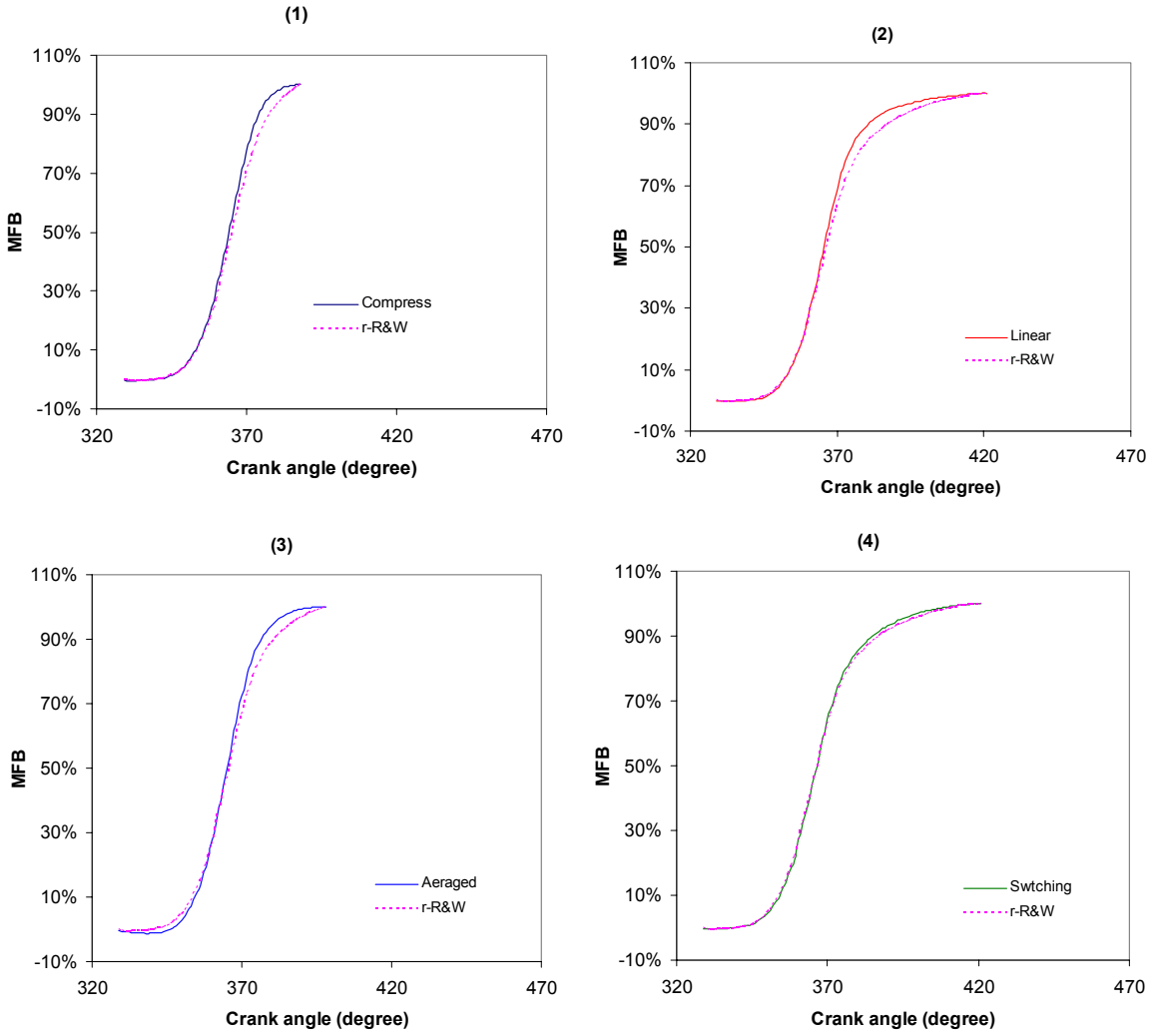

(1)	5%MFB ms (CA)	50%MFB ms (CA)	95%MFB ms (CA)	Total ms (CA)
Compress	-4.76%	-2.78%	-9.62%	4.917 (59)
r-R&W	1.750 (21)	3.000 (36)	4.333 (52)	

(2)	5%MFB ms (CA)	50%MFB ms (CA)	95%MFB ms (CA)	Total ms (CA)
Linear	0.00%	-2.70%	-13.24%	7.667 (92)
r-R&W	1.750 (21)	3.083 (37)	5.667 (68)	

(3)	5%MFB ms (CA)	50%MFB ms (CA)	95%MFB ms (CA)	Total ms (CA)
Averaged	4.76%	0.00%	-10.53%	5.750 (69)
r-R&W	1.750 (21)	3.000 (36)	4.750 (57)	

(4)	5%MFB ms (CA)	50%MFB ms (CA)	95%MFB ms (CA)	Total ms (CA)
Switching	0.00%	0.00%	-4.41%	7.667 (92)
r-R&W	1.750 (21)	3.083 (37)	5.667 (68)	

Figure 5-17 The comparison of MFB results between different polytropic index methods and revised R&W model. Data smoothing method: raw data; engine operated in higher load condition. Percentages stand for the deviation from the r-R&W model.

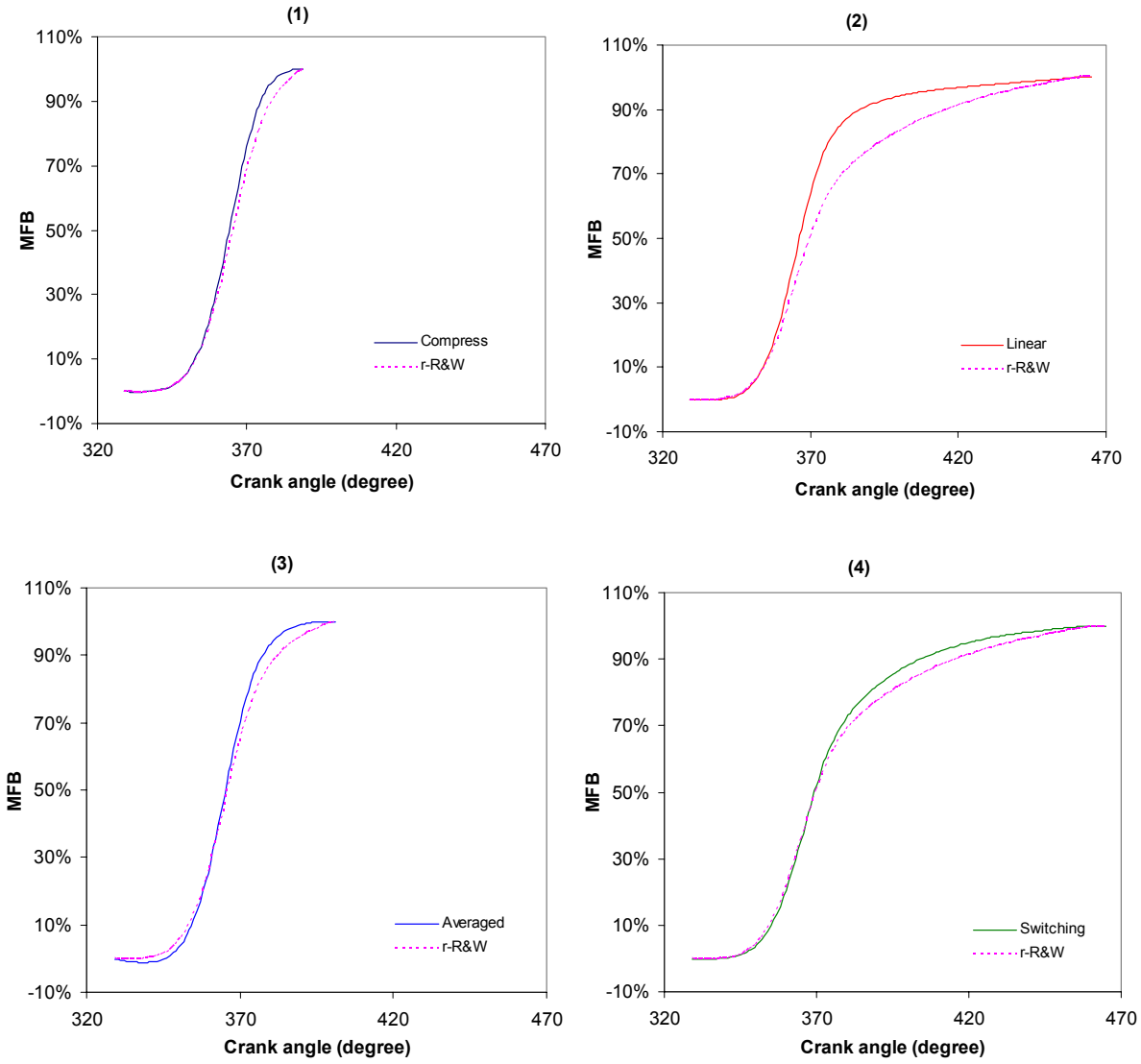

(1)	5%MFB ms (CA)	50%MFB ms (CA)	95%MFB ms (CA)	Total ms (CA)
Compress	0.00%	-2.78%	-9.43%	5.000 (60)
r-R&W	1.667 (20)	3.000 (36)	4.417 (53)	

(2)*	5%MFB ms (CA)	50%MFB ms (CA)	95%MFB ms (CA)	Total ms (CA)
Linear	0.00%	-7.5%	-18.28%	11.333 (136)
r-R&W	1.750 (21)	3.333 (40)	8.667 (104)	

(3)	5%MFB ms (CA)	50%MFB ms (CA)	95%MFB ms (CA)	Total ms (CA)
Averaged	9.96%	-2.69%	-11.94%	6.000 (72)
r-R&W	1.667 (20)	3.083 (37)	4.917 (59)	

(4)*	5%MFB ms (CA)	50%MFB ms (CA)	95%MFB ms (CA)	Total ms (CA)
Switching	4.74%	0.00%	-12.51%	11.333 (136)
r-R&W	1.750 (21)	3.333 (40)	8.667 (104)	

Figure 5-18 The comparison of MFB results between different polytropic index methods and revised R&W model. Data smoothing method: low pass filter; engine operated in higher load condition. Percentages stand for the deviation from the r-R&W model.

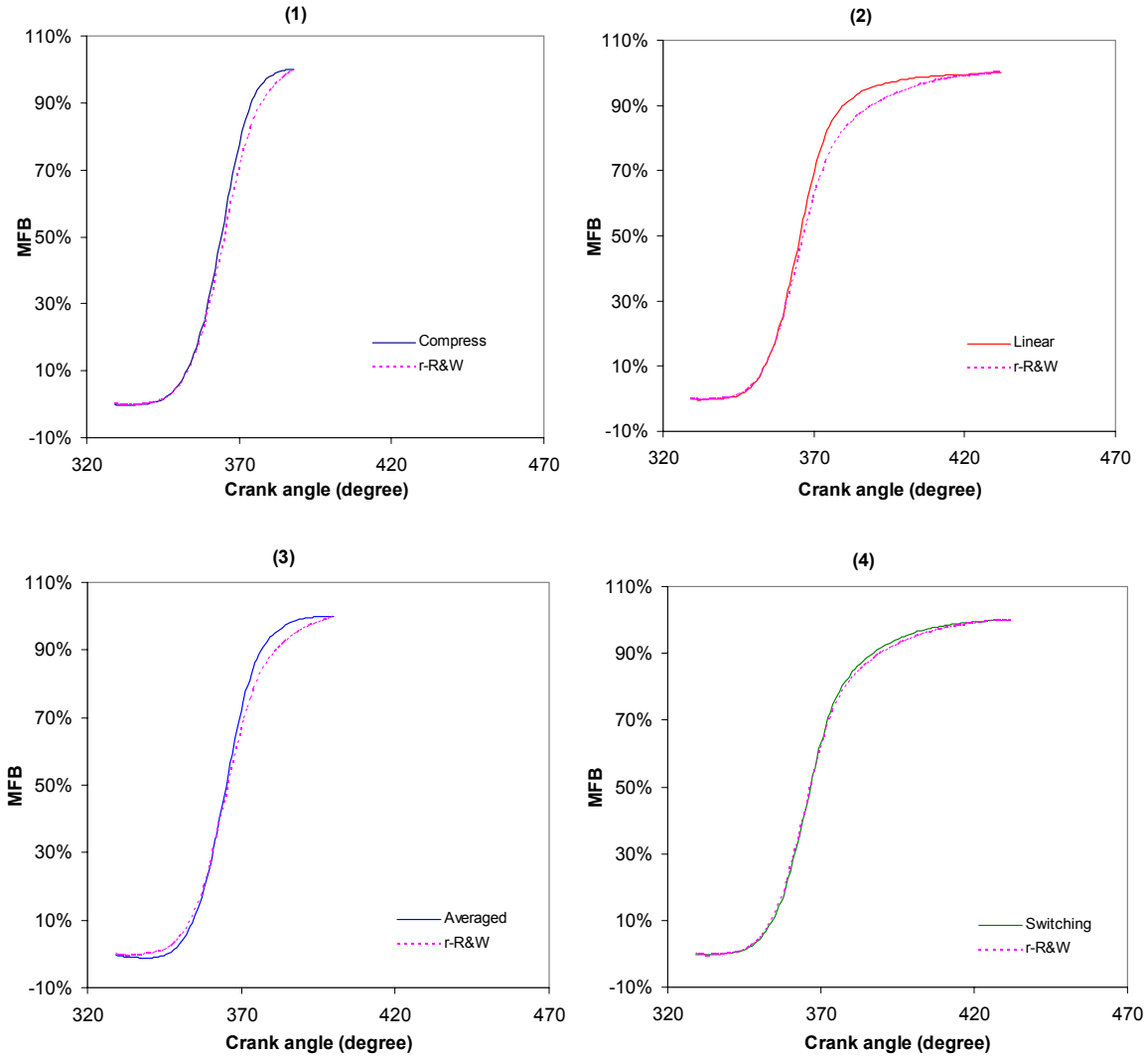

(1)	5%MFB ms (CA)	50%MFB ms (CA)	95%MFB ms (CA)	Total ms (CA)
Compress	0.00%	-2.78%	-9.62%	4.917 (59)
r-R&W	1.667 (20)	3.000 (36)	4.333 (52)	

(2)	5%MFB ms (CA)	50%MFB ms (CA)	95%MFB ms (CA)	Total ms (CA)
Linear	0.00%	-2.70%	-19.44%	8.583 (103)
r-R&W	1.750 (21)	3.083 (37)	6.000 (72)	

(3)	5%MFB ms (CA)	50%MFB ms (CA)	95%MFB ms (CA)	Total ms (CA)
Averaged	4.76%	0.00%	-12.07%	5.917 (71)
r-R&W	1.750 (21)	3.000 (36)	4.833 (58)	

(4)	5%MFB ms (CA)	50%MFB ms (CA)	95%MFB ms (CA)	Total ms (CA)
Switching	0.00%	0.00%	-5.56%	8.583 (103)
r-R&W	1.750 (21)	3.083 (37)	6.000 (72)	

Figure 5-19 The comparison of MFB results between different polytropic index methods and revised R&W model. Data smoothing method: 9 points weighted smoothing; engine operated in higher load condition. Percentages stand for the deviation from the r-R&W model.

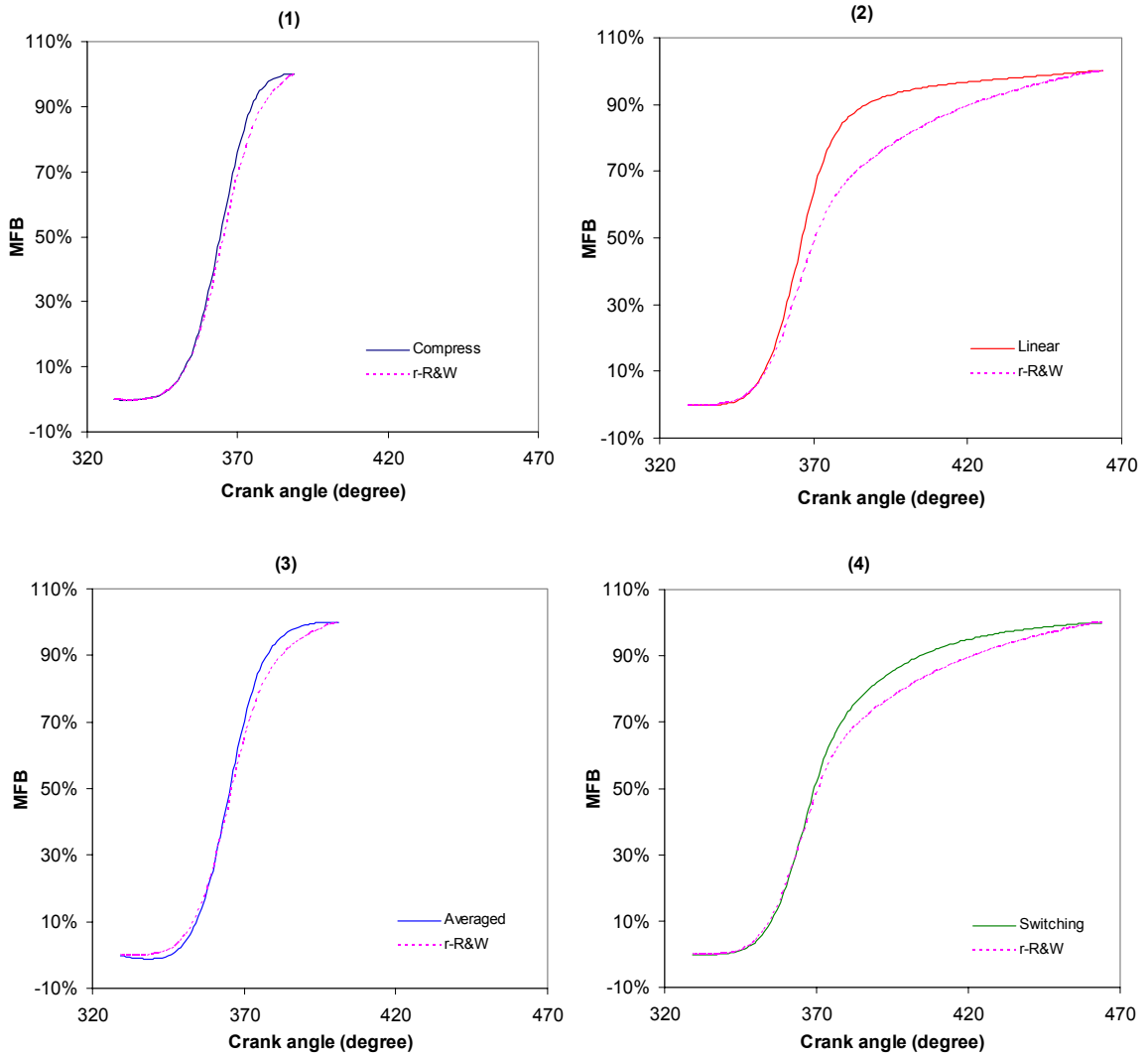

(1)	5%MFB ms (CA)	50%MFB ms (CA)	95%MFB ms (CA)	Total ms (CA)
Compress	0.00%	-2.78%	9.43%	5.000 (60)
r- R&W	1.667 (20)	3.000 (36)	4.417 (53)	

(2)*	5%MFB ms (CA)	50%MFB ms (CA)	95%MFB ms (CA)	Total ms (CA)
Linear	0.00%	-9.76%	-30.28%	11.250 (135)
r-R&W	1.750 (21)	3.417 (41)	9.083 (109)	

(3)	5%MFB ms (CA)	50%MFB ms (CA)	95%MFB ms (CA)	Total ms (CA)
Averaged	10.00%	-2.70%	-11.86%	6.000 (72)
r-R&W	1.667 (20)	3.083 (37)	4.917 (59)	

(4)*	5%MFB ms (CA)	50%MFB ms (CA)	95%MFB ms (CA)	Total ms (CA)
Switching	4.76%	-2.44%	-16.51%	11.250 (135)
r-R&W	1.750 (21)	3.417 (41)	9.083 (109)	

Figure 5-20 The comparison of MFB results between different polytropic index methods and revised R&W model. Data smoothing method: LPF + 9PWS; engine operated in higher load condition. Percentages stand for the deviation from the r-R&W model.

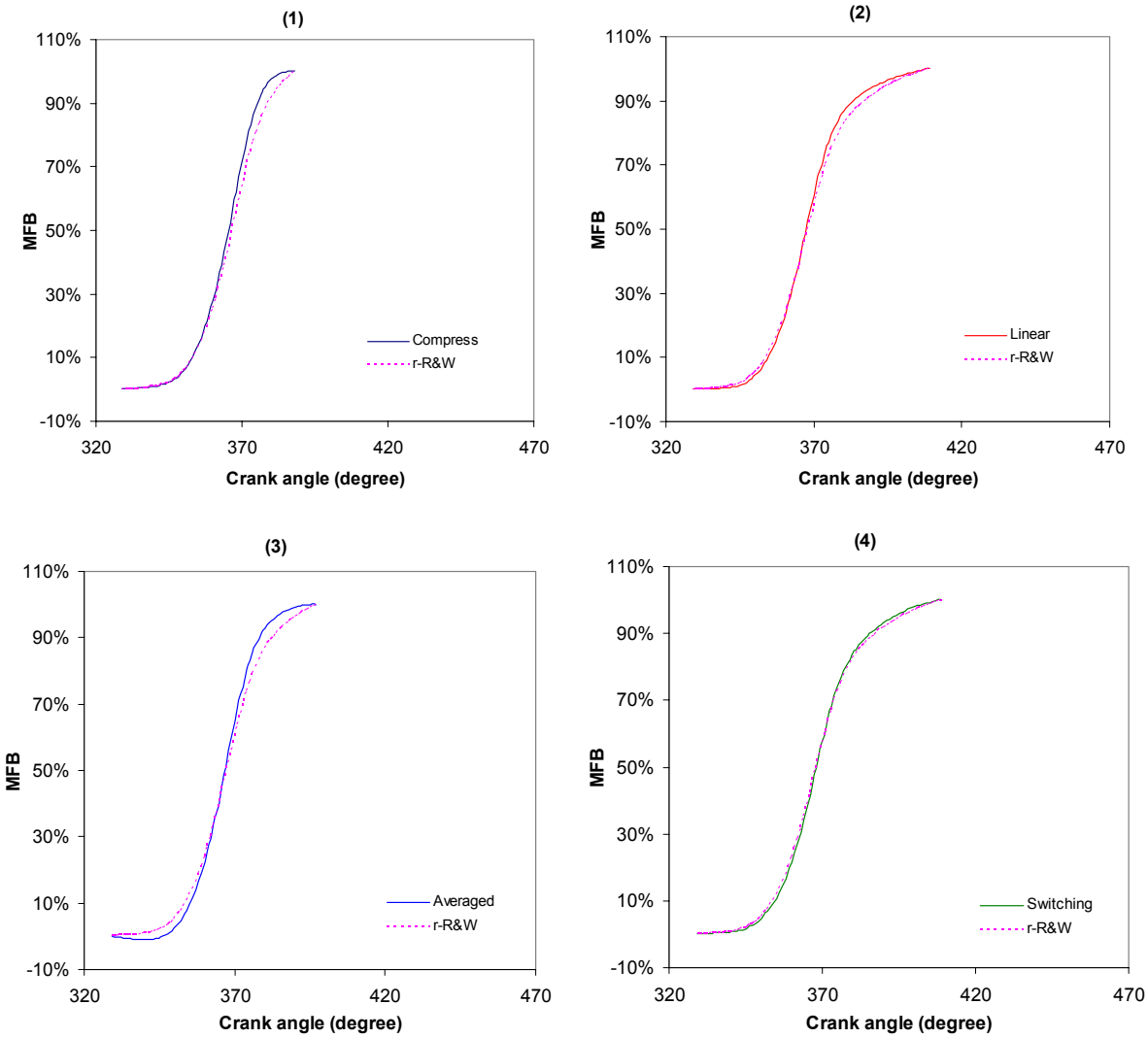

(1)	5%MFB ms (CA)	50%MFB ms (CA)	95%MFB ms (CA)	Total ms (CA)
Compress	0.00%	-2.70%	-9.43%	6.556 (59)
r-R&W	2.222 (20)	4.111 (37)	5.889 (53)	

(2)	5%MFB ms (CA)	50%MFB ms (CA)	95%MFB ms (CA)	Total ms (CA)
Linear	5.00%	-2.56%	-6.06%	8.889 (80)
r-R&W	2.222 (20)	4.333 (39)	7.333 (66)	

(3)	5%MFB ms (CA)	50%MFB ms (CA)	95%MFB ms (CA)	Total ms (CA)
Averaged	15.00%	-2.63%	-10.17%	7.556 (68)
r-R&W	2.222 (20)	4.222 (38)	6.556 (59)	

(4)	5%MFB ms (CA)	50%MFB ms (CA)	95%MFB ms (CA)	Total ms (CA)
Switching	5.00%	0.00%	-3.03%	8.889 (80)
r-R&W	2.222 (20)	4.333 (39)	7.333 (66)	

Figure 5-21 The comparison of MFB results between different polytropic index methods and revised R&W model. Data smoothing method: raw data; engine operated in lower speed condition (IG timing: -31° CA ATDC). Percentages stand for the deviation from the r-R&W model.

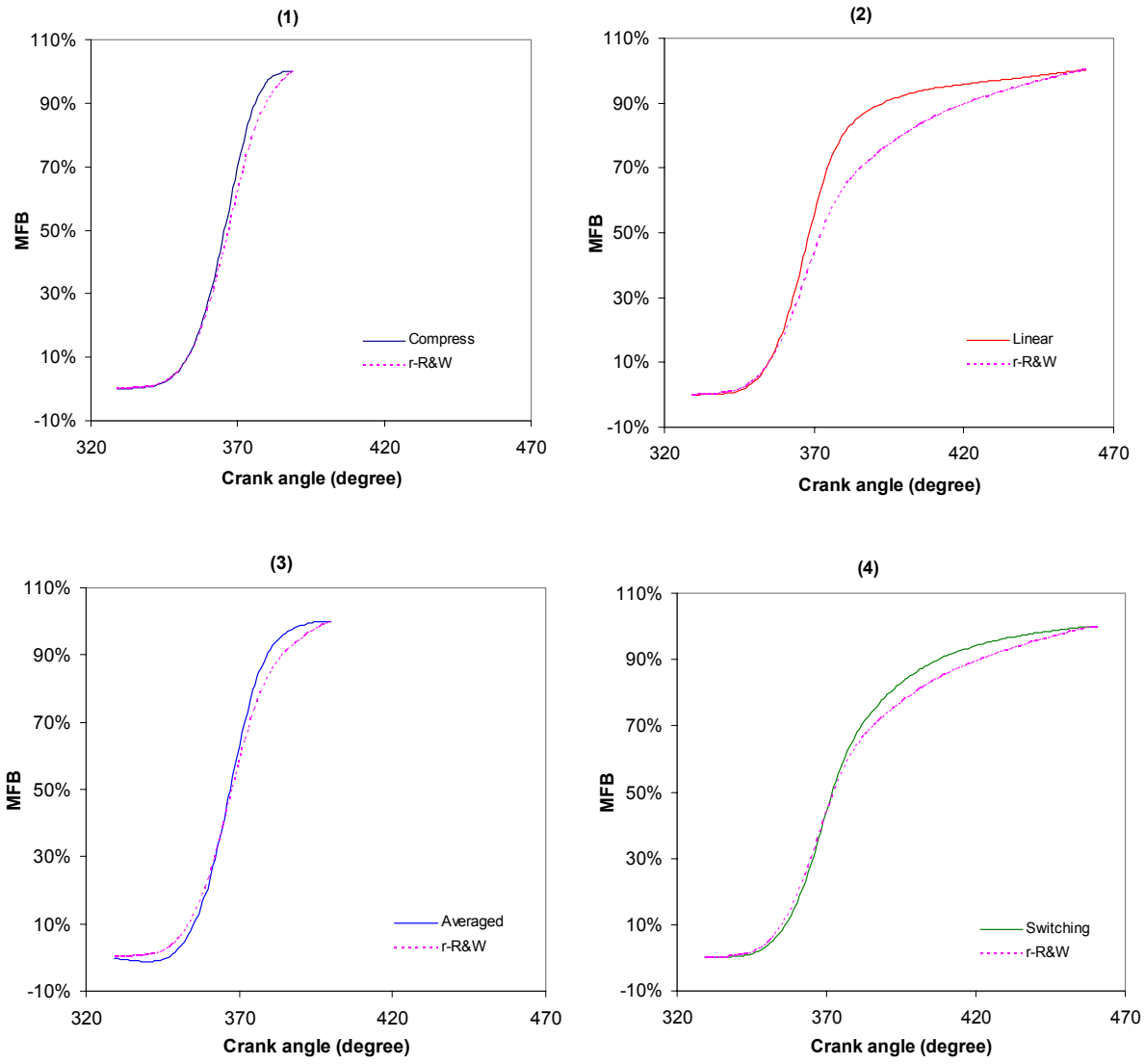

(1)	5%MFB ms (CA)	50%MFB ms (CA)	95%MFB ms (CA)	Total ms (CA)
Compress	0.00%	-2.70%	-9.26%	6.667 (60)
r-R&W	2.222 (20)	4.111 (37)	6.000 (54)	

(2)*	5%MFB ms (CA)	50%MFB ms (CA)	95%MFB ms (CA)	Total ms (CA)
Linear	4.76%	-9.30%	-22.94%	14.667 (132)
r-R&W	2.333 (21)	4.778 (43)	12.111 (109)	

(3)	5%MFB ms (CA)	50%MFB ms (CA)	95%MFB ms (CA)	Total ms (CA)
Averaged	15.00%	0.00%	-11.48%	7.889 (71)
r-R&W	2.222 (20)	4.222 (38)	6.778 (61)	

(4)*	5%MFB ms (CA)	50%MFB ms (CA)	95%MFB ms (CA)	Total ms (CA)
Switching	4.76%	-2.33%	-13.76%	14.667 (132)
r-R&W	2.333 (21)	4.778 (43)	12.111 (109)	

Figure 5-22 The comparison of MFB results between different polytropic index methods and revised R&W model. Data smoothing method: low pass filter; engine operated in lower speed condition (IG timing: -31° CA ATDC). Percentages stand for the deviation from the r-R&W model.

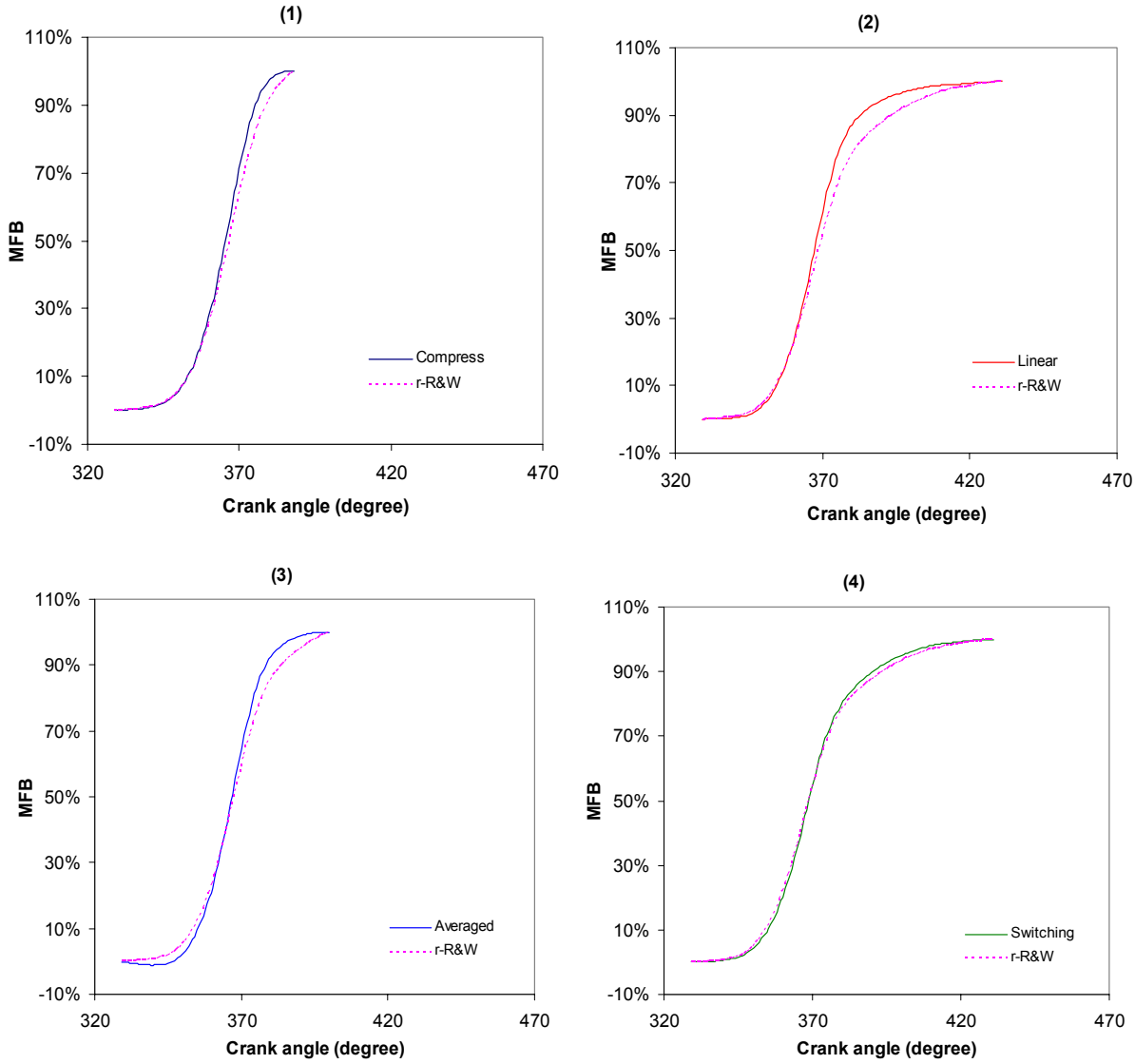

(1)	5%MFB ms (CA)	50%MFB ms (CA)	95%MFB ms (CA)	Total ms (CA)
Compress	0.00%	-2.70%	-9.43%	6.556 (59)
r-R&W	2.222 (20)	4.111 (37)	5.889 (53)	

(2)	5%MFB ms (CA)	50%MFB ms (CA)	95%MFB ms (CA)	Total ms (CA)
Linear	0.00%	-2.56%	-17.33%	11.333 (102)
r-R&W	2.333 (21)	4.333 (39)	8.333 (75)	

(3)	5%MFB ms (CA)	50%MFB ms (CA)	95%MFB ms (CA)	Total ms (CA)
Averaged	15.0%	-2.63%	-11.67%	7.889 (71)
r-R&W	2.222 (20)	4.222 (38)	6.667 (60)	

(4)	5%MFB ms (CA)	50%MFB ms (CA)	95%MFB ms (CA)	Total ms (CA)
Switching	0.00%	0.00%	-6.67%	11.333 (102)
r-R&W	2.333 (21)	4.333 (39)	8.333 (75)	

Figure 5-23 The comparison of MFB results between different polytropic index methods and revised R&W model. Data smoothing method: 9 points weighted smoothing; engine operated in lower speed condition (IG timing: -31° CA ATDC). Percentages stand for the deviation from the r-R&W model.

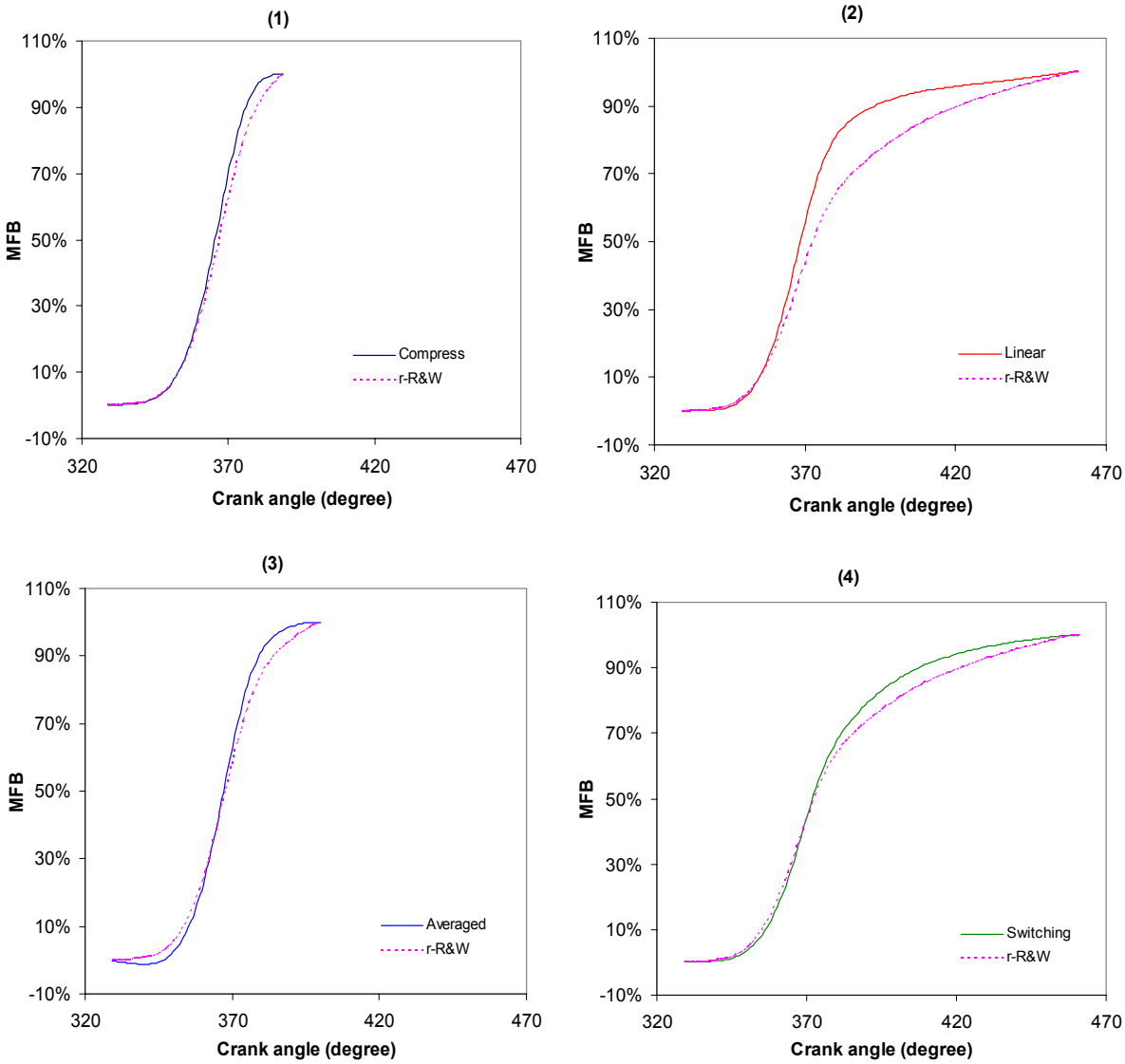

(1)	5%MFB ms (CA)	50%MFB ms (CA)	95%MFB ms (CA)	Total ms (CA)
Compress	0.00%	-2.70%	-9.26%	6.667 (60)
r-R&W	2.222 (20)	4.111 (37)	6.000 (54)	

(2)*	5%MFB ms (CA)	50%MFB ms (CA)	95%MFB ms (CA)	Total ms (CA)
Linear	4.76%	-9.30%	-22.94%	14.667 (132)
r-R&W	2.333 (21)	4.778 (43)	12.111 (109)	

(3)	5%MFB ms (CA)	50%MFB ms (CA)	95%MFB ms (CA)	Total ms (CA)
Averaged	15.00%	0.00%	-11.48%	7.889 (71)
r-R&W	2.222 (20)	4.222 (38)	6.778 (61)	

(4)*	5%MFB ms (CA)	50%MFB ms (CA)	95%MFB ms (CA)	Total ms (CA)
Switching	4.76%	-2.33%	-13.76%	14.667 (132)
r-R&W	2.333 (21)	4.778 (43)	12.111 (109)	

Figure 5-24 The comparison of MFB results between different polytropic index methods and revised R&W model. Data smoothing method: LPF + 9PWS; engine operated in lower speed condition (IG timing: -31° CA ATDC). Percentages stand for the deviation from the r-R&W model.

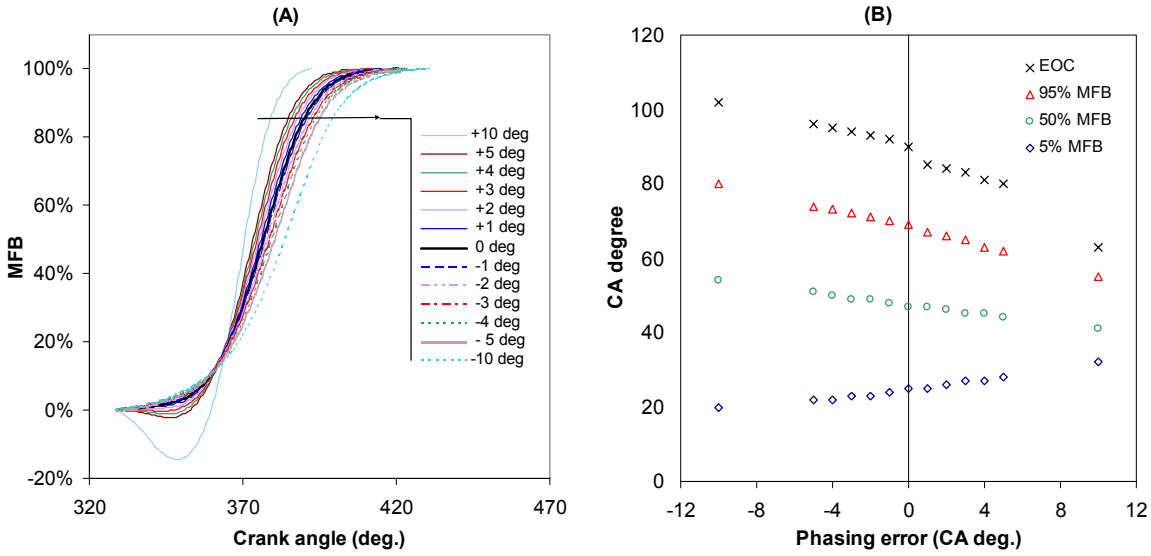

(C)

Phasing error (CA)	5%MFB (CA)	50%MFB (CA)	95%MFB (CA)	Total (CA)
-10	20	54	80	102
5	22	51	74	96
-4	22	50	73	95
-3	23	49	72	94
-2	23	49	71	93
-1	24	48	70	92
0	25	47	69	90
1	25	47	67	85
2	26	46	66	84
3	27	45	65	83
4	27	45	63	81
5	28	44	62	80
10	32	41	55	63

Figure 5-25 (A) Variations of MFB profile (B) Trend of each MFB stage (C) Table of required CA on each MFB stage – caused by phasing error in standard engine operating condition.

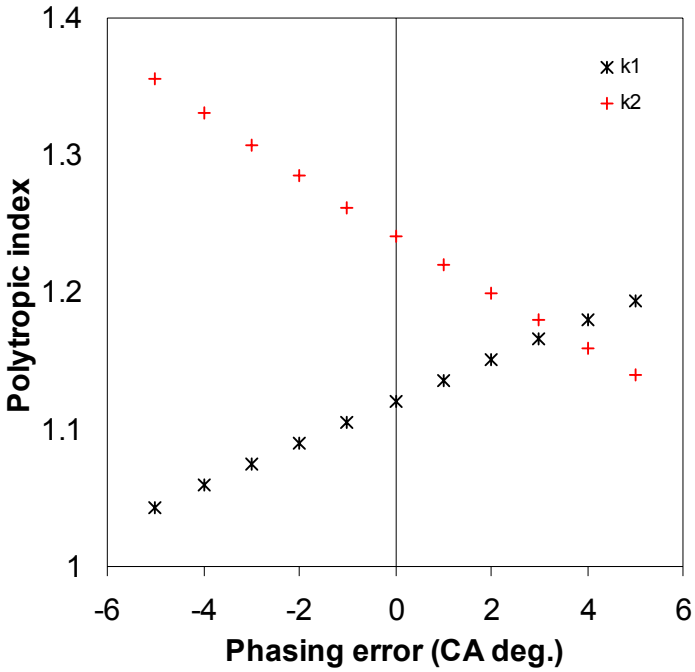

Figure 5-26 The influence of phasing error on the polytropic index.

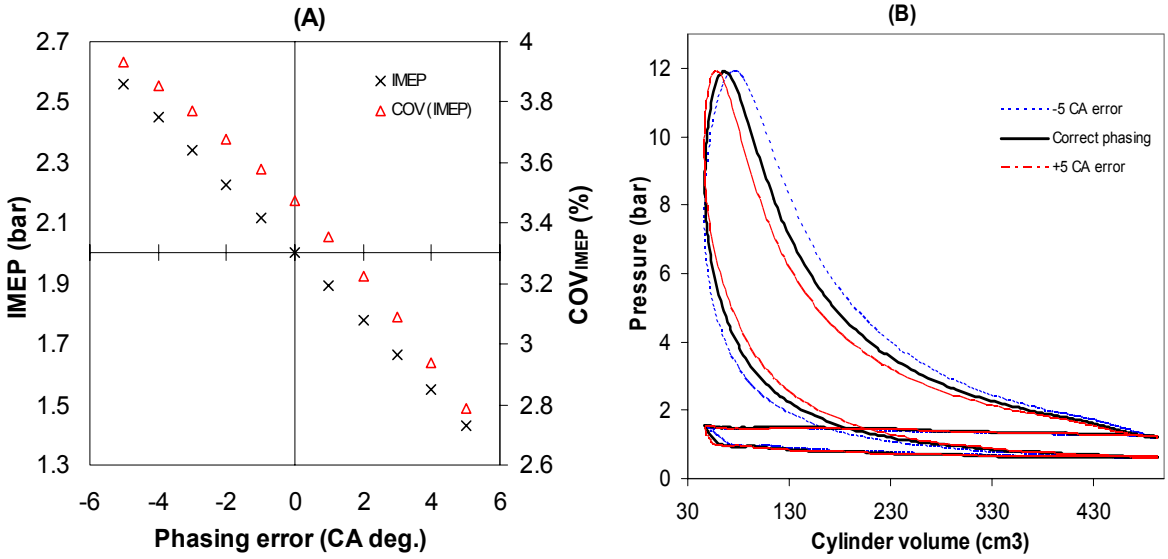

Figure 5-27 (A) Deviations of IMEP and COV_{IMEP} (B) Variations of P-V diagram – caused by phasing error in standard operating condition.

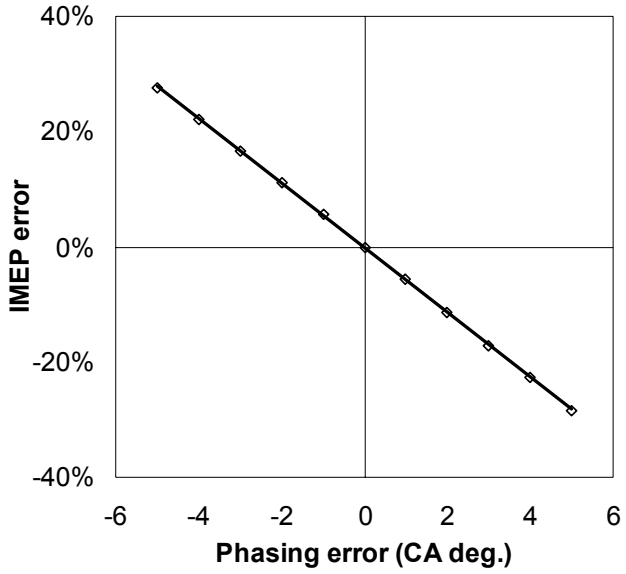

Figure 5-28 Correlation between IMEP error and phasing error.

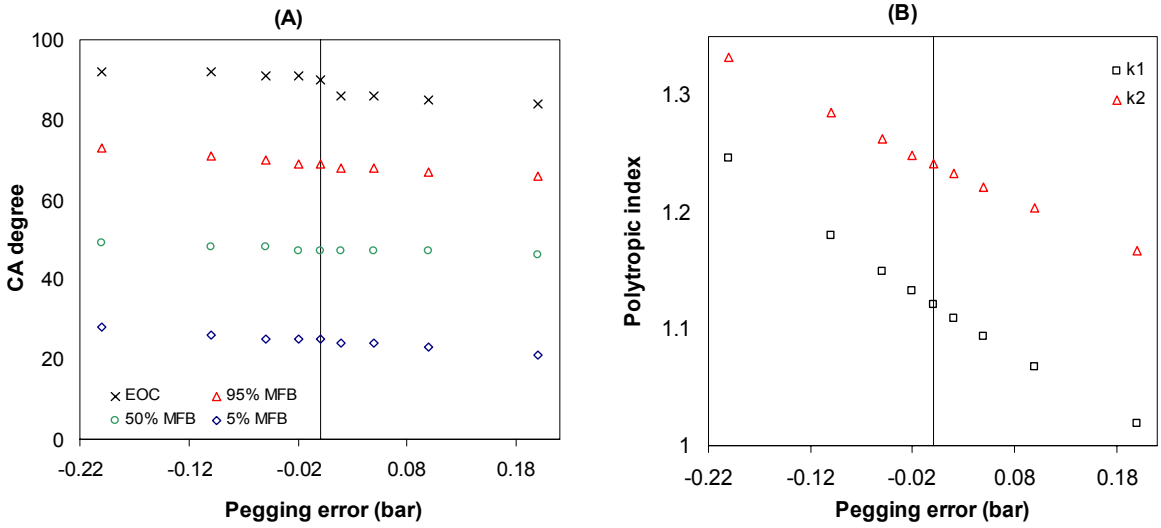

Figure 5-29 The effect of reference absolute pressure error on (A) MFB calculation, (B) Polytropic index values.

5.3. Validation of EOC point – the Comparison with 95% Mass Fraction Burned

Since now the EOC can be located more accurately by the method discussed above, it appears unnecessary to keep on using the 95% MFB as a combustion indicator; however, before the EOC finding mechanism can be verified by an optical observation research, the trends of EOC still needs to be verified with regard to 95% MFB by comparing the tendency of these two value in the same change of operating conditions.

The comparison will not be done individually here, but examined with the other following tests; therefore, the argument relating to this issue will be buried in the related discussions. Most of the figures showing the tendencies of MFB in this study will present both sets of information at the same time, which should make this assessment much easier.

6. EFFECTS ON COMBUSTION INDICATORS WHEN ADDING H_2/EGR INTO NATURAL GAS FUELLED ENGINE

Using the catalytic exhaust gas reforming reactor to produce hydrogen from NG fuel has been proved feasible by the Future Power Systems research group at the University of Birmingham; the product gas can then be applied in high level EGR dilution condition to increase the burn rate and maintain stable combustion. The relationship between hydrogen, EGR and the emissions results were discussed intensively in the IMechE paper by Allenby [99]. Hence, this chapter will concentrate on the effects of adding EGR and Hydrogen on the combustion indicators, i.e. IMEP, COV_{IMEP} and MFB. The correlations between the two additives and these indicators will be investigated firstly; results will then be used to explore the combined effects – conditions effectively similar to those when applying the fuel reforming method. With the use of hydrogen enriched natural gas fuel, the combustion stability (under 5% COV_{IMEP}) could still be maintained even when 25% EGR was added into the fuel.

6.1. Combustion Characteristics of Natural Gas

Methane is the main constituent of natural gas, although the composition may differ depending on the source gas field, the main components of natural gas in mass and volumetric

percentages are shown in Table 2-3. Compared with methane, natural gas has less specific energy (-4%), higher energy density (4%) and higher density (about 8%). However, the differences do not make any major difference to the combustion behaviours, Figure 6-1 illustrates the similarity. Base line tests in standard, higher load and lower speed conditions (the same definitions as Chapter 4.3) were conducted at the beginning of each set of tests, which aimed to set up reference data for comparing the additive effects, general results are shown in Figure 6-2. However, the real condition was slightly different in each test depending upon the actual engine operating condition and the environmental variables. In the standard condition, the smallest amount of crank angles rotation was needed to complete combustion; nevertheless, it required the longest ignition delay. The trend in 95% MFB does not agree with the tendency of EOC on the crank angle base because different speeds, however, the comparison in time base shows a similar behaviour between these two, which supports the accuracy of EOC finding mechanism used in this study.

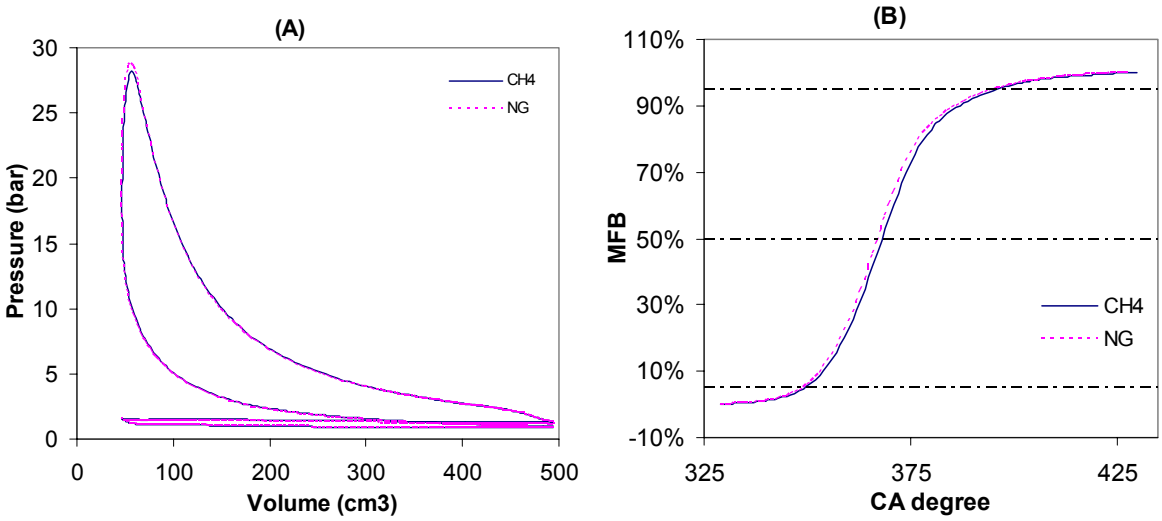

Figure 6-1 **Similar combustion behaviours between methane and natural gas fuel, engine ran at 2000 rpm, 4.3 bar IMEP and ignition timing -31° CA ATDC, (A) P-V diagram (B) MFB profile.**

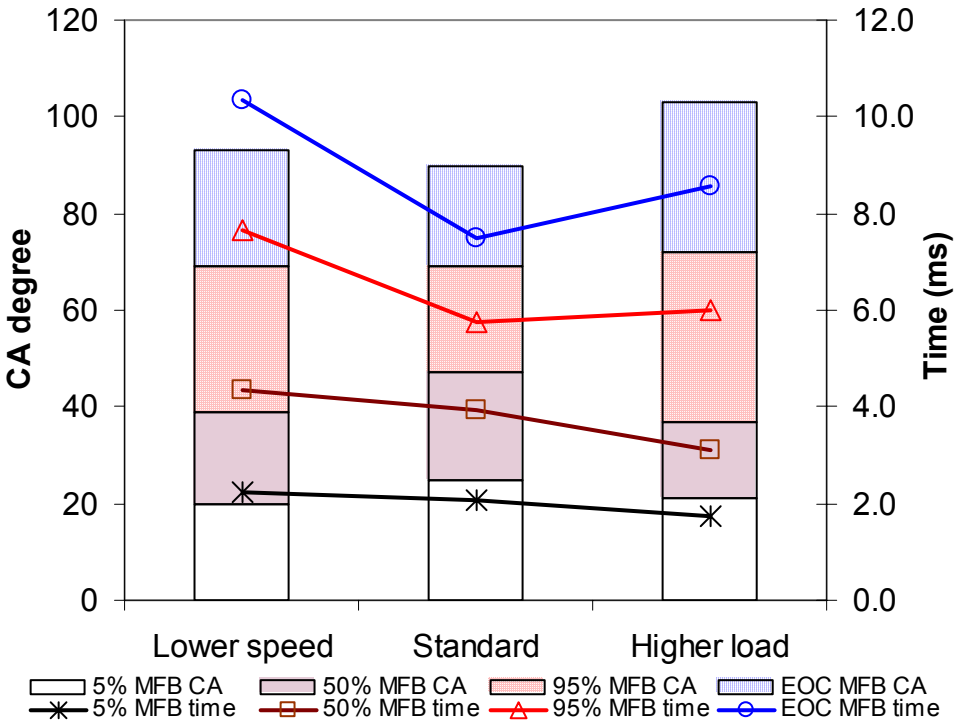

Figure 6-2 **The variations of required crank angles to reach MFB stage in three base line tests.**

6.2. The Combustion Indicators Affected when Adding EGR

6.2.1. IMEP, MFB and Cycle by Cycle Variations

Two major methods to control the nitric oxide emission have been used since 1970's, i.e. retarding ignition timing and adding EGR; the former measure suffers from the problem of the thermal inefficiency, therefore, EGR has more merit. EGR reduces nitric oxide emission from the engine by lowering the in-cylinder temperature, nevertheless the flame speed will be affected and cause longer combustion duration, thus advanced spark timing is needed to maintain 50% MFB at 10° ATDC, which is believed to have the maximum thermal efficiency. Moreover, the reduced combustion rate will make stable combustion condition more difficult to reach, which is probably because of the inert characteristic of EGR and the inlet mixture volume taken by EGR reducing the oxygen content.

Figure 6-3 (A) shows correlations between COV_{IMEP} and volume percentage of EGR, the relevant MFB trend lines demonstrate the delayed combustion durations caused by the increasing EGR. In Figure 5-4 and Figure 5-6, advancing the ignition timing has increased the peak pressure but still retained the MFB profile shape, which suggests a strategy to maintain the maximum thermal efficiency by advancing spark ignition timing. Figure 6-3 (B) compares the MFB profiles of different EGR content; the interval between two 50% MFB points under

different conditions presents required crank angles by which to advance the ignition. For example, in the 10.83% EGR case, to draw the thermal efficiency lost back to the base line, it is necessary to advance the ignition by 19 crank angle degrees.

In general, the peak pressure has more severe cycle by cycle variation than the IMEP; although both of them have similar tendencies to the increasing EGR, the peak pressure is relatively less sensitive. This phenomenon can be observed from Figure 6-4 (A) and (B). When 75% increasing COV_{IMEP} was observed, the COV_{Pmax} shows only an 11% increment. The evidence of EGR disturbing stability can easily be found in the upper part of a P-V diagram shown in Figure 6-4. The effects of advancing the spark ignition, which can not only maintain thermal efficiency, but also reduce the cycle by cycle variation; can be seen in Figure 6-4 (C).

6.2.2. Emissions - NO, UHC and CO

The previous section outlined the advantages of using advanced ignition timing to compensate for the loss in thermal efficiency caused by adding EGR, and the results do encourage such an application. However, like the trend shown in Figure 5-4, increasing the advancing ignition timing also yields an increase in NO emissions, which is in conflict with the effect of applying EGR hence raises a doubt about its use. The final effect on emissions results are shown in

Figure 6-5, the NO concentration still falls with increasing EGR although ignition timing has been advanced. Since the temperature and peak pressure inside cylinder both affect the formation of NO, they were then examined to explain the behaviour. Nevertheless, no relevant relationship can be found from temperature variation (only exhaust temperature is available in this study, which is not really relevant to the cylinder temperature), but the correlation between peak pressure and increasing EGR does show a very rough tendency which is slightly similar with the declined NO.

There are several sources of unburned hydrocarbon (UHC); the crevices in the combustion chamber are believed to be the main cause [100], another source of UHC occurs when the flame extinguishes itself in the chamber before the flame front reaches the walls. Such a condition arises if the temperature and pressure fall too fast, and it could be caused by adding too much EGR [101, Ch. 10], consequently the combustion quality becomes poorer and a substantial ignition delay occurs. This phenomenon can be observed from Figure 6-3 (A) and Figure 6-5. According to the result shown in Figure 5-5, advanced ignition timing will not affect the ignition delay, therefore, the increment of ignition delay is caused by EGR. In this case, adding 10% EGR induced 57% ignition delay growth and 88.6% UHC increase.

It is believed that the main determination of carbon monoxide (CO) emissions is the air/fuel ratio; Figure 6-6 presents the relationships between the relative air/fuel ratio (λ) and three

emissions. Result shows when A/F ratio was slightly higher than 14.59 ($\lambda > 1$) the CO emission became very close to zero. There is not enough data to correlate EGR content with CO emission; however, previous study has claimed there is no direct link between these two items.

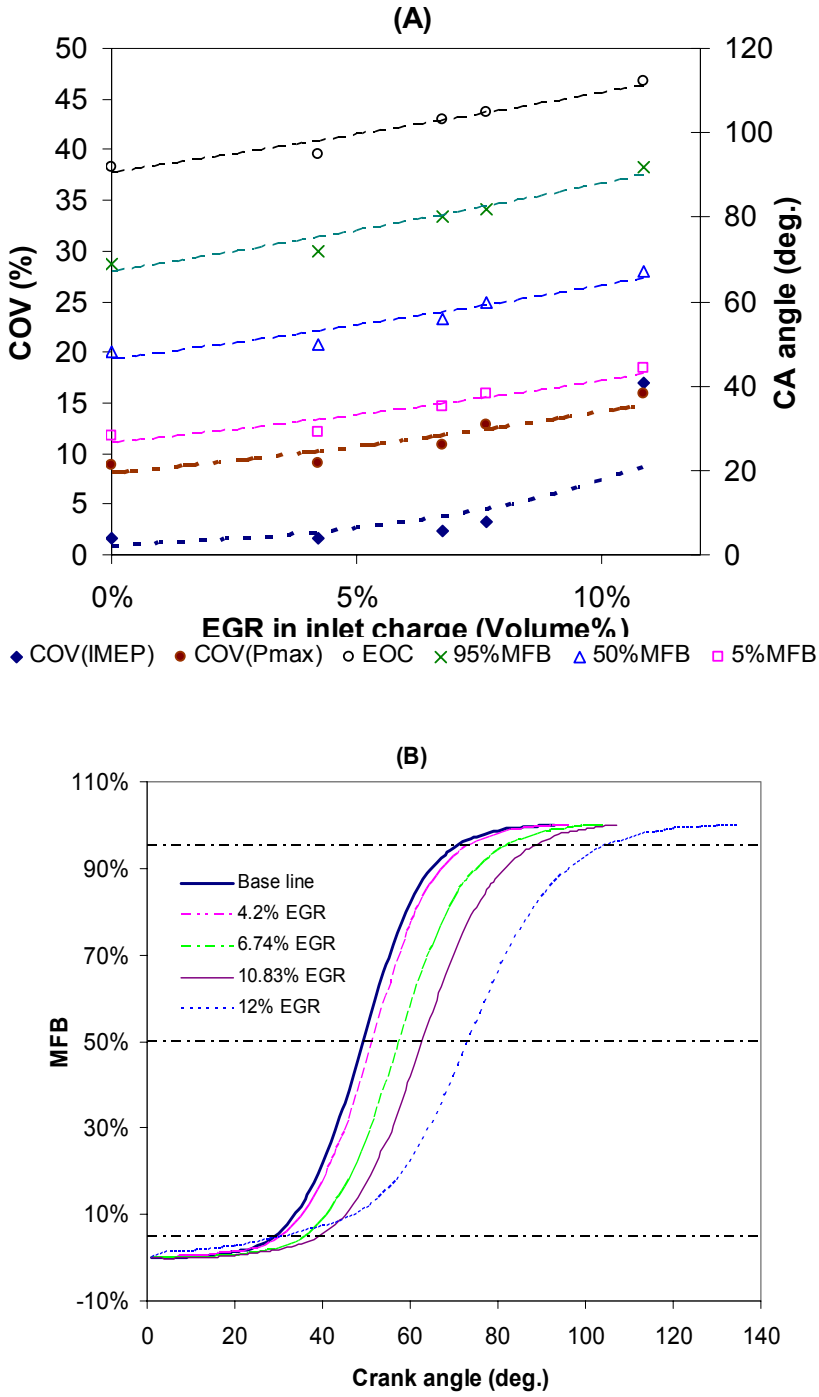

Figure 6-3 **(A) EGR versus COV_{IMEP}, the trend lines of mass fraction burned show an increasing tendency when 50% MFB is retained at 10° CA ATDC. (B) MFP profiles versus crank angle from igniting. Engine ran at 2000 rpm, 2 bar IMEP, ignition timing varied as necessary.**

(A) No EGR, COV_{Pmax}: 10.30%, COV_{IMEP}: 2.89%, ignition timing 31° CA BTDC

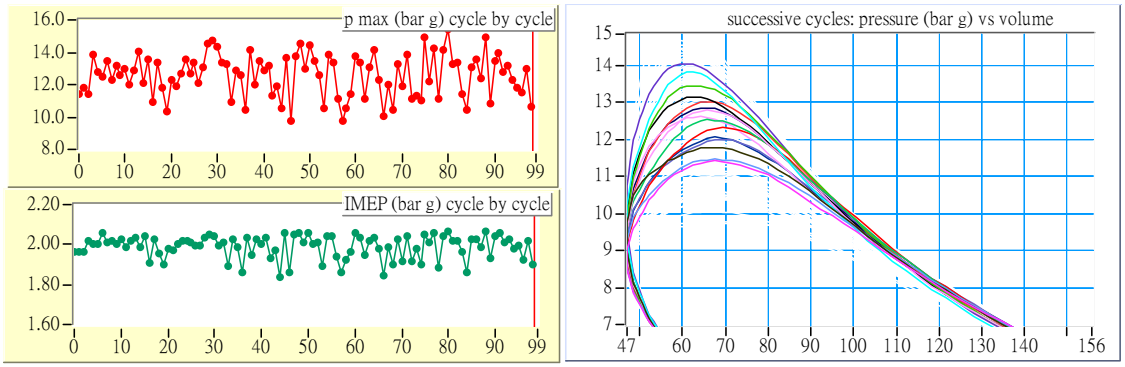

(B) EGR: 5.55%, COV_{Pmax}: 11.47%, COV_{IMEP}: 5.06%, ignition timing 31° CA BTDC

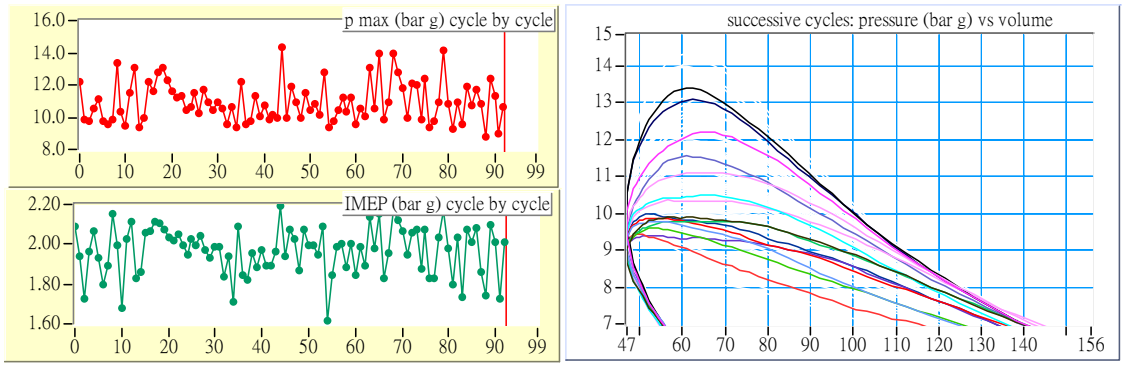

(C) EGR: 4.2%, COV_{Pmax}: 9.10%, COV_{IMEP}: 1.65%, ignition timing 40° CA BTDC

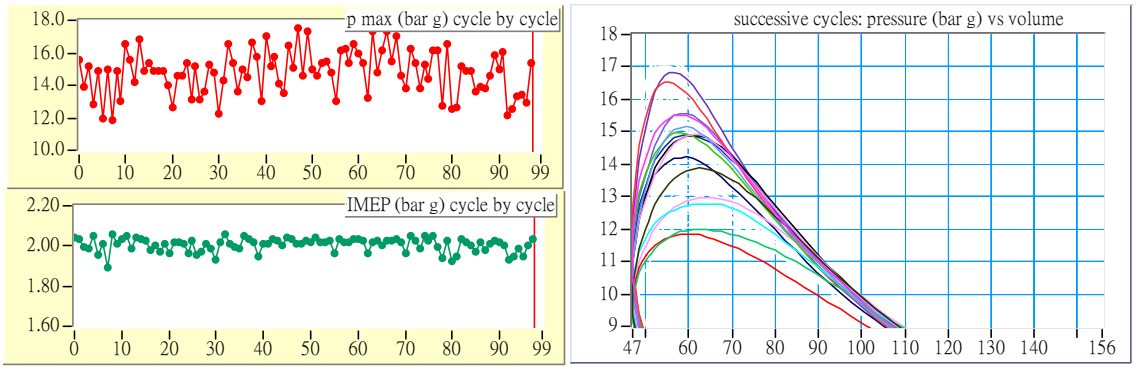

Figure 6-4 Comparisons of the cycle by cycle variations among three engine operating conditions (A) MBT timing, (B) MBT timing with EGR and (C) advanced spark timing to keep 50% MFB at 10° CA ATDC, in all cases the engine ran at 2000 rpm, 2bar IMEP.

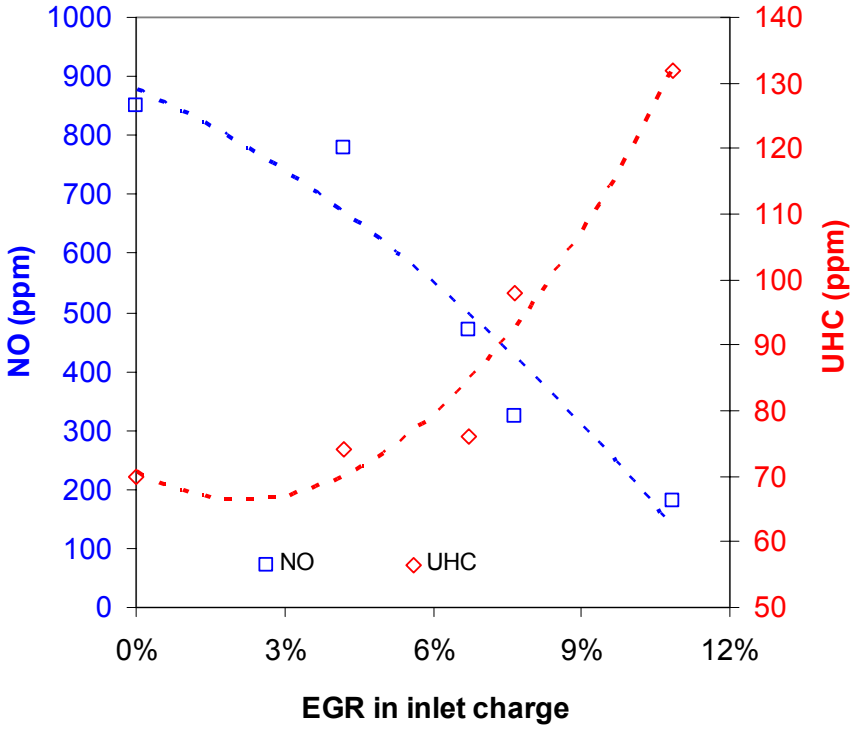

Figure 6-5 **The variations of NO and HC in emissions when applied advanced ignition timing method to EGR application. Engine operating condition: 2000 rpm, 2 bar IMEP, spark ignition varying to keep 50% MFB at 10° CA ATDC.**

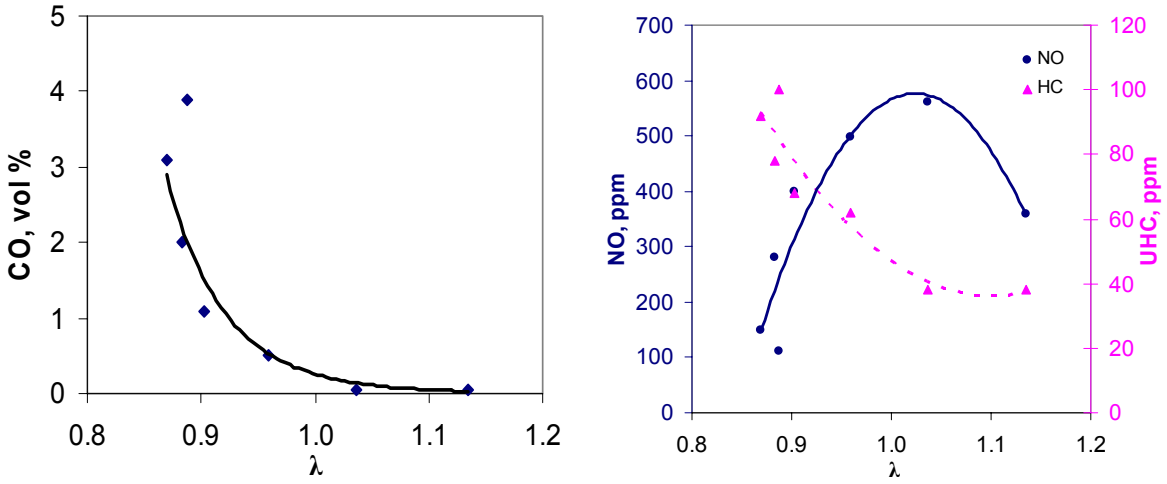

Figure 6-6 **Variations of CO, NO and HC emissions with air/fuel ratio, engine ran without EGR at 2000 rpm, 2 bar IMEP, ignition timing: 31° CA BTDC.**

6.3. Adding H_2 as an Additive in NG Fuel

Adding hydrogen to an engine as an additive has been found to produce a general trend of enhancing the rate of combustion; as for emissions, UHC is observed reducing but NO becomes higher when adding hydrogen. The characteristic stable combustion due to its fast combustion rate can also make it efficient for extending the limit EGR that can be used. Figure 6-7 presents the trends of combustion durations when adding H_2 while varying the ignition timing to retain 50% MFB at 10° CA ATDC, the reductions in combustion duration can be observed in all stages of MFB. Figure 6-8 shows the trends of emissions from the test in Figure 6-7, both of them shown the same tendencies as when adding hydrogen alone.

The combustion stabilizing effect of hydrogen can not be clearly recognized from the values of COV_{IMEP}, it fluctuated around the same level (1.4% in this case); however, the expected increasing COV_{IMEP} did not happen as shown in Figure 5-3 (A) when the ignition was advanced from MBT timing, which shows the potential of using this strategy without causing drivability problems. Through the comparisons between the cases with and without hydrogen in Figure 6-9, a higher peak pressure and a steeper pressure rise can be clearly seen when adding hydrogen (2.6% in volume this case). In the case of adding 4.8% EGR, the higher pressure (in terms of crank angle) in the expansion stroke is further evidence of longer combustion duration, which is correspondent to Figure 6-3 (A).

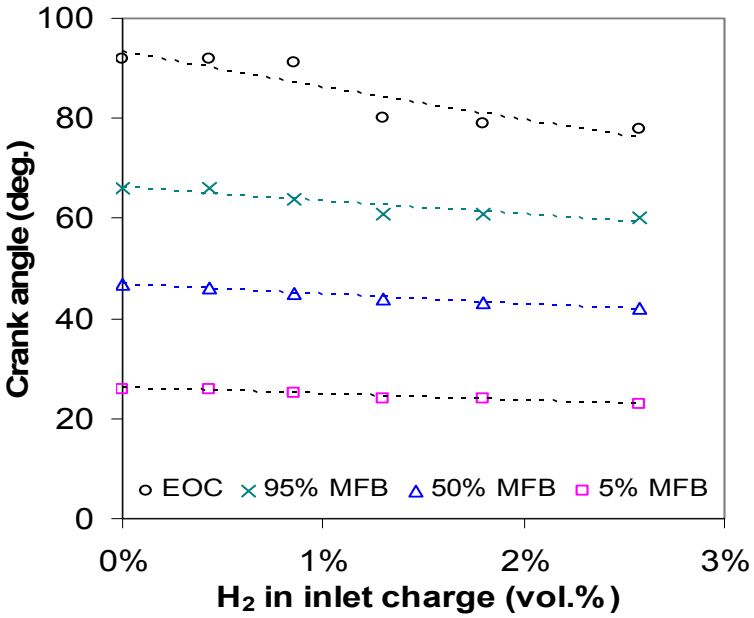

Figure 6-7 **The variation of required crank angles in each MFB stage with increasing hydrogen, engine ran at 2000 rpm, 2 bar IMEP, ignition timing varying to keep 50% MFB at 10° CA ATDC.**

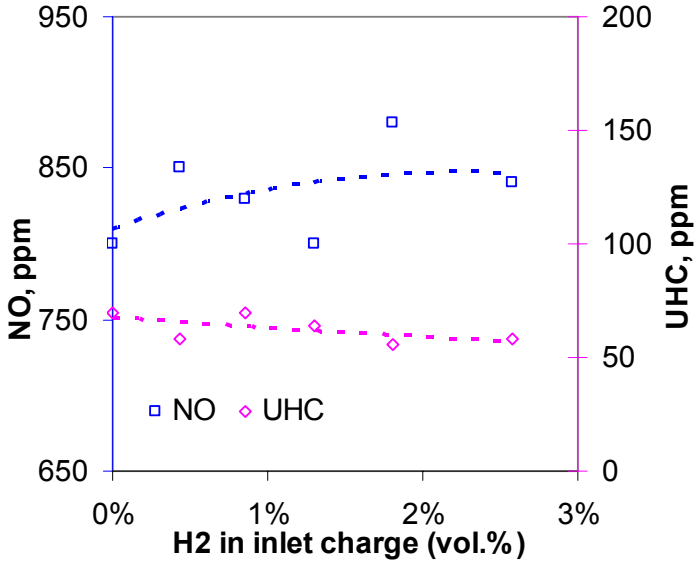

Figure 6-8 **Variations of NO and HC emissions with hydrogen in the inlet charge, engine ran at 2000 rpm, 2 bar IMEP, ignition timing varying to keep maximum thermal efficiency.**

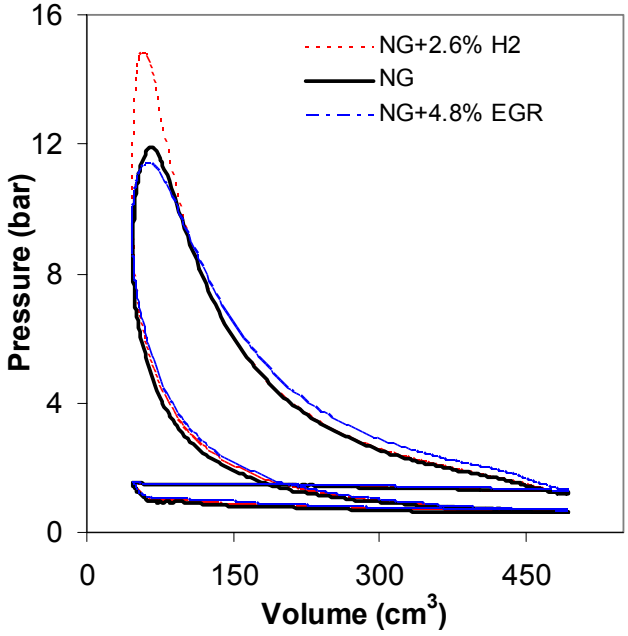

Figure 6-9 The variations of pressure versus volume when adding hydrogen or EGR into the NG fuel, engine ran in the standard condition.

6.4. Combined effects of EGR & H_2 – Fuel Reforming Simulation

6.4.1. Adding EGR and H_2 Alternately – Investigation of the Trade-off Effect

Individual effects of EGR and hydrogen as additives in a NG fuelled engine have already been discussed, one of the interesting topics in the present study is the combustion behaviour when catalyst reformed gas is supplied to the engine, which means both EGR and hydrogen are introduced into combustion and a trade-off effect will happen. Under such situation, the combustion behaviour becomes complicated and hard to explain because there are too many

parameters; therefore, the comparisons will be based on some basic variations and with fewer changes involved.

The approach of adding hydrogen to extend the EGR tolerance of a NG fuelled engine were achieved through a 'step increase' method with 5% COV_{IMEP} used as a criterion. The test procedure starts once the base line condition has been reached, EGR is then added until the criterion is slightly over, followed by applying hydrogen to bring the cycle by cycle variation back to below 5%, meanwhile the ignition timing may be varied as required; by continuing to do this, the limit of EGR can be gradually elevate until stable combustion can no longer be retained by increasing hydrogen and/or varying the ignition timing.

6.4.1.1. Test 1.1 - Fixed Ignition Timing Test

5% and 50% MFB results in Figure 6-10 (A) show slightly decreasing trends, which are good signs for the maximum thermal efficiency control. However, 95% MFB and EOC both reveal a tendency to increase. At the beginning of combustion, hydrogen has a stronger effect on the flame development period, which is why a shorter ignition delay was observed. However, EGR delayed the burn duration - becoming severe even though the cycle by cycle variation was controlled by the hydrogen, which implied the combustion rate should still remain within a certain degree of its original speed, see the overlap of expansion stroke in Figure 6-10 (B).

Alternatively, this phenomenon can be explained by the fast flame speed characteristic of hydrogen, which helped to reduce the ignition delay in the initial stage of combustion, however, because of the small amount and its quicker combustion, hydrogen was burned out before the middle stage of combustion, therefore the effect from EGR became stronger in the later part of combustion, which increased the burn duration dramatically. The differences between two of the compared MFB profiles in Figure 6-10 (C) support this explanation.

The emissions results of base line and final stable condition in this test are tabulated below, the reduction percentage of each emission is also shown in parentheses:

Test 1.1	EGR%	H2%	HC (ppm)	NO (ppm)	CO (%)
Base line	-	-	62	510	0.47
Final stable condition	18.2%	5.6%	8 (87.1%)	16 (96.9%)	0.01 (97.9%)

Table 6-1 Emissions results of base line and final stable condition in Test 1.1.

6.4.1.2. Test 1.2 - Maximum Thermal Efficiency Test

Keeping 50% MFB at 10° CA ATDC is believed to have the maximum thermal efficiency of the engine, hence the above test needs to be further restricted by this requirement to obtain the most advantage of such trade-off effect, and Figure 6-10 presents a small requirement of advancing the spark timing to do so. Therefore, the test process becomes very easy. When EGR and H_2 are both present in the charge mixture, once the ignition timing has been optimised for the maximum thermal efficiency the first time, the procedure for further

increasing the additives will become the same as test 1.1. Figure 6-11 illustrates such condition; after the first time hydrogen was added to stabilize the combustion at spark timing 49° CA BTDC (5.67% EGR and 0.52% H_2), the trend spark timing becomes level in the continuative tests.

The emissions results of the base line and final stable conditions in this test are tabulated below, the reduction percentage of each emission is also shown in parentheses:

Test 1.2	EGR%	H2%	HC (ppm)	NO (ppm)	CO (%)
Base line	-	-	90	710	0.51
Final stable condition	13.0%	1.7%	48 (46.7%)	126 (82.3%)	0.08 (84.3%)

Table 6-2 Emissions results of base line and final stable condition in Test 1.2.

6.4.2. Test 2 - Reformed Fuel Test

A synthetic gas with a volume composition of 75% H_2 and 25% CO was used, aiming to simulate the main reactive components of the product from the reforming reactor. Comparisons between this gas and pure hydrogen were concentrated on the beneficial effects in terms of combustion, i.e. whether the gas can maintain the stable combustion characteristic and the low emissions level which are the greatest concerns in this study.

The trends of required crank angle degrees versus EGR in Figure 6-12 show very similar behaviours at each MFB stages as in Figure 6-10. Results show that without sacrificing the

driving stability, 22.5% EGR in the inlet charge can be reached if the natural gas has 12.9% enriched hydrogen. This outcome confirms the application of the exhaust gas reforming method in terms of stable combustion.

The emissions results of the baseline and final stable conditions in this test are tabulated as below, the reduction percentage in each emission is also shown in parentheses:

Test 2	EGR%	H2%	HC (ppm)	NO (ppm)	CO (%)
Base line	-	-	60	520	0.22
Final stable condition	22.5%	12.9%	48 (20%)	54 (89.6%)	0.1 (54.5%)

Table 6-3 Emissions results of base line and final stable condition in Test 2.

6.4.3. Peak Pressure

Figure 6-13 shows the correlation between peak pressure and the required crank angle degrees in the above three tests, 5% MFB, 95% MFB and EOC are compared. Although the three dotted trend lines all show similar declined tendencies, 5% MFB is more consistent, which can be linked with the burn rate, thus more combustion will be conducted before TDC and this causes higher pressure inside the cylinder, Figure 6-10 (B) and (C) shows these phenomena.

The other signifier which should be addressed here is the consistency between the tendencies of 95% MFB and EOC, this again confirms the EOC point has been acquired correctly.

6.4.4. Emissions Control

Figure 6-14 compares three emissions results from the above tests. They all show falling tendencies with the increasing level of EGR, which supports the use of exhaust gas fuel reforming and ensures its ability of exhaust control.

The synthetic gas did not perform better in terms of controlling CO and UHC; flatter curves can be seen in related diagrams compared with the effect of adding pure hydrogen. The result showing lean condition by adding EGR in test 1.2 has small effect on reducing CO, and this can be ascribed to the CO content of synthetic gas.

A comparison of emissions control of the three tests is shown in Table 6-4. With similar EGR content in the inlet charge, the synthetic gas performed very well, especially in NO control.

	EGR%	H2 %	HC	NO	CO
Test 1.1	12.2%	4.9%	38.7%	65.7%	91.5%
Test 1.2	13.0%	1.7%	46.7%	82.3%	84.3%
Test 2	13.8%	5.9%	20.0%	75.8%	63.6%

Table 6-4 Percentage reductions of three emissions. Results shown are the comparisons between the baseline and the stable condition with similar EGR content in each test.

The strategy of increasing the tolerance of EGR using hydrogen enriched natural gas can be achieved by interpolating the step procedure in Figure 6-10 ~ Figure 6-12, detailed method can be found in the aforementioned IMechE paper by Allenby.

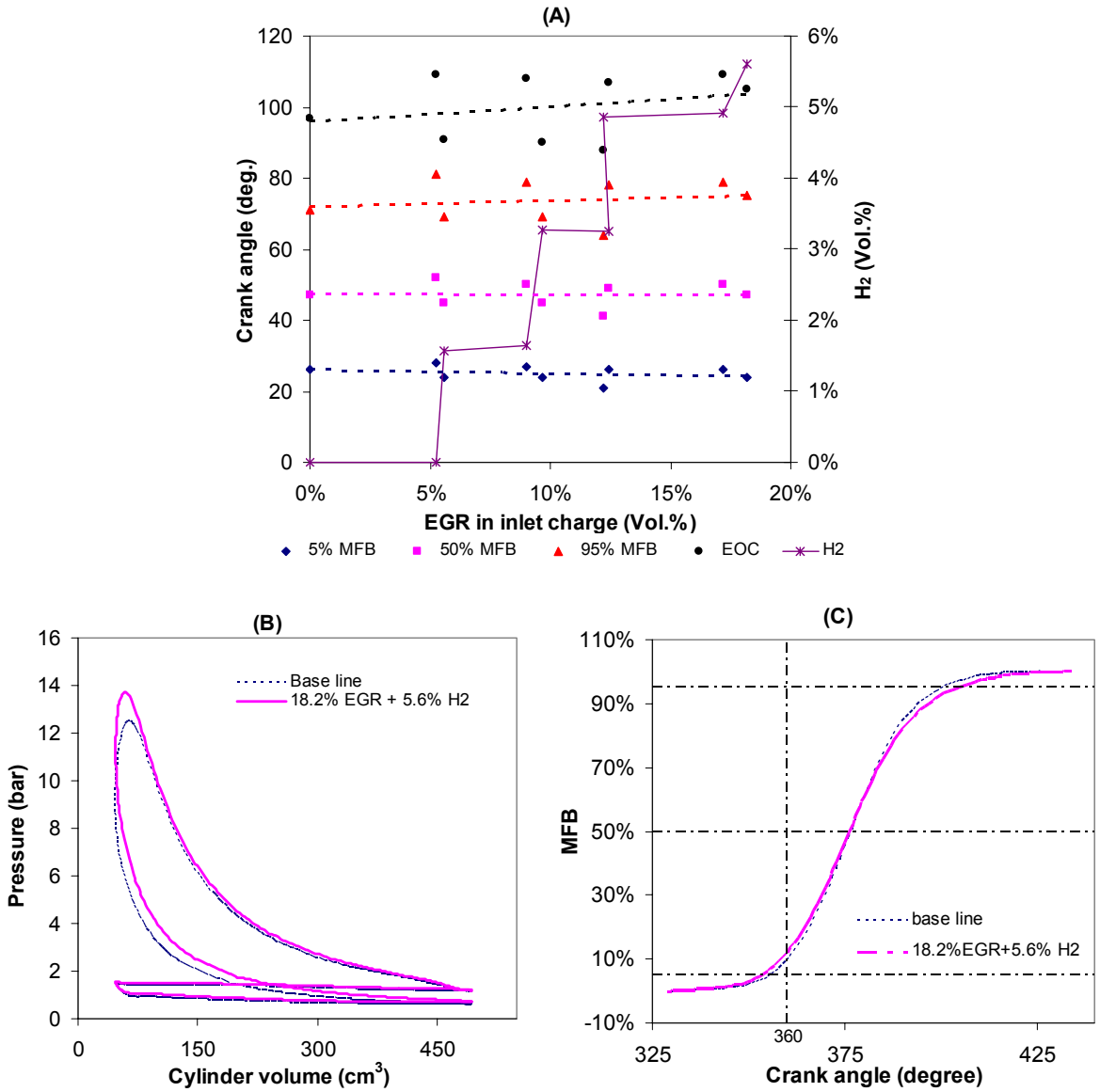

Figure 6-10 **(A) Required crank angle degrees versus EGR. Comparison of different MFB stages. Real line shows the test procedures in which EGR and H_2 were added alternately. (B) P-V diagram and (C) MFB profile are comparisons between base line and test final condition. Engine ran in the standard condition with COV_{IMEP} fluctuating about 5% (Test 1.1).**

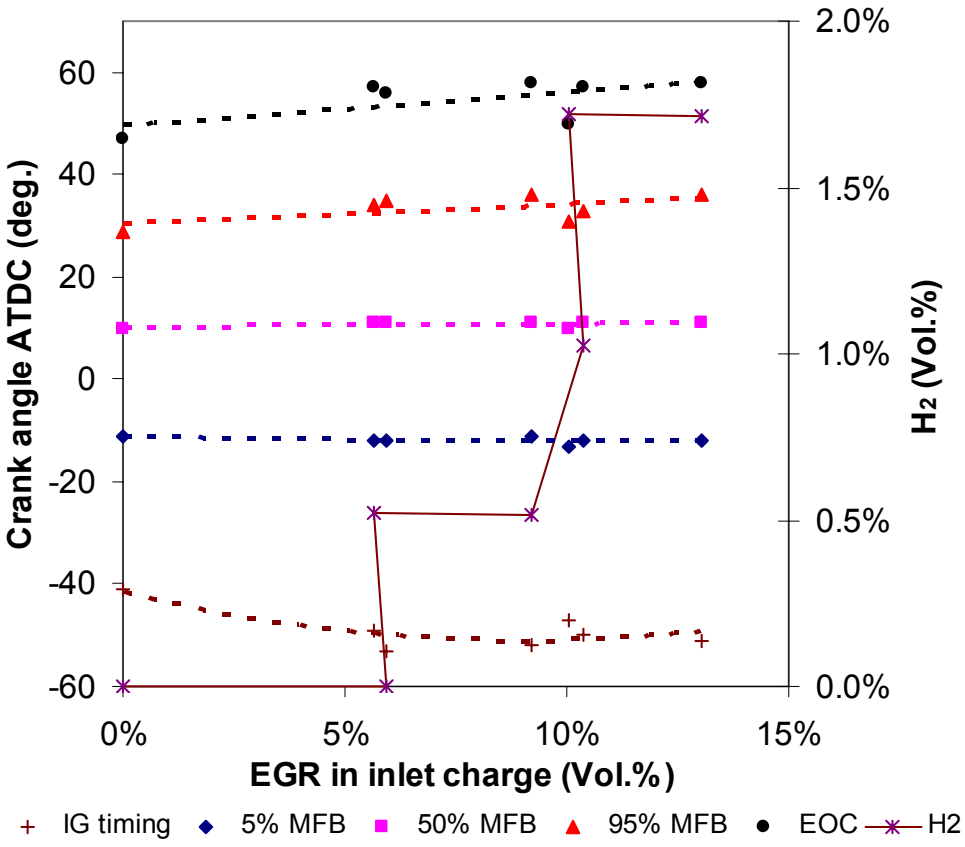

Figure 6-11 **Required crank angle degrees versus EGR. Comparison of different MFB stages. Real line shows the test procedures in which EGR and H_2 were added alternately. Engine ran in the standard condition with COV_{IMEP} fluctuating about 5%, ignition timing was adjusted to keep 50% MFB at 10° CA ATDC (Test 1.2).**

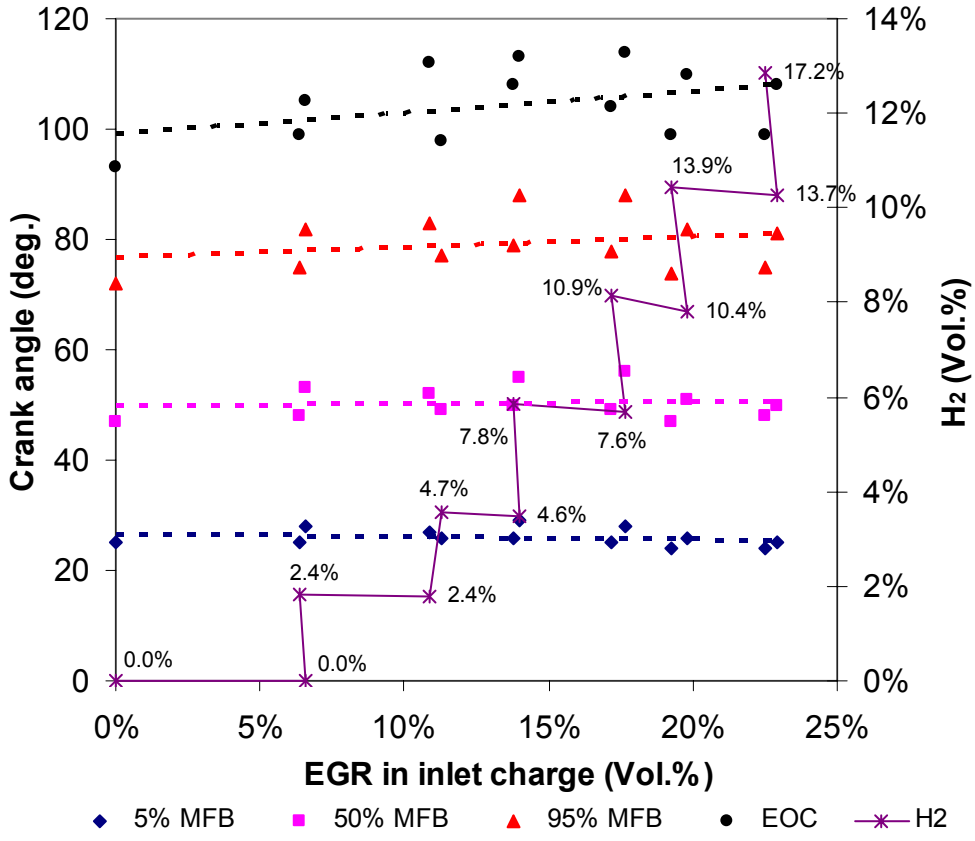

Figure 6-12 **Required crank angle degrees versus EGR. Comparison of different MFB stages. Real line with H_2/CO volume percentages shows the test procedure in which EGR and H_2/CO were added alternately. Engine ran in the standard condition with COV_{IMEP} fluctuating about 5%. (Test 1.3).**

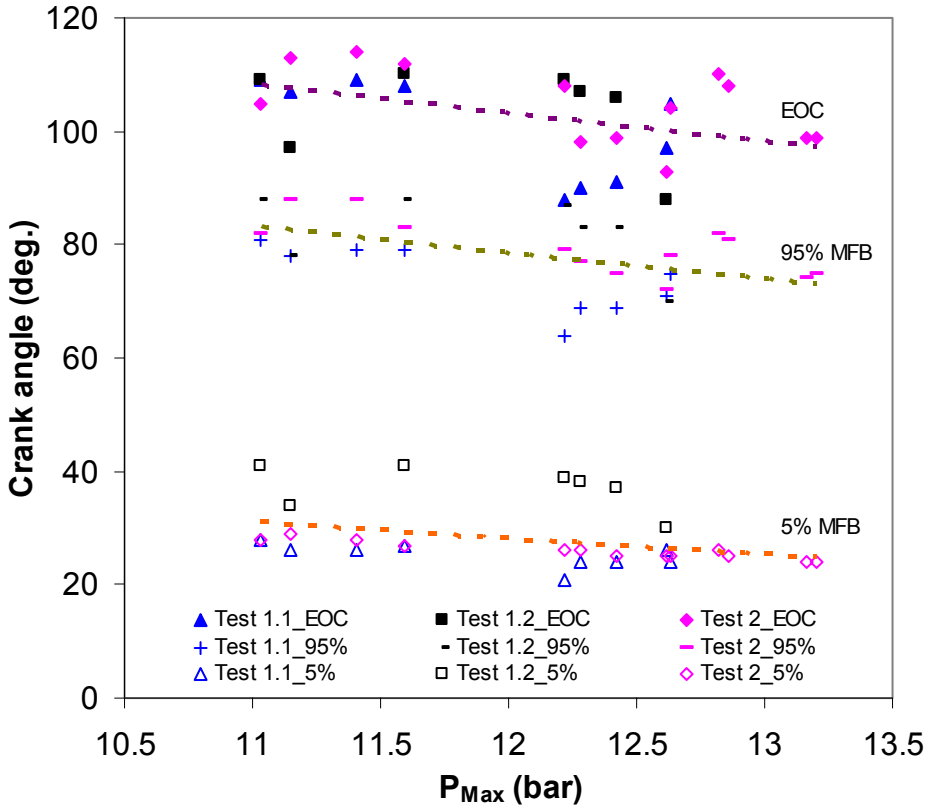

Figure 6-13 Required crank angle degrees versus peak pressure. Comparison of 5%, 95% and total mass fraction burned.

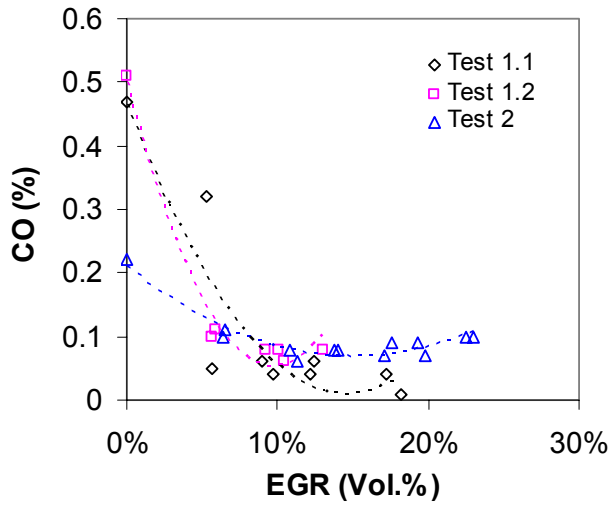

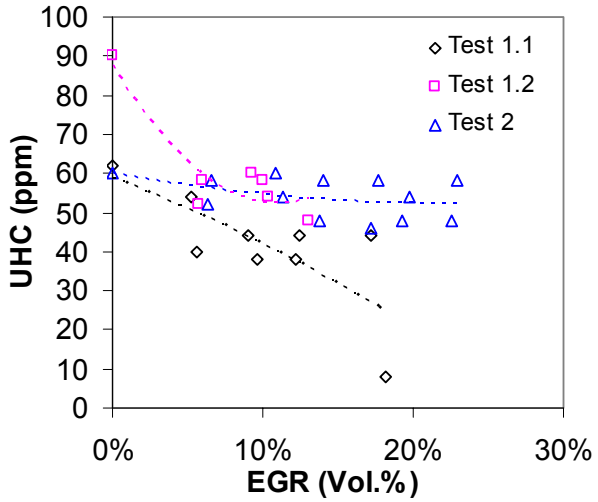

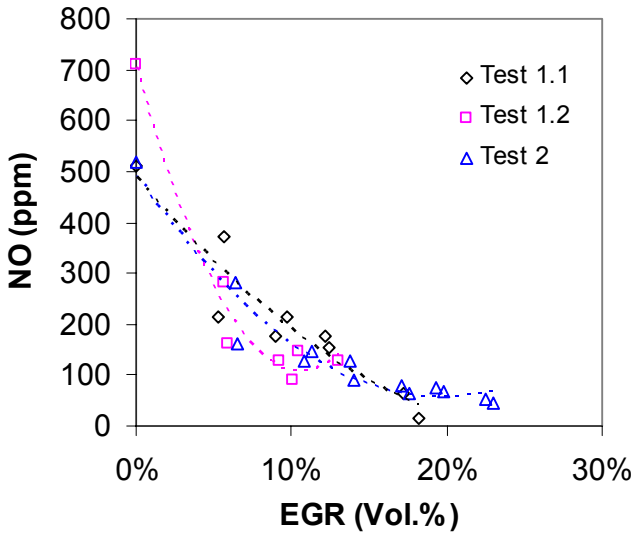

Figure 6-14 EGR versus emissions. Comparison of three combined effects tests.

7. APPLICATIONS OF DIFFERENTIAL PRESSURE DATA

Through the third differential of pressure data it is possible to detect the engine knocking, as mentioned in the literature survey, which sheds lights on using the derivative of pressure data to correlate with some other combustion phenomena. Differential pressure data are used to locate the initial value of EOC in the improved method of MFB calculation, hence the first and second derivatives of pressure traces are both available to provide for any further applications. Work in this chapter will concentrate on two issues: MFB and emissions, using the existing differential data to investigate the correlations.

Analysed pressure data were filtered by the nine points weighted smoothing method, the differential values were derived by the following equation suggested by Checkel and Dale [8].

$$dP(\theta)=\left\{\begin{matrix}86\times\left[P(\theta-4)-P(\theta+4)\right]+142\times\left[P(\theta+3)-P(\theta+3)\right]\\+193\times\left[P(\theta+2)-P(\theta-2)\right]+126\times\left[P(\theta+1)-P(\theta-1)\right]\end{matrix}\right\}\Big/(1188\times d\theta) \quad \text{Eq. 7-1}$$

where

dP(θ) is the derivative value at crank angle *θ*.

dθ is the pressure data interval, one crank angle degree in this study.

P(θ) is the original pressure data at crank angle *θ*, (*θ* + 1) indicates the succeeding crank angle and the same application applied for other items in the equation.

7.1. Prediction of MFB

7.1.1. By Derivative Value

The second derivatives of cylinder pressure can be used to locate the ignition delay of a diesel engine, 2% MFB, it has been said that it corresponds to $d^2p/d\theta^2 = 0$ [94], although this value is not adopted as the definition of ignition delay in this study, this relationship can be useful as a validation method of MFB calculation.

Owing to the different working principles, the differential pressure patterns of spark ignition engine are very different from those of a diesel engine, see Figure 7-1, and the pressure data derived real time by data acquisition are not analogous, this will make the differential value analysis more complex and unpredictable. Thus, after comparing with the three operating conditions in Chapter 5, only the point ($d^2p/d\theta^2 = 0$) in the standard operating condition corresponds to 2% MFB as shown in Figure 7-1 (D). For the other two tests, they show little relevant link at all, see Figure 7-2.

The method used in the program to estimate the initial EOC point for MFB calculation also adopts a differential pressure tracking mechanism, which is also suggested by an application to diesel engine [35]. Two options can be chosen in this method:

1. 1st derivative value: EOC locate at the minimum value position.

2. 2nd derivative value: EOC is the first zero point after the minimum value.

The same results from the above three operating conditions can be used again for comparing the difference between these two methods. The comparative results are shown below:

	Standard	Lower speed	Higher load
1st derivative value	396° CA	385° CA	384° CA
2nd derivative value	396° CA	385° CA	384° CA
Final EOC point derived by improved method	419° CA	431° CA	432° CA

Table 7-1 Estimated EOC point by 1st and 2nd derivative value methods.

Both methods agree with each other, and all points happened earlier than the final EOC positions, which means this method underestimates the EOC of a natural gas fuelled SI engine, on the other hand, this proves that it is adequate as a starting point for the 'approaching' method, and both methods can be used without causing any difference in the end result.

For a mathematical aspect, these two options should reach the same result as shown in the table; however, considering the discrete data condition, the second derivative value is highly recommended for diesel engines.

7.1.2. By Integral of 2nd Derivative Values

This section investigates the potential method of predicting the required crank angles in each MFB stage. The integration period was chosen from spark timing to the peak value of first

differential pressure, this period is the most rapid combustion period which affects the cylinder pressure pronouncedly. However, the results have also been compared with the integral values calculated throughout the whole combustion period, trends with different directions but similar relationships were acquired. Trapezoidal rule is adopted to integrate the data due to its simplicity.

The three tests conducted in Chapter 6 are compared to investigate the accuracy of the prediction. Results in Figure 7-3 show pronounced consistency in each test; the linear relationship can be applied through nearly all MFB stages in three tests, except the EOC with higher variability. 5% and 50% MFB show very good correlations with the integral of 2nd derivative, these phenomena can be contributed to the integration period which is roughly the same as 50% MFB and the interval probably determines the whole pressure shape in the diagram.

The linear relationship can be represented by the form as an equation $y = Ax + B$, the relative parameters for each trend line are listed below:

	5% MFB	50% MFB	95% MFB	EOC
Test 1.1	$y = -202.58x + 37.93$	$y = -305.45x + 68.54$	$y = -458.17x + 106.97$	-
Test 1.2	$y = -23.3x + 42.38$	$y = -20.43x + 64.3$	$y = -85.62x + 101.86$	-
Test 2	$y = -40.96x + 28.83$	$y = -69.18x + 53.61$	$y = -119.88x + 84.77$	$y = -172.23x + 116.07$

Table 7-2 The linear equations of trend lines. Each equation represents the correlations between the integral of 2nd derivative of pressure data and required crank angles at relative MFB stage.

By mathematics, the integral of second derivative value should be equal to the subtraction of the last and first value in the same period. Previous section also showing the EOC point derived from the 1st derivative method or 2nd derivative method does not cause differences. The results of comparison on the deviation between the values derived by the integration of the 2nd derivative of pressure data during the ignition timing and peak pressure position, and the subtraction value of the 1st derivative of pressure data between the ignition timing and peak pressure, showing consistence in three compared cases, see Figure 7-4. The result recommends the method of using the integration of 2nd derivative value is unnecessary; the subtraction by the 1st derivative data can also perform the same function, which will make this method more efficient.

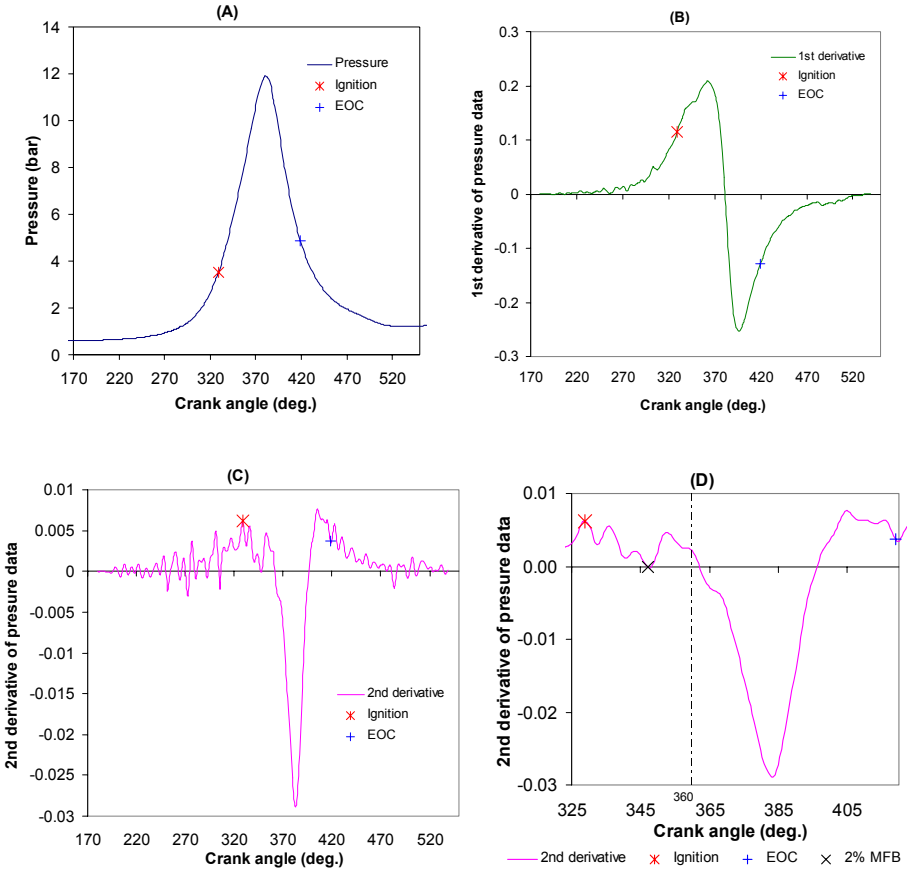

Figure 7-1 **Pressure data patterns of natural gas fuelled engine. (A) Original pressure data (B) 1st derivative of pressure data (C) 2nd derivative of pressure data (D) Relevant window of 2nd derivative of pressure data. Data shown are from a baseline test of the standard operating condition.**

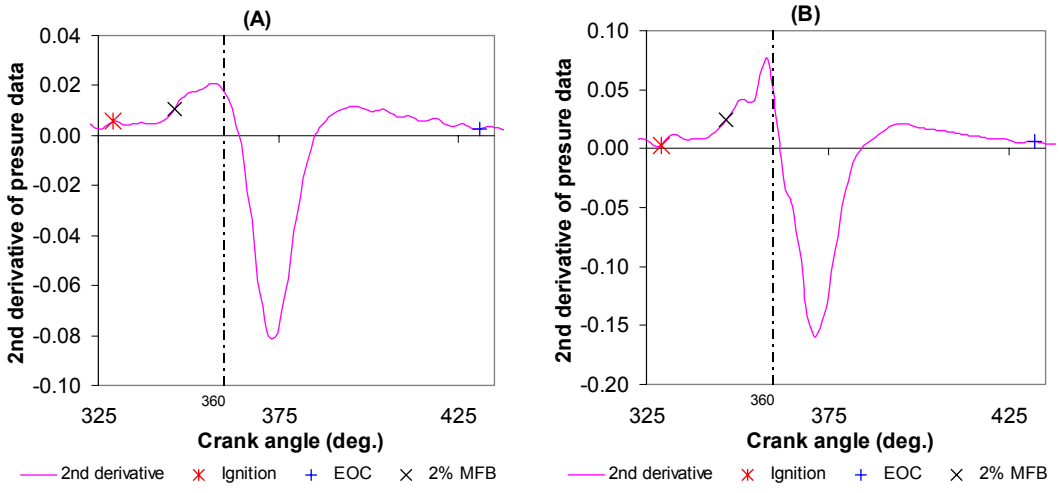

Figure 7-2 **2% MFB position on the second differential pressure curve. Comparison of (A) lower speed and (B) higher load conditions.**

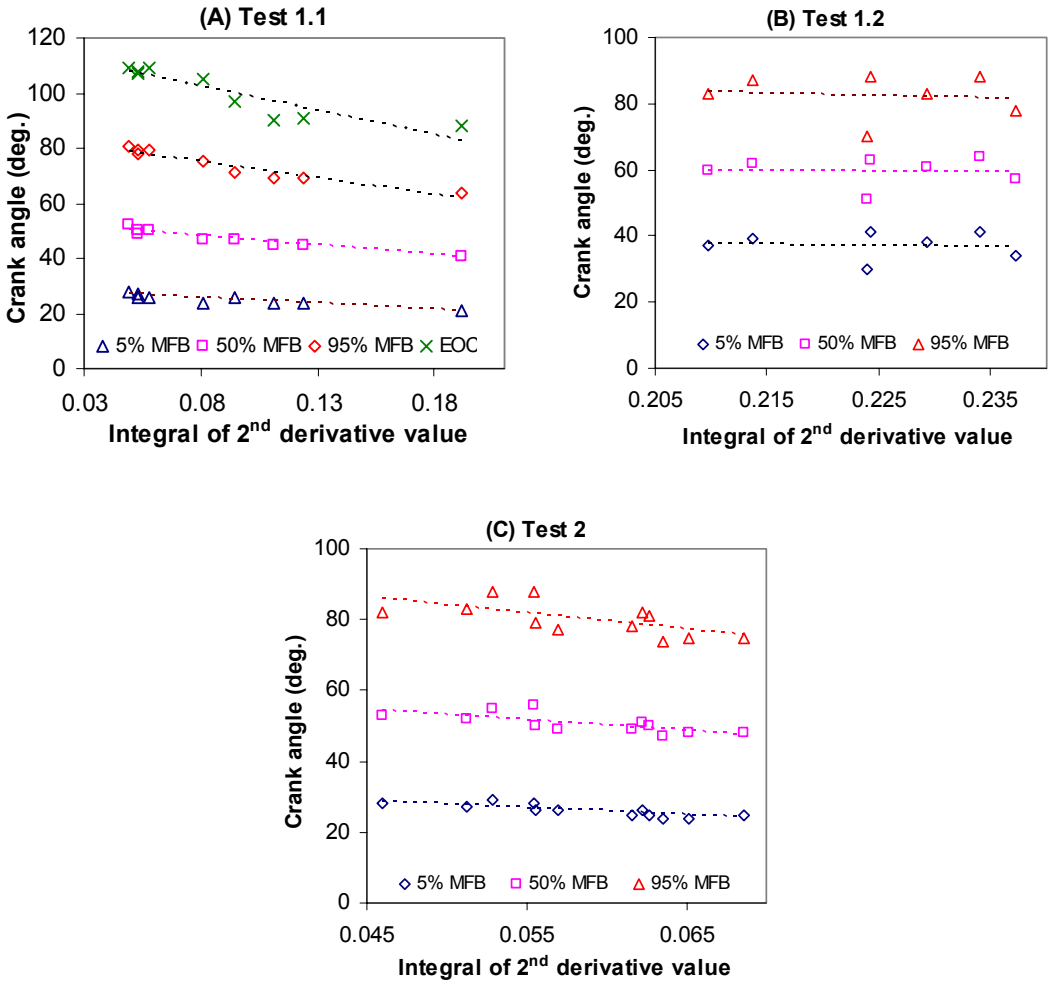

Figure 7-3 Correlation between MFB and integral of 2nd derivative of pressure data.

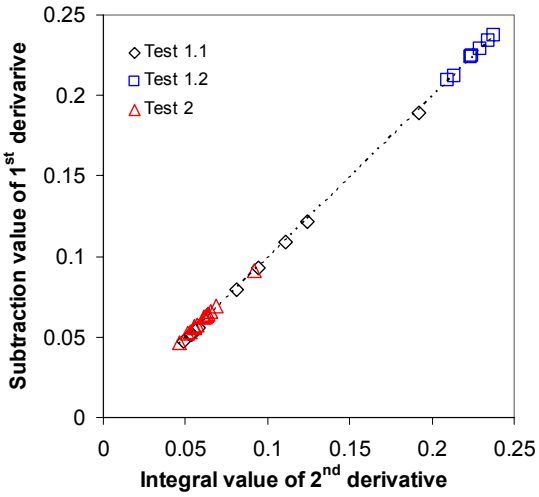

Figure 7-4 The deviation between the integral value of 2nd derivative of pressure data and the subtraction value of 1st derivative of pressure data.

7.2. Emissions pattern prediction

Natural gas fuelled engines normally produce lower emissions such as CO, UHC and particulate than the traditional hydrocarbon fuels. Due to this clean characteristic, it stands a better chance of the emissions being predictable by simply extracting information from the combustion related data, e.g. differential pressure traces.

May [10] successfully correlated the integral of the second differential pressure data to predict the emissions behaviour in a gasoline fuelled SI engine, this encourages a feasibility investigation on applying such a mechanism to an SI engine with exhaust gas reformed fuel. Although the above discussions has proved the 1st derivative can perform the same result, its slight deviation might still cause some unexpected problems, therefore, the 2nd derivative value is still adopted for comparing. The integral results from the last section are further investigated for the correlation between the value and emissions results; however, in May's experiments, the comparisons were set up between different equivalence ratios and fuels, which intended to minimize the change of the emission results. The attempt here is to try to correlate the exhaust emissions from a more complicated mixture, which includes EGR and H_2 inside the natural gas fuel, although the stoichiometric condition was supposed to be maintained, the inlet charge condition still fluctuated occasionally. Hence, IMEP and maximum pressure are introduced to normalize the variability, these two values have direct

links with the air/fuel ratio; hence, dividing by one of them can normalize the variation.

7.2.1. Nitric Oxide

The formation of NO is linked to temperature and peak pressure as mentioned in Chapter 6; hence, the integral value is divided by the peak pressure to normalize the variation. After comparison, the whole combustion period was found not to improve the correlation, and the best fit for this relationship is a linear behaviour, the results and the correlation equations are shown in Figure 7-5. Correlation of Test 1.2 has higher variation mainly because the effect of advanced ignition timing, which increased the peak pressure and will abate the effect of normalization. This result is different with May's, which an exponential function as Eq. 2-17 was reported, the reason is probably because the engine operation conditions were not stable and the air/fuel ratio moved up and down between the stoichiometric, in May's consideration, they should be separated for comparison.

7.2.2. Carbon Monoxide

The deduction in the last section has already implied the impossibility of using this method to predict the CO in these compared cases. Based on previous discussion, the air/fuel ratio

determines the amount of CO in the exhaust, however, the result with the same comparison measure (by May's method) is show in Figure 7-6. The expected logarithmic relationship can not be clearly identified.

Although only NO can be correlated with the integral values in the present study, the application is still optimistic, under more rigorous experimental set up, it is possible to foretell the exhaust emissions behaviour simply from cylinder pressure data. The demonstration of successful prediction of NO in this study is a good example.

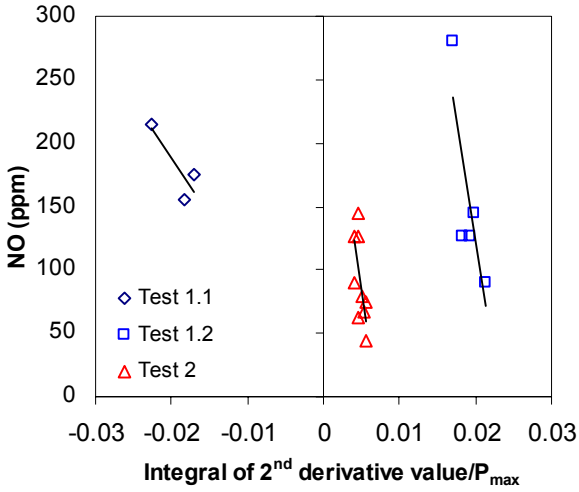

Test 1.1	y = -9281.7x + 2.561
Test 1.2	y = -39042x + 902.15
Test 2	y = -39238x + 279.4

Figure 7-5 Correlations of NO and the integral of 2nd derivative of pressure data divided by peak pressure

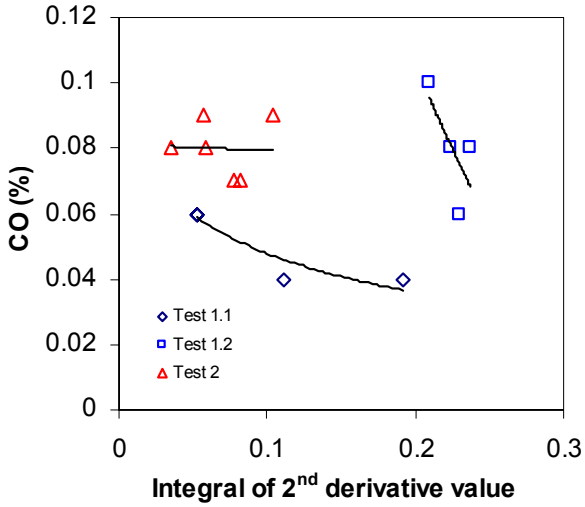

Figure 7-6 CO versus the integral of 2nd derivative of pressure data.

8. CONCLUSIONS AND FUTURE WORK

8.1. Conclusions

According to the test results and previous discussions, a number of conclusions can be drawn and generally classified into three categories.

8.1.1. Accuracy of Improved Methods

The accuracy of the improved method has been verified for three operating conditions, the deviation at each MFB stage between this method and other traditional measures, even with the same combustion period, can be very high, e.g. 15% at 5% MFB, 9.76% at 50% MFB and 30.28% at 95% MFB. This also reveals the importance of choosing the data processing method; the difference in MFB calculation result between the raw data and smoothed signals has been found to deviate by 65% deviation in some cases.

A mechanism for finding the EOC position without objective judgement involved has been established and associated with the MFB calculation, the results always shows a convergence in the approaching process. The compression and expansion polytropic indices are both derived from the pressure data by a curve fitting method to gain linear regressions with better approximations, and then used together with the approached EOC point in the calculation of

the revised R&W model to derive the final MFB result.

8.1.2. The Correlations between Additives and Combustion Related Indicators

The effects of EGR and hydrogen on the natural gas fuelled SI engine have been investigated in terms of combustion duration. These effects were quantified and then used successfully to correlate the more complicated behaviour in the operating condition with reformed fuel.

The use of synthetic gas containing 75% H_2 and 25% CO was verified as performing well in terms of emissions control, while the burn duration can be maintained at nearly the same level as for the condition when adding pure hydrogen is added. This phenomenon also confirms the envelope of benefits of using exhaust gas fuel reforming in a NG fuelled SI engine.

8.1.3. Using Differential Pressure Data to Predict the MFB and Emissions

The first CA point after ignition with the value $d^2p/d\theta^2 = 0$ has been found to correspond to 2% MFB in only some special cases, which is not suitable to be used in a natural gas fuelled SI engine. Also, the first occurrence of the zero value seems to be quite random, in conclusion this method is not very relevant to establishing the ignition delay. In contrast, tracking the first and second derivative value to locate the EOC point has shown that it underestimates the

combustion duration, however, it can be used as an initial value in the EOC finding mechanism.

The integral of the 2nd derivative of pressure data has proved itself a useful tool for predicting the required crank angles at each MFB stage. However, the method using the subtraction of two relative 1st derivatives can reach the consistent results has shown the possibility of using a simpler method to perform the same prediction. To the author's knowledge, other researchers have not previously used both methods.

The model of predicting the emission behaviour has shown some interesting results, NO level can be foretold using the normalized integral value of the 2nd derivative of pressure data in a linear equation form.

8.2. Future Work

8.2.1. Data Acquisition Rig

The data acquisition rig has at times suffered from the missing signals and system malfunction problems during the tests. A signal conditioner, which was not used in this study, should be used before signals pass to the data acquisition card. For reducing noise and any interference, a better shielding material for cable and connections is also necessary. Instead of

smoothing data through program, a hardware filter might be added for dada accuracy.

8.2.2. Program

There are still too many parameters that have to be manually input to the program, and some values have to be acquired from other sources, such as pressure gauge and flow meter, which will reduce the accuracy. A self calibrating function can be employed to the in-house program without too much effort, e.g. engine speed and absolute pressure pegging, which both affect the MFB calculation. The former work can be done by just programming, but the latter will need one more pressure transducer to be installed on the inlet manifold pipe. This way human error can be avoided and tests will become more efficient.

To make it easy to obtain the data for comparison, the current program has not been automated with the improved approaches with r-R&W model, the switching procedure needs to be done manually. Besides, the MFB calculation has repeated the EOC finding mechanism and polytropic index acquiring procedures in the program, which might cause delay for real time study, therefore the program needs to be reprogrammed for better efficiency.

8.2.3. MFB Model

The r-R&W model is derived from the original R&W model. Although the use of two polytropic index values in the revised model has already adopted the idea of two different thermodynamics processes, which means some heat loss has occurred, the final result still shows 100% of energy conversion. This can not be true in the real world, therefore a heat transfer model has to be employed if the surface area of engine is known precisely.

The EOC position could be verified by an observation in an optical engine to confirm the accuracy; an overestimated duration is expected without a heat transfer model.

The linear change of polytropic index method for MFB calculation has shown some consistence with the improved method, which might be worth further studying in terms of its thermodynamics aspect.

8.2.4. Emissions prediction

The method needs to be applied under more rigorous set up such as control of air/fuel ratio condition, it is necessary to build up some baseline data before moving on to the reformed fuel investigation, e.g. fuelling tests for different air/fuel ratio conditions with natural gas alone, individual effect of additive on emissions in different air/fuel ratios, etc. The 1st

derivative and 2nd derivative of pressure data should both be examined the possibility of prediction.

REFERENCES

1. Stone, R., et al., *Combustion analysis in the Rover K4 optical engine.* Proceeding of Institution of Mechanical Engineers C524/033/97, 1997. v. AutoTech '97(Automotive Engines and Powertrains): pp. 1-12.

2. Reeves, M., et al., *Particle image velocimetry analysis of IC engine in-cylinder flows.* Optics and Lasers in Engineering, 1996. v. 25(6): pp. 415-432.

3. Amann, C.A., *Cylinder-pressure measurement and its use in engine research.* SAE 852067, 1985.

4. Wibberley, P. and Clark, C.A., *An investigation of cylinder pressure as feedback for control of internal combustion engines.* SAE 890396, 1989.

5. Hayes, I.K., Savage, L.D., and Sorenson, S.C., *Cylinder pressure data acquisition and heat release analysis on a personal computer.* SAE 860029, 1986.

6. Chun, K.M. and Heywood, J.B., *Estimating heat-release and mass-of-mixture burned from spark-ignition engine pressure data.* Combustion Science and Technology, 1987. v. 54: pp. 133-143.

7. Stone, C.R. and Green-Armystage, D.I., *Comparision of methods for the calculation of mass fraction burnt from engine pressure-time diagrams.* Proceeding of Institution of Mechanical Engineers, 1987. v. 1201(D1): pp. 61-67.

8. Checkel, M.D. and Dale, J.D., *Computerized knock detection from engine pressure recoeds.* SAE 860028, 1986. v. 95: pp. 221-231.

9. Rosseel, E. and Sierens, R., *Knock detection in a hydrogen engine.* SAE 970039, 1997: pp. 37-47.

10. May, J.M. and Gyorog, D., *A second derivation of cylinder pressure characterization of exhaust emissions.* ASME, 1997 Spring Techanical Conference 97-ICE-30, 1997. v. 28-3: pp. 55~60.

11. Heywood, J.B., *Internal combustion engine fundamentals*. Automotive Technology. 1988: McGraw-Hill Book Company, ISBN 0-07-100499-8.

12. Ramos, J.I., *Internal combustion engine modeling*. 1989: Hemisphere Publishing Corporation, ISBN 0-89116-157-0. pp. 236-239.

13. Chow, A. and Wyszynski, M.L., *Thermodynamic modelling of complete engine systems - a review.* Proceeding of Institution of Mechanical Engineers, Part D: Journal of Automobile Engineering D03198, 1999. v. 213.

14. Rassweiler, G.M. and Withrow, L., *Motion pictures of engine flames correlated with pressure cards.* SAE, 1938. v. 42(5): pp. 185-204.

15. Larminie, J. and Dicks, A., *Fuel cell systems explained*. 2000: John Wiley & Sons, LTD, ISBN 0-471-49026-1.

16. Kordesch, K. and Simader, G., *Fuel cells and their applications*. 1996: VCH, ISBN 3-527-28679-2.

17. Blarigan, P.V. and Keller, J.O., *A hydrogen fuelled Internal combustion engine designed for single speed/power operation.* Internation Jurnal of Hydrogen Energy, 1998. v. 23(7): pp. 603-609.

18. Yamin, J.A.A., et al., *Effect of combustion duration on the performance and emission characteristics of a spark ignition engine using hydrogen as a fuel.* International Journal of Hydrogen Energy, 2000. v. 25: pp. 581-589.

19. Borroni-Bird, C.E., *Fuel cell commercialization issues for light-duty vehicle applications.* Journal of Power Sources, 1996. v. 61: pp. 33-48.

20. Ekdunge, P. and Raberg, M., *The fuel cell vehicle analysis of energy use, emissions and cost.* International Journal of Hydrogen Energy, 1998. v. 23: pp. 381-385.

21. Meyer, A.P., et al., *Progress in the development of PEM fuel cell engines for transportation.* SAE 2001-01-0540, 2000.

22. Taraza, D., Henein, N.A., and Bryzik, W., *The frequency analysis of the crankshaft's speed variation: A reliable tool for diesel engine diagnosis.* Journal of Engineering for Gas Turbines and Power, 2001. v. 123(2): pp. 428-432.

23. Chan, S.H., *Thermodynamics in a turbocharged direct injection diesel engine.* Proceedings of the Institution of Mechanical Engineers, Part D: Journal of Automobile Engineering, 1998. v. 212(1): pp. 11-24.

24. Saitzkoff, A., et al., *In-cylinder pressure measurements using the spark plug as an ionization sensor.* SAE 970875, 1997. v. 106.

25. Brown, W.L., *Methods for evaluating requirements and errors in cylinder pressure measurement.* SAE 670008, 1967. v. 76: pp. 50-77.

26. Lancaster, D.R., Krieger, R.B., and Lienesch, J.H., *Measurement and analysis of engine pressure data.* SAE 750026, 1975

27. Randolph, A.L., *Cylinder-pressure-transducer mounting techniques to maximize data accuracy.* SAE 900171, 1990. v. 99.

28. Collings, N., Dinsdale, S., and Eade, D., *Knock detection by means of the spark plug.* SAE 860635, 1986.

29. Ohashi, Y., et al., *The application of ionic current detection system for the combustion condition control.* SAE 1999-01-0550, 1999. v. SP-1419.

30. VanDyne, E.A., et al., *Misfire detection from ionization feedback utilizing the SmartFire plasma ignition technology.* SAE 2000-01-1377, 2000.

31. Byttner, S., Rognvaldsson, T., and Wickstrom, N., *Estimation of combustion variability using in-cylinder ionization measurements.* SAE 2001-01-3485, 2001.

32. Daniels, C.F., *The comparison of mass fraction burned obtained from the cylinder pressure signal and spark plug ion signal.* SAE 980140, 1998. v. SP-1348: pp. 15-23.

33. Daw, C.S. and Kahl, W.K., *Interpretation of engine cycle-to-cycle variation by chaotic time series analysis.* SAE 902103, 1990. v. 99: pp. 2188-2199.

34. Guezennec, Y.G. and Gyan, P., *A novel approach to real-time estimation of the individual cylinder combustion pressure for S.I. engine control.* SAE 1999-01-0209, 1999: pp. 55-65.

35. Reddy, P.R., et al., *Evaluation of combustion parameters in direct injection diesel engines - An easy and reliable method.* SAE 930605, 1993. v. SP-971: pp. 159~165.

36. Gatowski, J.A., et al., *Heat release analysis of engine pressure data.* SAE 841359, 1984: pp. 961-977.

37. Cheung, H.M. and Heywood, J.B., *Evaluation of a one zone burn-rate analysis procedure using production SI engine pressure data.* SAE 932749, 1993. v. 102: pp. 2292-2303.

38. Cartwright, A. and Fleck, R., *Cylinder pressure analysis in high performance two-stroke engines.* SAE 962535, 1996. v. 105.

39. Jensen, T.K. and Schramm, J., *A three-zone heat release model for combustion analysis in a natural gas SI engine - effects of crevices and cyclic variations on UHC emissions.* SAE 2000-01-2802, 2000.

40. Hassaneen, A.E., et al., *A study of the flame development and rapid burn durations in a lean-burn, fuel-injected natural gas S.I. engine.* SAE 981384, 1998. v. SP-1371.

41. Brunt, M.F.J. and Emtage, A.L., *Evaluation of IMEP routines and analysis errors.* SAE 960609, 1996: pp. 87-101.

42. Rocco, V., *D.I. diesel engine in-cylinder pressure data analysis under T.D.C. setting error.* SAE 930595, 1993.

43. Stas, M.J., *Thermodynamic determination of T.D.C. in piston combustion engines.* SAE 960610, 1996. v. SP-1157: pp. 103-108.

44. Morishita, M. and Kushiyama, T., *An improved method for determining the TDC position in a PV-diagram (First report).* SAE 970062, 1997. v. 106: pp. 233-244.

45. Morishita, M. and Kushiyama, T., *An improved method of determining the TDC position in a PV-diagram.* SAE 980625, 1998. v. SP-1330.

46. Tazerout, M., Corre, O.L., and Rousseau, S., *TDC determination in IC engines based on the thermodynamic analysis of the temperature-entropy diagram.* SAE 1999-01-1489, 1999. v. 108.

47. Brunt, M.F.J. and Emtage, A.L., *Evaluation of burn rate routines and analysis errors.* SAE 970037, 1997: pp. 19-30.

48. Brunt, M.F.J. and Pond, C.R., *Evaluation of techniques for absolute cylinder pressure correction.* SAE 970036, 1997. v. SP-1267: pp. 7-18.

49. Randolph, A.L., *Methods of processing cylinder-pressure transducer signals to maximize data accuracy.* SAE 900170, 1990. v. 99.

50. Brunt, M.F.J. and Lucas, G.G., *The effect of crank angle resolution on cylinder pressure analysis.* SAE 910041, 1991.

51. Karim, G.A. and Khan, M.O., *An examination of some of the error normally associated with the calculation of apparent rates of combustion heat release in engines.* SAE 710135, 1971.

52. Shayler, P.J., Wiseman, M.W., and Ma, T., *Improving the determination of mass fraction burnt.* SAE 900351, 1990.

53. Ball, J.K., Raine, R.R., and Stone, C.R., *Combustion analysis and cycle-by-cycle variations in spark ignition engine combustion Part 1: An evaluation of combustion analysis routines by reference to model data.* Proceedings of the Institution of Mechanical Engineers, Part D: Journal of Automobile Engineering D04197, 1998. v. 212: pp. 381-339.

54. Homsy, S.C. and Atreya, A., *An experimental heat release rate analysis of a diesel engine operating under steady state conditions.* SAE 970889, 1997. v. SP-1246.

55. Rauckis, M.J. and McLean, W.J., *The effects of hydrogen addition on ignition delays and flame propagation in spark ignition engines.* Combustion Science and Technology, 1998. v. 19: pp. 207-216.

56. Grimm, B.M. and Johnson, R.T., *Review of simple heat release computations.* SAE 900445, 1990.

57. Hribernik, A., S*tatistical determination of correlation between pressure and crankshaft angle during indication of combustion engines.* SAE 982541, 1998.

58. Mendis, K.J.S., et al., *Modelling and measurements from a natural gas fuelled engine.* SAE 930927, 1993. v. SP-958: pp. 143-161.

59. Ferguson, C.R. and Kirkpatrick, A.T., *Internal combustion engines applied thermosciences.* 2nd ed. 2001: John Wiley & Sons, Inc, ISBN 0-471-35617-4.

60. Stone, C.R., Brown, A.G., and Beckwith, P., *Cycle-by-cycle variations in spark ignition engine combustion - Part II: Modelling of flame kernel dispalccements as a cause of cycle-by-cycle variations.* SAE 960613, 1996. v. SP-1157.

61. Ozdor, N., Dulger, M., and Sher, E., *An experimental study of the cyclic variability in spark ignition engines.* SAE 960611, 1996. v. SP-1157.

62. Johansson, B., *Cycle-to-cycle variations in S.I. engines - the effects of fluid flow and gas composition in the vicinity of the spark plug on early combustion.* SAE 962084, 1996. v. 105: pp. 2281-2296.

63. Brunt, M.F.J., Rai, H., and Emtage, A.L., *The calculation of heat release energy from engine cylinder pressure data.* SAE 981052, 1998. v. SP-1315: pp. 101-112.

64. Ishii, K., et al., *Investigation of cyclic variation of IMEP under lean burn operation in spark-ignition engine.* SAE 972830, 1997. v. SP-1301: pp. 55-64.

65. Austen, A.E.W. and Lyn, W.T., *The application of heat release analysis to engine combustion study.* CIMAC Conference, International Council on Combustion Engines, 1962.

66. Krieger, R.B. and Borman, G.L., *The computation of apparent heat release for internal combustion engines.* ASME 66-WA/DGP-4, 1966.

67. Goering, C.E., *Engine heat release via spread sheet.* American Society of Agricultural Engineers, 1998. v. 41(5): pp. 1249-1253.

68. Woschni, G., *A universially applicable equation for the instantaneous heat transfer coefficient in the internal combustion engine.* SAE 670931, 1967. v. 76.

69. Eichelberg, I.G., *Some new investigations on old combustion engine problems - II.* Engineering, 1939. v. 148: pp. 463-466, 547-550.

70. Annand, W.J.D., *Heat transfer in the cylinders of reciprocating internal combustion engines.* Proceeding of Institution of Mechanical Engineers, 1963. v. 177(36): pp. 973~990.

71. Annand, W.J.D. and Ma, T.H., *Instantaneous heat transfer rates to the cylinder head surface of a small compression-ignition engine.* Proceeding of Institution of Mechanical Engineers, 1971. v. 185(Part 1): pp. 976~987.

72. Whitehouse, N.D., *Heat transfer in a quiescent chamber diesel engine.* Proceeding of Institution of Mechanical Engineers, 1971. v. 185, Part 1: pp. 963-975.

73. Han, S.B., et al., *Empirical formula for instantaneous heat transfer coefficient in spark ignition engine.* SAE 972995, 1997. v. SP-1306.

74. Patro, T.N., *Combustion study of hydrogen fueled DI diesel engine: Simplified heat release analysis.* International Journal of Hydrogen Energy, 1993. v. 18(3): pp. 231-241.

75. Goodger, E.M., *Alternative fuels - Chemical energy resources.* 1980: The Macmillan Press Ltd, ISBN 0-333-25813-4.

76. Poulton, M.L., *Alternative fuels for road vehicles.* 1994: Computational Mechanics Publications, ISBN 1-85312-301-3.

77. Maxwell, T.T. and Jones, J.C., *Alternative fuels: emissions, economics, and performance.* 1995: Society of Automotive Engineers, ISBN 1560915234.

78. Kato, K., et al., *Development of engine for natural gas vehicle.* SAE 1999-01-0574, 1999. v. SP-1436

79. Swain, M.R., et al., *The effects of hydrogen addition on natural gas engine operation.* SAE 932775, 1993. v. 102: pp. 1592-1601.

80. Liss, W.E. and Thrasher, *Natural gas as a stationary engine and vehicular fuel.* SAE 912364, 1991. v. SP-888

81. Das, L.M. and Mathur, R., *Exhaust gas recirculation for NOx control in a multicylinder hydrogen-supplemented S.I. engine.* Internation Jurnal of Hydrogen Energy, 1993. v. 18(12): pp. 1013-1018.

82. Lumsden, G., Eddleston, D., and Sykes, R., *Comparing lean burn and EGR.* SAE 970505, 1997. v. SP-1267

83. Sakonji, T. and Shoji, F., *Study on improvement of natural gas fueled spark ignition engines - effect of EGR utilization.* SAE 971714, 1997.

84. Apostolescu, N. and Chiriac, R., *A study of combustion of hydrogen-encriched gasoline in a spark Ignition engin.* SAE 960603, 1996. v. SP-1157.

85. Stocky, J.F., Dowdy, M.W., and Vanderbrug, T.G., *An examation of the performance of spark ignition engines using hydrogen-supplemented fuels.* SAE 750027, 1975.

86. Shrestha, S.O.B. and Karim, G.A., *Hydrogen as an additive to methane for spark ignition engine applications.* International Journal of Hydrogen Energy, 1999. v. 24: pp. 577-586.

87. Jones, M.R., Dunn, J.W., and Wyszynski, M.L., *Thermodynamics feasibility studies of the exhaust-gas reforming of hydrocarbon fuels.* Proceeding of Institution of Mechanical Engineers, Part D, C384/014, 1990.

88. Jones, M.R. and Wyszynski, M.L., *Onboard generation of hydrogen-based gaseous engine fuels by exhaust-gas reforming of liquid hydrocarbons.* Auto Tech '93, 1993.

89. Jamal, Y. and Wyszynski, M.L., *On-board generation of hydrogen-rich gaseous fuels-a review.* International Journal of Hydrogen Energy, 1994. v. 19(7): pp. 557-572.

90. Wagner, T., Jamal, Y., and Wiszynski, M.L., *Advantages of fractional addition of hydrogen to internal combustion engines by exhaust gas fuel reforming.* Hypothesis Conference, Cassino-Gaete, Italy. 26-29 June, 1995.

91. Jamal, Y., Wagner, T., and Wyszynski, M.L., *Exhaust gas reforming of gasoline at moderate temperatures.* International Journal of Hydrogen Energy, 1996. v. 21(6): pp. 507-519.

92. Wyszynski, M.L., et al., *On-board generation and IC engine use of hydrogen-rich gaseous fuels.* Hydrogen 94,10th World Hydrogen Conference, 1994: pp. 1-10.

93. Smith, J.A. and Bartley, G.J.J., *Stoichiometric operation of a gas engine utilizing synthesis gas and EGR for NO_x control.* ASME, 1998 Spring Techanical Conference 98-ICE-107, 1998. v. 30(3): pp. 59-66.

94. Sher, E. and Hacohen, Y., *Ignition delay and combustion duration in H2-enriched gasoline SI engine.* Combustion Science and Technology, 1989. v. 65: pp. 263-275.

95. Tabaczynski, R.J., Ferguson, C.R., and Radhakrishnan, K., *A turbulent entrainment model for spark-ignition engine combustion.* SAE 770647, 1977. v. 86.

96. Hires, S.D., Tabaczynski, R.J., and Novak, J.M., *The prediction of ignition delay and combustion intervals for a homogeneous charge, spark ignition engine.* SAE 780232, 1978. v. 78.

97. Blizard, N.C. and Keck, J.C., *Experimental and theoretical investigation of turbulent burning model for internal combustion engines.* SAE 740197, 1974. v. 83.

98. Stone, R., *Introduction to internal combustion engines.* 3rd ed. 1999: MacMillan Press Ltd., ISBN 0-333-74013-0.

99. Allenby, S., et al., *Hydrogen enrichment: A way to maintain combustion stability in a natural gas fuelled engine with exhaust gas recirculation, the potential of fuel reforming.* Proceeding of Institution of Mechanical Engineers, 2001. v. 215(Part D: Journal of Automobil Engineering): pp. 405~418.

100. Namazian, M. and Hwywood, J.B., *Flow in the piston cylinder ring crevices of a spark ignition engine, effect on hydrocarbon emissions, efficiency and power.* SAE 820088, 1982

101. Degobert, P., *Automobiles and Pollution.* 1995: SAE, ISBN 1-56091-563-3.

APPENDIX - A

Dead weight calibrations for pressure transducer and charge amplifier set.

Pressure(bar)	1	2	3	4	Average
0	-0.146	-0.179	-0.154	-0.177	-0.164
1	-0.089	-0.123	-0.097	-0.119	-0.107
1.5	-0.063	-0.093	-0.069	-0.091	-0.079
2	-0.038	-0.064	-0.042	-0.064	-0.052
2.5	-0.012	-0.037	-0.015	-0.038	-0.0255
3	0.012	-0.011	0.011	-0.01	0.0005
3.5	0.037	0.014	0.039	0.015	0.02625
4	0.064	0.04	0.066	0.042	0.053
4.5	0.089	0.067	0.092	0.068	0.079
5	0.115	0.094	0.117	0.094	0.105
5.5	0.142	0.12	0.144	0.119	0.13125
6	0.169	0.148	0.17	0.148	0.15875
6.5	0.197	0.174	0.195	0.175	0.18525
7	0.224	0.201	0.222	0.201	0.212
7.5	0.25	0.228	0.249	0.227	0.2385
8	0.276	0.253	0.277	0.254	0.265
8.5	0.301	0.279	0.304	0.281	0.29125
9	0.324	0.306	0.329	0.308	0.31675
9.5	0.351	0.334	0.355	0.335	0.34375
10	0.379	0.361	0.38	0.362	0.3705
10.5	0.405	0.387	0.408	0.388	0.397
11	0.431	0.416	0.434	0.415	0.424
11.5	0.458	0.444	0.46	0.442	0.451
12	0.484	0.471	0.486	0.468	0.47725
12.5	0.511	0.497	0.509	0.495	0.503
13	0.538	0.524	0.536	0.521	0.52975
13.5	0.565	0.55	0.563	0.547	0.55625
14	0.592	0.576	0.589	0.575	0.583
14.5	0.618	0.603	0.616	0.601	0.6095
15	0.645	0.63	0.644	0.627	0.6365
15.5	0.671	0.656	0.671	0.653	0.66275
16	0.698	0.681	0.7	0.681	0.69
16.5	0.724	0.708	0.727	0.708	0.71675
17	0.75	0.735	0.753	0.736	0.7435
17.5	0.777	0.761	0.777	0.762	0.76925
18	0.805	0.789	0.801	0.79	0.79625
18.5	0.83	0.814	0.829	0.816	0.82225
19	0.857	0.843	0.856	0.843	0.84975
19.5	0.883	0.87	0.883	0.87	0.8765
20	0.91	0.896	0.909	0.897	0.903
20.5	0.935	0.924	0.935	0.923	0.92925

Pressure(bar)	1	2	3	4	Average
21	0.965	0.949	0.962	0.949	0.95625
21.5	0.992	0.976	0.99	0.975	0.98325
22	1.014	1.003	1.013	1.002	1.008
22.5	1.043	1.03	1.04	1.029	1.0355
23	1.074	1.059	1.066	1.054	1.06325
23.5	1.093	1.083	1.094	1.079	1.08725
24	1.123	1.112	1.121	1.104	1.115
24.5	1.15	1.138	1.148	1.13	1.1415
25	1.174	1.166	1.172	1.155	1.16675
25.5	1.199	1.192	1.198	1.182	1.19275
26	1.225	1.216	1.223	1.213	1.21925
26.5	1.255	1.242	1.259	1.24	1.249
27	1.283	1.272	1.285	1.264	1.276
27.5	1.308	1.297	1.311	1.29	1.3015
28	1.332	1.326	1.335	1.32	1.32825
28.5	1.355	1.347	1.356	1.345	1.35075
29	1.385	1.375	1.384	1.375	1.37975
29.5	1.409	1.405	1.41	1.402	1.4065
30	1.438	1.429	1.436	1.432	1.43375
30.5	1.464	1.459	1.463	1.458	1.461
31	1.491	1.482	1.49	1.485	1.487
31.5	1.519	1.509	1.515	1.509	1.513
32	1.543	1.538	1.543	1.538	1.5405
32.5	1.565	1.562	1.569	1.566	1.5655
33	1.594	1.588	1.591	1.593	1.5915
33.5	1.616	1.611	1.615	1.616	1.6145
34	1.646	1.637	1.649	1.644	1.644
34.5	1.674	1.664	1.674	1.672	1.671
35	1.694	1.699	1.701	1.698	1.698
35.5	1.72	1.72	1.727	1.723	1.7225

APPENDIX - B

The deduction of IMEP calculation used in the program:

Substitute Eq. 4-4 into Eq. 4-3

$$V = V_c + \frac{\pi B^2}{4}\left[l + \frac{L}{2}\left(1 - \cos\theta\right)\right] - \frac{\pi B^2}{4}\sqrt{l^2 - \frac{L^2}{4}\sin^2\theta} \qquad \text{Eq. B-1}$$

$$\frac{dV}{d\theta} = \frac{\pi B^2}{4}\left(\frac{L}{2}\sin\theta + \frac{\frac{L^2}{8}\sin\left(2\theta\right)}{\sqrt{l^2 - \frac{L^2}{4}\sin^2\theta}} \right) \qquad \text{Eq. B-2}$$

Substitute Eq. B-2 into Eq. 2-8

$$IMEP = \frac{\Delta\theta}{V_s}\sum_{i=\theta_0}^{\theta_n} p\left(i\right)\frac{\pi B^2}{4}\left(\frac{L}{2}\sin i + \frac{\frac{L^2}{8}\sin\left(2i\right)}{\sqrt{l^2 - \frac{L^2}{4}\sin^2 i}} \right) \qquad \text{Eq. B-3}$$